Modelling the future of aviation

Developing a comprehensive, user-friendly model able to assess the climate impact of policy and technological measures

Joris Neuman 4178106

Msc Thesis
AE5211

Aerospace Engineering

TU Delft

18th November, 2021

Contents

Nomenclature

Acronyms

AIM	Aviation Integrated Model
APMT	Aviation Portfolio Management Tool
ASK	Available Seat Kilometer
ATK	Available Tonne Kilometer
BADA	Base of Aircraft Data
CAEP	Committee on Aviation Environmental Protection
EASA	European union Aviation Safety Agency
ERF	Effective Radiative Forcing
FESG	Forecasting and Economic Sub-Group
FFWD	Fast ForWarD
FLEET	FleetLevel Environmental Evaluation Tool
FSDM	Fleet System Dynamics Model
GDP	Gross Domestic Product
GREAT	Global and Regional Environmental Aviation Tradeoff tool
IATA	International Air Transport Association
ICAO	International Civil Aviation Organisation
IPCC	Internation Panel of Climate Change
ISSR	Ice Super Saturated Region
LF	Load factor
MLW	Maximum Landing Weight
MTOW	Maximum Take Off Weight
MZF	Maximum Fuel Weight
NRMSE	Normalised Root Mean Square Error
OECD	Organisation for Economic Co-operation and Development
OEW	Operative Empty Weight
RMSE	Root Mean Square Error
RPK	Revenue Passenger Kilometer
RTK	Revenue Tonne Kilometer
SC	Size Category

SRES	Special Report on Emissions Scenarios
SSP	Shared Socioeconomic Pathway

Chemical species

CH	Hydrocarbons
CH_3	Methyl radical
CH_4	Methane
CO	Carbon monoxide
CO_2	Carbon dioxide
HO_2	Hydroperoxy radical
M	Third body
N_2	Nitrogen
NO_x	Nitrogen oxides
$O(^3P)$	Atomic oxygen
O_2	Oxygen
OH	Hydroxyl radical
SO_2	Sulphur dioxide
SO_3	Sulphur trioxide

Greek symbols

β	Demand coefficients
η	Coefficient values
η	Efficiency [-]
η	Performance scaling parameter [-]
μ	Routing inefficiency parameter [nm]
ϕ	Proportion between the total energy requirement of the aircraft and the constant weight energy source
θ	Aircraft size category scaling parameter [-]
ζ	Cruise distance scaling parameter

Roman symbols

a	Scaling factor [-]
b	Maturity growth rate [-]
D	Drag [N]
D	Dummy variable [-]
D	Stage length [km]
d	Distance [nm]
d	Segment distance [nm]
E	Total energy carried on aircraft at start of the cruise phase [J]
e	Specific energy [J kg^{-1}]
f	Route fare [$]

g	Gravitational acceleration [m s^{-2}]
g	Growth rate [-]
h	Airport hub status [-]
HHI	Airline passenger share [-]
I	Income [$]
K	Asymptotic value [km $\$^{-1}$]
k	Propulsive efficiency scaling constant [-]
L	Lift [N]
LF	Passenger load factor [-]
N	Passenger demand [passengers]
NLCC	Number of low cost carriers [-]
O	Fraction of fuel mass per RTK [km^{-1}]
P	Population [persons]
PL	Load factor [-]
pr	Proportion of flights for aircraft size category [-]
q	Flight frequency [-]
R	Longest runway length [m]
R	Range [m]
t	Time [years]
t	Time in years [year]
t	Travel time [m]
U	Size category parameter [-]
VAR	Variable under consideration [-]
vot	Value of time [-]
W	Weight [N]
x	Example variable [-]

Subscripts

0	Initial
bat	Battery
c	Constant fuel
co2	Carbon dioxide
d	Destination
f	Fuel
fr	Freight
GC	Great circle
gt	Gas turbine
inc	Increase of constant

m	Origin airport
n	Destination airport
new	New
NM	Nautical miles
o	Origin
OD	Origin destination
OE	Operative empty
p	Flight phase
p	Propulsive
pax	Passenger
PL	Payload
pl	Payload
pos	Possible
r	Region
s	Aircraft type
tot	Total

Abstract

The aviation sector accounted for 3.4 to 4.0% of the total anthropogenic radiative forcing in 2015. The sectors' growth is several percentage points larger than the annual fuel efficiency gain, resulting in an increasing climate change impact. The world formulated goals for 2050 to limit anthropogenic climate change, the aviation sector requires a mix of fuel consumption reducing technology, increased operational efficiency and carbon offsetting to contribute to the goals.

The Aviation Integrated Model (AIM) developed at the University of Cambridge resolves the impact of technological and operational choices, but requires detailed knowledge of the technological development. This work is directed to retain the air traffic and fleet resolution model of AIM, while utilising a different performance model. Aircraft performance is modelled by technology trends to assess a range of technology options (such as hybrid electric flight or different aerodynamic configurations) at limited required knowledge while retaining the model's physical basis.

The model uses the Breguet range equation and fuel fractions updated with Lissys' Piano-X data to resolve aircraft fuel consumption with limited modelling error. The fuel and carbon dioxide emissions have an average normalised root-mean-square error of three percent compared to AIM, while nitrous oxide emissions incur a 1.5% error.

A case study to demonstrate the capability of the model has been performed to investigate the possibilities for hybrid electric flight serving a significant market share before 2050. The current trends in annual fuel efficiency increase and increase in battery specific energy do not result in a significant market share or reduction of aviation emissions for hybrid electric aircraft before 2050.

To achieve a 10% decrease in carbon dioxide emissions, the annual increase of the aircraft fuel efficiency has to be increased from 1.1% per year to 1.5% and the annual battery specific energy increase is required to go up to 5.67%. The required increase in both battery specific energy and the aircraft performance parameters is significant, which makes a substantial reduction of emissions of the aviation sector by hybrid electric aircraft before 2050 improbable.

1 Introduction

This following chapter aims to provide an overview of the challenge the aviation industry faces due to the increased attention to aviation's share in global warming. First a quantification of the problem is provided in Section 1.1. The reaction of the industry to the discussion and the current performance is presented in Section 1.2 and Section 1.3, respectively. The research objective of the work in this report is presented in Section 1.4.

1.1 Impact

Since the beginning of powered flight in the start of the twentieth century, the world has become more interconnected. Commercial aviation has contributed to this effect by decreasing long range travel time substantially. The sector has enjoyed tax exemptions and benefits due to its perceived positive effects on economic growth. During the past decade, the aviation sector has been increasingly scrutinised for the industries' role in global warming.

The CO_2 effects of aviation are estimated to account for 3.5% of the total anthropogenic forcing in 2018 [1]. Due to uncertainty the 90% likelihood range of anthropogenic Radiative Forcing (RF) caused by aviation is estimated to be between 3.4-4.0% in 2015 [2]. Revenue Passenger Kilometres (RPK) have increased by a factor 2.2 between 2005 and 2019 accompanied by an increase in fuel consumption to 363 billion litres from 257 billion litres [3][4].

The aviation sector has not only increased in the absolute term of emissions, the relative contribution has increased as well. The report on the national greenhouse gas inventories in 2012 by the United Nations Framework Convention on Climate Change shows aircraft emissions have grown by 76% between 1990 and 2012 in the Organisation for Economic Co-operation and Development (OECD) countries including the Russian Federation, the Baltic States, and several Central and Eastern European States [5]. For comparison marine fuel usage increased by 10% over this period [5].

1.2 Goals

The increase in public and governmental pressure has led to action by the United Nations International Civil Aviation Organisation (ICAO) and the International Air Transport Association (IATA) which is the aviation sector's trade organisation. Both have pledged all growth from 2020 to be carbon-neutral, with the baseline level to be set by the average of the emissions in 2019 and 2020 [6][7]. Due to the COVID-19 crisis, which is expected by the ICAO to reduce air passenger numbers by 60% in 2020, 2019 has been set as the new baseline, effectively resulting in a new pledge of carbon-neutral growth after 2019 [8].

Both IATA and the ICAO have set annual fuel efficiency targets in 2010 and 2009, respectively. The efficiency goal of IATA is set at 1.5% improvement in annual fuel efficiency up and till 2020, whereas the ICAO strives for 2% improvement until 2050 [6][7]. The IATA goal required fuel efficiency to improve by 15.3% between 2009 and 2020 and the ICAO targets resulted in an overall fuel efficiency improvement of 55.4% between 2010 and 2050. The IATA has further specified the goal of net-zero carbon emissions in aviation CO_2 emissions in 2050 [9].

The European Commission has specified targets for aviation emissions in 2050 as well. The European Green Deal specifies a reduction of 90% in transport emissions as compared to 1990 levels, in which aviation is expected to contribute. [10]

1.3 Performance

Between 1960 and 2014 the aviation sector has achieved an average fuel efficiency improvement of 1.3% per year, leading up to a total reduction of 45% on a seat-km basis [11]. It should be noted that most of the fuel efficiency improvements were made in the period between 1960 and 1970 and the period between 1980 and 1990 at an annual rate of 2.6% [11]. In the period between 2000 and 2010, 0.5% improvement was reached on a yearly basis and between 2010 and 2014 1.1% [11]. The annual fuel efficiency targets of 1.5% (IATA) and 2% (ICAO) have therefore not been met between 2009 and 2014.

The increase in RPK has been 5.79% annually between 2005 and 2019 [3][6]. If the trend in RPK growth continues post 2020, the difference between the RPK growth and annual fuel efficiency has to be compensated through increased operational efficiency and carbon offsetting.

If the 1.5% goal annual fuel efficiency goal of IATA is achieved between 2019 and 2050, the fuel efficiency will have increased by 58.7% in 2050 as compared to 2020. If in the same period the annual increase in RPK seen between 2005 and 2019 continues, the total RPK will increase with 472.5% between 2019 and 2050. Combined with the RPK growth between 2005 and 2019 of 120.8%, the sector will have grown 1110% in 45 years.

To decrease the deficit between the expected annual fuel efficiency improvement and the increase in passenger traffic, will require a mix between technological- and operational innovation and carbon offsetting.

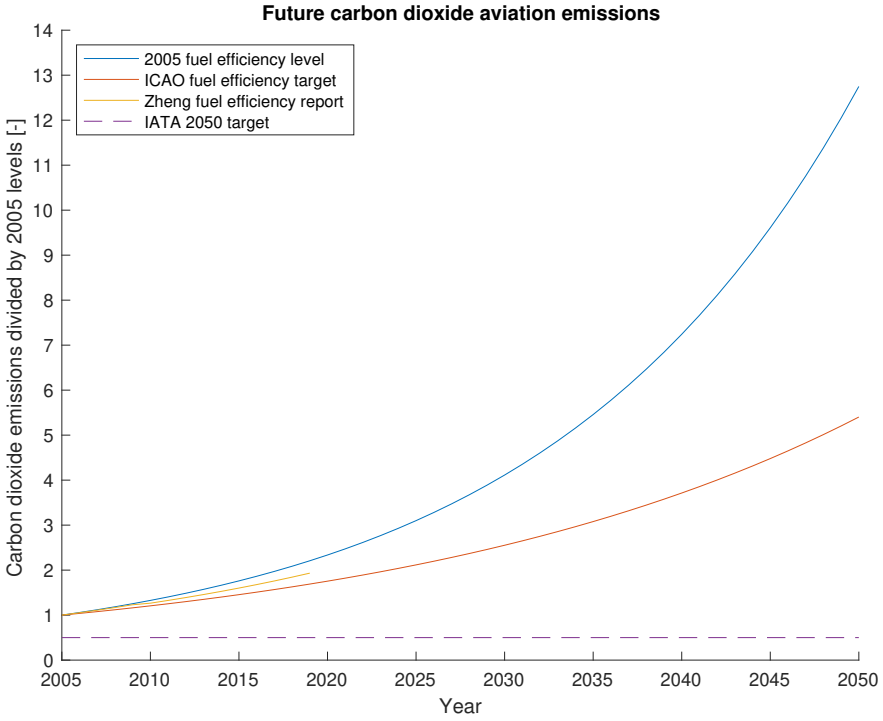

Figure 1.1: Emission projection based on RPK growth, reported fuel efficiency and ICAO and IATA fuel efficiency targets [3][4][6][7][12].

1.4 Research objective

The objective of the research in this work is formulated as follows:

> *Provide insight in required technological capability to reduce the emissions of the aviation industry by connecting a preliminary design model with a fleet simulation model.*

The research goal is to be obtained by answering the following main research question:

> *How can a user-friendly model be constructed which can determine the impact of technological and operational development on aviation emissions in the 21st century?*

The main research question is subdivided into the following research questions:

- Which model architecture is best suited to answer the research question?
- Which models exist for the preliminary design and performance of aircraft?
- Which models exist to determine the type and sizes of the global fleet?
- Which models exist to simulate fleet activity?
- Which combination of models is best suited to answer the research question?
- How can the performance be modelled for every flight phase?
- How does the model perform for a base case scenario against other models?
- How sensitive is the required trend in battery technology against other design parameters?

2 | Literature review

Aviation impacts the environment in several ways, which consists mainly of noise and atmospheric emissions [13]. Aerodynamic interactions and engines cause noise that affect populations around airports. Emissions from aircraft engines influence local air quality near airports and are associated with global warming. This chapter focuses on the global warming effect caused due to aviation. First the combustion process and the chemical species involved are analysed in Section 2.1. The species are further discussed in Section 2.2. A quantification of the impact of the species is provided in Section 2.3. A discussion of state-of-the-art models is presented in section 2.4. The chapter concludes with the model selection procedure and selection in Section 2.5.

2.1 Combustion process

The global fleet of subsonic aircraft makes use of jet fuel as an energy source for the propulsive systems. The propulsion unit is used to generate and maintain the velocity of the aircraft by overcoming or matching the incurred drag of the aircraft. Jet fuel consists of hydrocarbons (C_nH_m), with a mean C/H ratio of $C_{12}H_{23}$, which is combusted in the engine with oxygen (O_2) supplied from atmospheric air [14][15].

In addition to oxygen, atmospheric air consists for 79% out of nitrogen (N_2) [16]. Jet fuel specifications dictate a sulphur content lower than 0.3%, however low levels of sulphur exists in jet fuel which oxidises during combustion [17]. During oxidation, carbon dioxide (CO_2), water and sulphur dioxide (SO_2) are formed in the ideal exothermic reaction. Residual nitrogen and oxygen are emitted.

As the fuel is combusted, less than ideal conditions in the engine, it results in incomplete combustion. Unburned hydrocarbons (HC), carbon monoxide (CO) and soot (carbon molecules) are the result of incomplete combustion [13]. Due to the high pressure and temperature environment in the combustion chamber, atmospheric nitrogen and oxygen start to react and form nitrogen oxides (NO_x) [17]. The chemical reaction of the combustion process is illustrated in Figure 2.1.

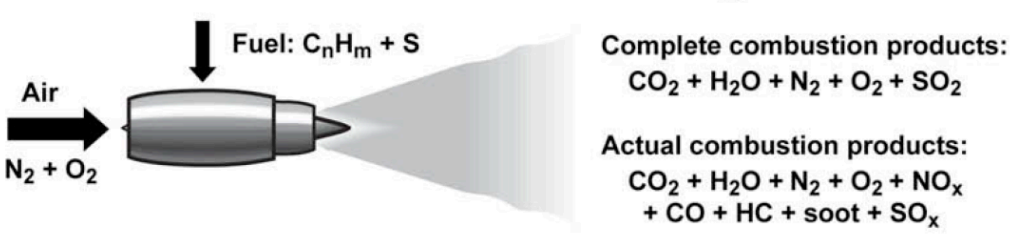

Figure 2.1: Combustion species in an aircraft engine. Illustration from Lee et al. [2]

2.2 Emissions species

The species encountered during combustion in aircraft engines are further discussed with regard to the atmospheric interaction of the species. First carbon dioxide, water vapour and nitrogen oxide are discussed in Section 2.2.1 to Section 2.2.3. The mechanics of soot, sulphur and hydrocarbons and carbon monoxide are presented in Section 2.2.4 to Section 2.2.6, respectively.

2.2.1 Carbon dioxide

Carbon dioxide is one of the primary products obtained in complete combustion of jet fuel. For every kilogram of jet fuel oxidised, 3.160 kilograms of carbon dioxide is formed [14][17]. Within the atmosphere CO_2 does not

Species	Emission index [g kg^{-1}]
CO_2	3160
H_2O	1231
NO_x	14.12 - 15.14
CO	2 - 3
SO_2	1.2
HC	0.1 - 0.6
Soot	0.03

Table 2.1: Mean emission index for jet fuel. Data obtained from Lee et al. [1][2]

interact, but on the earths surface the biosphere and oceans absorb and emit CO_2 [18]. The CO_2 mixes in the atmosphere and the emission location does not influence its effects [18]. The residence time of carbon dioxide in the atmosphere depends on the process by which it is removed [19]. Carbon dioxide uptake by land through photosynthesis involves a timeline of one year to one century [19]. The timescale of absorption by the ocean is equal to one decade to twenty centuries determined by the IPCC [19][20].

The insulating effect of carbon dioxide makes it a greenhouse gas, as it reflects radiation from the earths surface and passes incoming sunlight, of which the scale depends on the atmospheric concentration [18]. Radiative forcing is a parameter in which the perturbation of the earth energy budget is expressed, with positive radiative forcing indicating a warming effect [2]. The combination of carbon dioxides insulating properties and a long lifetime causes the warming effect to continue over a long time even if anthropogenic emissions of the species would cease.

2.2.2 Water vapour

As one kilogram of jet fuel is burned, 1.24 kg of water vapour is released into the atmosphere. The direct effect of water vapour emissions into the atmosphere is similar to CO_2, absorbing radiation from the earths surface, of which the scale depends on the atmospheric concentration [17]. The flux in water vapour concentration in the troposphere is small compared to the natural hydrological cycle and has a low residence time of nine days, therefore the global warming effect is regarded as negligible [18]. The negligible global warming effect is valid for the direct water vapour impact and does not account for the significant contribution of contrails. The stratosphere contains a lower concentration of water, and slower atmospheric processes that remove aircraft water emissions, leading to residence time of months to years.

Water vapour emissions from aircraft have a second, indirect global warming effect. When hot, moist air from the exhaust mixes with colder air it can form line-shaped cirrus clouds [14]. The critical temperature at which contrails form is specified by the Schmidt-Appleman criterion [14]. The critical temperature depends on ambient pressure, humidity, temperature and engine parameters [21]. Under the right conditions the water vapour in the exhaust condensates when it mixes with the cold ambient air, and freezes due to the low ambient temperature forming a condensation trail (contrail) [22].

The duration of the contrails depends on the saturation level of the air with respect to ice. If the air is subsaturated the contrail will persist for minutes, but if the air is supersaturated the contrail can persist for hours [21]. If a contrails persists for more than ten minutes it is defined as a persistent contrail [18]. Contrails which are formed in moist air and Ice Super Saturated Regions (ISSR), grow by taking up water vapour contained in the ambient air [22]. The growing contrails are similar to natural cirrus clouds and are referred to as contrail cirrus [21]. Contrails reflect both incoming radiation from the sun and the outgoing surface radiation from the earth, however the outgoing radiation is reflected more efficiently leading to a net positive global warming effect [14].

The formation of contrails depends heavily on the atmospheric conditions and the propensity for contrail development varies throughout the atmosphere and has seasonal dependency. The poles and equator have a higher propensity to form persistent contrails as illustrated in Figure 2.2, but the regions are situated at a different pressure altitude [23]. When moving from winter to summer the regions with higher persistent contrail sensitivity decrease at the poles and increase at the equator. Most air traffic occurs within the dotted lines, indicated in Figure 2.2, between 30° and 60° latitude in regions with heightened persistent contrail coverage [24].

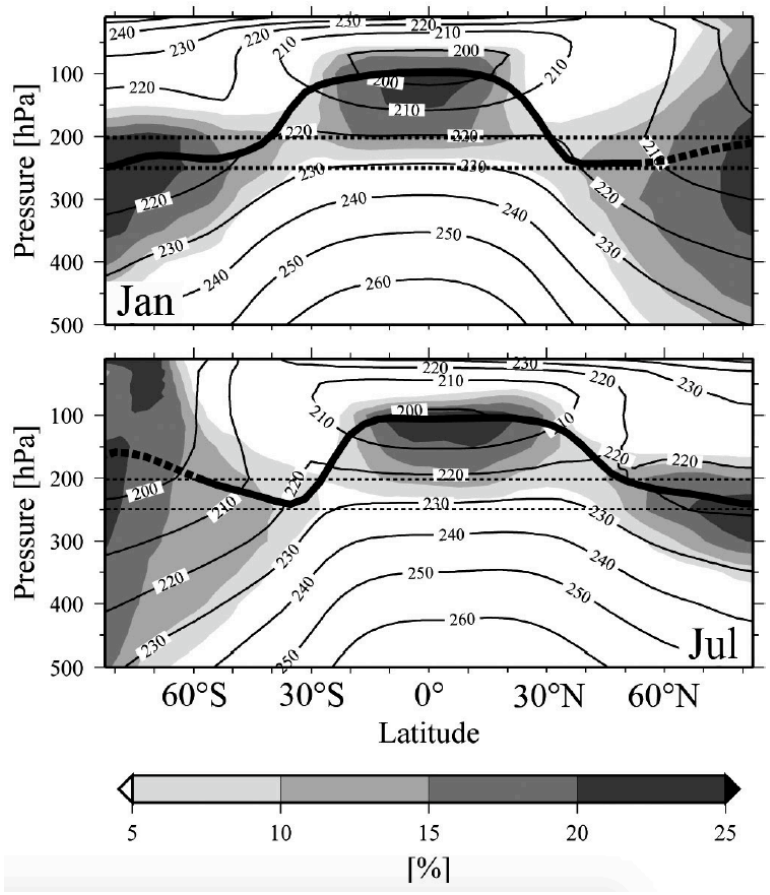

Figure 2.2: Sensitivity to contrail formation. Taken from Dahlmann et al. [24]. The original illustration is from Fichter et al. [25].

2.2.3 Nitrogen oxides

The high temperature and pressure conditions in the engine cause nitrogen and oxygen to react forming nitrogen oxides [17]. Nitrogen oxides consist of nitrogen oxide (NO) and nitrogen dioxide (NO_2). Aviation emitted NO_x impacts the atmosphere in three ways [2]. NO_x is an indirect effect which depends on the location in the atmosphere [26]. Most air traffic occurs in the higher troposphere, tropopause and lower stratosphere where emissions of NO_x influence the concentration of ozone and methane which are both gasses with positive radiative forcing [2].

Ozone formation

Ozone formation occurs through the chemical reaction in Equation (2.1), where atomic oxygen ($O(^3P)$) and oxygen (O_2) combine to form ozone in the vicinity of a third body (M).

$$O(^3P) + O_2 + M \rightarrow O_3 + M \tag{2.1}$$

In the troposphere, the formation of ozone is controlled by a series of reactions involving NO_x. NO combines with a hydroperoxy radical to form nitrogen dioxide and hydroxyl radicals as shown in Equation (2.2).

$$HO_2 + NO \rightarrow NO_2 + OH \tag{2.2}$$

Nitrogen dioxide photolyses into nitrogen oxide and atomic oxygen Equation (2.3), which in turn is used in Equation (2.1).

$$NO_2 \xrightarrow{h\nu} NO + O(^3P) \tag{2.3}$$

As ozone has positive radiative forcing and ozone concentration is increased through NO_x emissions, aviation NO_x is regarded to attribute to global warming [14].

Methane and ozone depletion

The chemical process involved in the depletion of ozone in the atmosphere occurs through reaction with hydroxyl or hydroperoxyl radicals as shown in Equation (2.4) and Equation (2.5) [14].

$$O_3 + HO_2 \rightarrow 2O_2 + OH \tag{2.4}$$

$$O_3 + OH \rightarrow O_2 + HO_2 \tag{2.5}$$

An emission of NO_x increases the hydroxyl radicals concentration in the atmosphere through Equation (2.2). The increase in ozone formation through NO_x triggers ozone to increase hydroxyl radical formation through Equation (2.4). Atmospheric methane (CH_4) is oxidised by hydrogen radicals through Equation (2.6).

$$CH_4 + OH \rightarrow CH_3 + H_2O \tag{2.6}$$

The reduction of methane and ozone leads to less radiative forcing as both are greenhouse gasses [14]. However, the increase in radiative forcing from ozone formation due to NO_x outweighs the radiative forcing decrease caused by reductions in methane and on the longer term small reductions in ozone, leading to a net positive radiative forcing effect due to aviation NO_x emissions [2].

2.2.4 Soot

Solid particles of carbon called soot are emitted in small quantities due to incomplete combustion (0.04 g kg^{-1} for the year 2002 from AERO2K [14]). Soot particles directly affect the global radiation budget by a net positive radiative forcing [2]. An indirect effect of soot particles is caused by the hydrophilic properties upon which water vapour condensates, triggering the formation of contrails and aerosols [14].

2.2.5 Sulphur

The sulphur contained in jet fuel is oxidised in combustion to sulphur dioxide as shown in Equation (2.7). Sulphur dioxide has a negative radiative forcing [2].

$$S + O_2 \rightarrow SO_2 \tag{2.7}$$

The sulphur dioxide can form into sulphur trioxide (SO_3) through the reaction with oxygen or a hydroxyl radical. Sulphur trioxide reacts with water vapour in the atmosphere forming sulphuric acid (H_2SO_4) with a low vapour pressure [14]. Sulphuric acid is regarded the most important precursor for aerosols. Aerosols reflect incoming solar radiation at a higher rate than outgoing terrestrial radiation causing surface cooling [18]. Aerosols have an impact on the microphysical and radiative properties of clouds of which the effect is not quantified [18].

Furthermore, sulphur emissions have been shown to possess a nonlinear relationship with ultrafine particles in aviation exhaust plumes [27].

2.2.6 Hydrocarbons and carbon monoxide

Hydrocarbons and carbon monoxide are formed due to incomplete combustion. The impact of the hydrocarbon methane on the radiative budget of the earth has been discussed in Section 2.2.3. Other hydrocarbons and carbon monoxide suppress the formation of radical hydroxyls which in turn leads to reduced depletion of ozone (Equation (2.5)) [17]. Unburned hydrocarbons are also known to facilitate nucleation, increase particle growth and form aerosols of which the mechanics have been discussed in Section 2.2.5 [18].

2.3 Climate impact of emission

In the preceding sections, the individual aircraft emission species and the mechanics of the atmospheric interaction have been discussed. Lee et al. have quantified the impact of aircraft emissions for the year 2005 and have updated it for the year 2018 in 2020 [1][2]. Figure 2.3 contains the quantification in which the uncertainty margins have been included. In the figure the Effective Radiative Forcing (ERF) and Radiative Forcing (RF) are used to quantify the impact of the individual emission species. The ERF has been introduced to account for the effects of non-homogenously distributed emission species which have a different efficacy due to the spatial distribution [1].

The largest uncertainty margin is incurred for aviation induced cirrus cloudiness. Excluding aviation CO_2 emissions when reviewing the determined best estimates for the radiative forcing of the emission species, results in an effective radiative forcing of 66.6 mW m^{-2}, of which 57.4 mW m^{-2} (86%) is caused by aviation induced contrail cirrus. The influence of NO_x on ozone production and methane reduction incur high uncertainty margins, however the total NO_x impact has a smaller uncertainty margin, contributing to about a quarter (17.5 mW m^{-2}) of the radiative forcing. The contribution of water vapour and soot aerosols is marginal with a reduction of the ERF by sulphur aerosol radiation interaction of -7.4 mW m^{-2} (-11%). Taking the contribution of CO_2 on the ERF into account, the total effective radiative forcing due to aviation increases by 51% to 100.9 mW m^{-2}.

The subdivision of the relative shares in the RF due to the different emission species, indicates that the fuel efficiency and emissions goals stated by the ICAO and IATA (Section 1.2) are drafted from the perspective of the current technical state and operational methods. The targets set are specified by fuel efficiency improvement and carbon dioxide emissions. If these targets are met with accompanying large increases in, for example, NO_x and contrail formation, it could lead to a net increase in RF. Evaluating the potential of operational measures and technological innovation should analyse the effect on all aforementioned emissions' species.

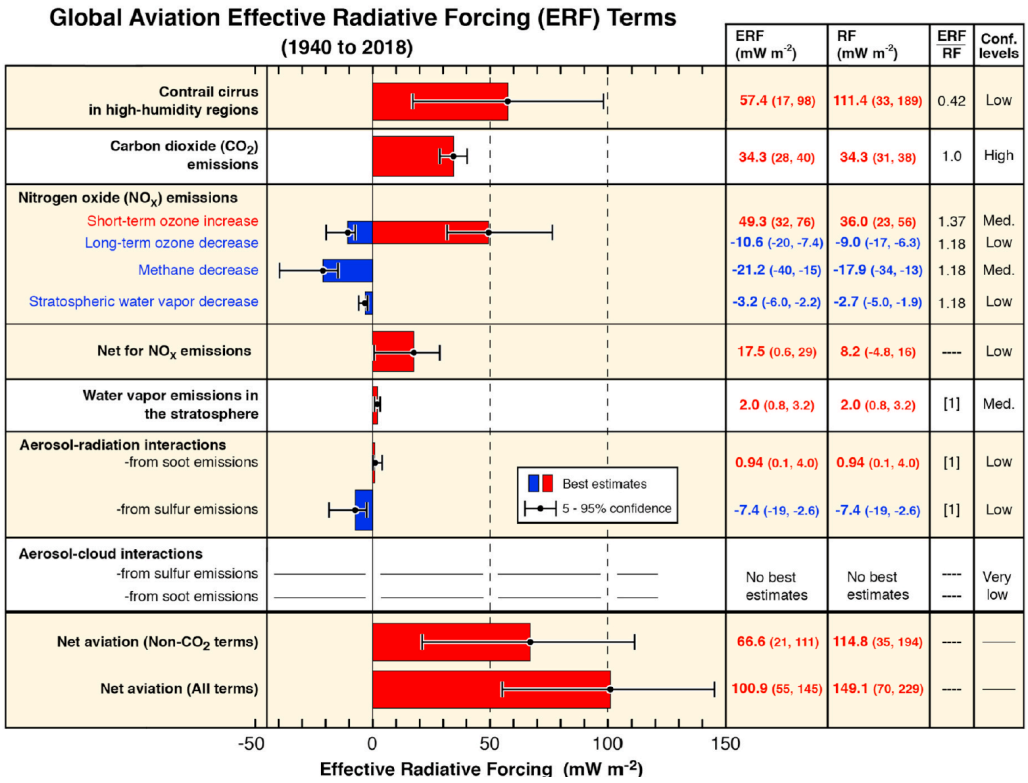

Figure 2.3: Quantification of the climate impact of the individual aviation emission species. Illustration from Lee et al. [1].

2.4 State-of-the-art aviation development and emission models

The emissions of the aviation sector has been modelled extensively to determine the current and future impact of aviation on the climate. Submodels used to evaluate design, fleet composition and the impact of emissions in the high troposphere and low stratosphere have been developed for various objectives. The following chapter provides an overview of these models.

First the models which simulate the future of aviation and the climate impact are discussed in Section 2.4.1. These models have been developed to support the drafting of effective policy and are referred to as policy models throughout this document for the sake of clear distinction. Section 2.4.2 discusses models to evaluate the performance of preliminary aircraft design, followed by fleet and traffic models in Section 2.4.3.

2.4.1 Policy based models

The development of models to assess the impact of aviation has started in the last decade of the twentieth century [18][28]. In 2019 Oguntona provided a review on nine different models, with an emphasis on the emissions inventories in 2050 as compared to the goals stated by IATA and the ICAO [29]. These models are listed in Table 2.2 and share a commonality in composition. The Aviation Integrated Modelling project (AIM), Future Civil Aviation Scenario Software Tool (FAST) and Aviation Emissions and evaluation of Reduction Options Modelling System (AERO-MS) start with an air traffic demand model discussed in the following section. Afterwards the fleet and traffic simulation. The performance evaluation of the aircraft in the fleet is analysed in the subsequent section, where an overview of the submodels is provided in Table 2.3.

	Applicability for this research	**Motivation**
1. Aviation Integrated Model (AIM)	Yes	-
2. Future Aviation Scenarios Tool (FAST)	Yes	-
3. Global and Regional Environmental Aviation Tradeoff (GREAT) tool	No	US National Airspace only
4. Fast ForWarD (FFWD)	No	CO_2 only
5. FleetLevel Environmental Evaluation Tool (FLEET)	No	US Domestic and International flights only
6. Aviation Emissions and evaluation of Reduction Options Modelling System (AEROMS)	Yes	-
7. Aviation Portfolio Management Tool (APMT)	No	Overlap with AERO-MS
8. Fleet System Dynamics Model (FSDM tool)	No	Short term
9. Combining aviation environmental design tool, IMPACT and FAST	No	CO_2 & NO_x only

Table 2.2: Overview of the models reviewed by Oguntona [29].

Air traffic demand

The AIM project starts with known flight data for a base year accounting for 95% of the flown RPK in that year [30]. It matches demand between city pairs based on population, income, fare and travel time. It also takes into account alternative methods of transportation. To model population and income, projected values are taken for different scenarios based on the Shared Socioeconomic Pathways (SSPs) by O'Neill et al. in 2013 [31].

The FAST model uses the 4D flight trajectory data from the Eurocontrol AERO2K database to determine the air traffic for the base year 2000 [32]. From the base year up and till 2020 it uses ICAO projections for global aviation traffic demand. For the period between 2020 and 2100 the FAST model uses a statistical relation between GDP and RPK growth to model the change in air traffic demand. The Special Report on Emissions Scenarios (SRES) are used to allow for different global development narratives by corrections in regional demand. The regional demand is represented by route groups which represent travel between and within regions [33].

The AERO-MS model of European Union Aviation Safety Agency (EASA) starts with a base year of 2006 for which the data is taken from the Eurocontrol WISDOM database, which contains global flight trajectory information. The future demand in air traffic is then modelled by taking into account demographic and macroeconomic development [28].

Both the AIM and AERO-MS models take into account the relation between demand and a change in fares. The fares are determined in other modules, which will be discussed in the next section. This relation is accounted for indirectly in the FAST model, where the effect of a change in fares is represented by the interpretation of the IPCC SRES.

Fleet and air traffic simulation

When the demand is determined, the models schedule aircraft to determine the aircraft movements. The AIM, AERO-MS and FAST model first define a set of aircraft groups to represent current and future aircraft [28][29][30].

The AIM model defines nine different groups based on seat capacity at the design range. The AERO-MS subdivides aircraft in seven seat capacity sizes and three range bands, which due to overlap leads to ten different aircraft groups [28]. The FAST model differentiates between sixteen aircraft and engine types to represent the global fleet [29].

Within the AIM project a multinomial logit model is used for every route to determine which share of the demand is flown by which aircraft class [30]. The logit model takes into account the route distance, if the airports are hub airports, the number of passengers on the route, the average passenger load factor, runway length and the number of low-cost carriers operating the route.

The AERO-MS model determines the operating costs for each route per aircraft category, which could feasibly operate on the route [28]. The operating costs include depreciation and interest rates as well as direct operating costs such as fuel and crew salaries.

The FAST model starts with the flight movements in the base year as the starting point for simulating aircraft movement. Fleet development was then modelled based on fleet forecasts, which depends on which IPCC SRES scenario is used [32].

Aircraft performance

AIM determines block fuel usage and NO_x per reference aircraft type (s) based on stage length (D) and load factor (PL) for the flight phases (p) climb, cruise and descent. The equations are derived by use of the Piano-X software, through which the coefficient values (η) have been determined, and leads to the relation shown in (2.8).

$$VAR_{sp} = \eta_{sp,0} + \eta_{sp,1} \cdot D + \eta_{sp,2} \cdot D \cdot PL + \eta_{sp,3} \cdot D^2 + \eta_{sp,4} \cdot PL + \eta_{sp,5} \cdot D^2 \cdot PL \tag{2.8}$$

The other flight phases are covered by either a fuel burn rate or a set amount of fuel required for the flight phase. Future technology, retrofits and operation measures are modelled as a percentage reduction in required fuel for the relevant flight phases. The associated change in costs (e.g. acquisition) is provided to determine the effect on lifetime costs of introducing an aircraft into the fleet [30]. The choice to adopt a measure to reduce fuel usage is determined by maximising profit. As revenue does not change due to a fuel saving measure, effectively the cost is minimised.

Within the AERO-MS model, a Flight and Emissions module determines the flight trajectory and emissions. For each of the ten different aircraft types, a reference aircraft is chosen based on market share of that aircraft type in the base year [28]. The Eurocontrol Base of Aircraft Data (BADA) database is used in conjunction with the ICAO Aircraft Engine Emission database as a source for the required parameters to simulate the aircraft trajectory, fuel flow and NO_x emissions [34]. The aircraft fuel usage is adjusted for suboptimal flight trajectories by a detour factor, which scale depends on the region where the flight takes place [28]. Technological improvements are then modelled as an increase in fuel efficiency. This means that if a yearly fuel efficiency increase of 1% is assumed, an aircraft produced in year $x+1$ will use 99% of the fuel for the same mission as an aircraft produced in year x uses [28]. Increased operational efficiency is incorporated by adjusting the detour factor.

The procedure to determine the aircraft performance in FAST is analogous to the method employed for the AIM model. First, simulations are run in Piano-X per aircraft type for a set of flight altitude and mission distance for the cruise phase [33]. Then the operations data is matched to a Piano-X simulation which bears the most resemblance [33]. By combining the trajectory and performance data, FAST projects the moment and location of emissions. As FAST uses an optimal trajectory (great circle distance and no holding patterns) in simulation, a detour factor as seen with the AERO-MS model is used. The detour factor is determined by comparing the total fuel usage in the base year and the fuel sales data. A 10% discrepancy between the fuel usage in the base year and the modelled fuel usage was found, which is used as a correction factor for future fuel usage in the model [32]. Increases in fuel efficiency are modelled in the scenarios as a yearly reduction in aviation emissions, of which the scale depends on which scenarios are modelled.

	Air traffic demand	**Fleet and air traffic simulation**	**Aircraft performance**
Aviation Integrated Modelling project (AIM)	City pair demand with socioeconomic projection	9 aircraft groups with a multinomial logit model	Piano-X extrapolation with fuel usage discount future technology and operational improvements
Future Civil Aviation Scenario Software Tool (FAST)	Base year extrapolation with regional growth	10 aircraft groups with base year operations. Fleet and traffic growth dictated by the IPCC SRES	Piano-X extrapolation with optimal trajectory adjusted by detour factor with year-on-year efficiency improvements
Aviation Emissions and evaluation of Reduction Options Modelling System (AERO-MS)	Base year extrapolation growth through demographic and economic projections	16 aircraft groups with minimisation of operating costs per route	Reference aircraft in BADA database with year-on-year efficiency improvements

Table 2.3: Overview of the submodels for the AIM, FAST and AERO-MS models.

2.4.2 Aircraft performance models

As underlined in the policy based models, advances in aircraft technology are evaluated in performance models. The performance models determine the quantity and location of emissions for a given mission.

Breguet range equation

The Breguet range equation is a physics based equation describing the relation between aircraft range, aerodynamic efficiency, structural efficiency, specific energy of the energy source and energy source to propulsion efficiency for the cruise phase. The traditional form of the equation, as shown in (2.9), is used in the Class-I sizing phase for aircraft [35][36].

$$R = \eta_{gt} \cdot \eta_p \cdot \left(\frac{L}{D}\right) \cdot \left(\frac{e_f}{g}\right) \cdot ln\left(\frac{W_{OE} + W_{PL} + W_f}{W_{OE} + W_{PL}}\right) \tag{2.9}$$

The range an aircraft is able to fly is depicted by the variable R. η_{gt} and η_p are the gas-turbine and propulsive efficiency, respectively [35]. The aerodynamic efficiency, the relation between how much drag an aircraft incurs

while generating the lift force, is represented by $\frac{L}{D}$. The specific energy of the fuel is e_f, and g the gravitational acceleration. The weight of the aircraft at the start of the flight phase is depicted by the sum of the operative empty weight W_{OE}, the payload weight W_{PL} and the fuel weight W_f. During the flight, the fuel weight W_f decreases as fuel is burned, and the aircraft becomes lighter, leading to the logarithmic relation in the Breguet equation [35].

As the Breguet range equation is used in the conceptual design phase of the aircraft, the variables are estimates determined from empirical relations or set as design goals. The consecutive design phases will allow a more exact determination of the design variables. This leads to both versatility and inaccuracy of the Breguet equation. The inaccuracy of the Breguet equation is caused by the assumptions made in derivation of the equation. The aircraft is assumed to be in steady, level flight which approaches but not matches the situation at cruise [37]. By merely using the Breguet function to compute the required mission fuel, the discrepancy becomes larger for short haul flight as compared to long haul flights. As long haul flights spend a higher proportion of the mission time operating in cruise conditions, the mission is more similar to the conditions described in the Breguet equation [38]. In order to account for the other flight phases, fuel fractions can be employed. Fuel fractions are generic, empirical values for what proportion of the mission fuel is used in which flight phase, to obtain a better estimate of the total mission fuel [36].

The versatility of the Breguet equation stems from the fact that it is used in the conceptual design phase, where detailed knowledge of the aircraft is not yet known. In the conceptual design phase, the aircraft configuration or engine type are researched to determine what aircraft layout is best in terms of fuel usage to perform a mission. Aircraft design is multidisciplinary, and optimisation in one field may lead to unacceptable performance in another. However, by reviewing Equation (2.9) three design fields can be discerned: aerodynamic design, propulsive design and structural design. Aerodynamic design is represented by $\frac{L}{D}$ relating the incurred amount of drag to the required amount of lift, the aerodynamic efficiency of the aircraft. The combined efficiency from the gas turbine and propulsive efficiency (η_{gt} and η_p) represent the propulsive design, and the operative empty weight (W_{OE}) is a measure of the structural design of the aircraft. An increase in performance from one of these disciplines can be evaluated through the Breguet equation, if the effect on the other disciplines is known.

The Breguet equation as shown in Equation (2.9) assumes a depleting fuel source, which leads to decreasing aircraft weight during the flight. The Breguet function can also be tailored to accommodate a constant weight energy source such as battery powered aircraft shown in Equation (2.10) [39].

$$R = \eta_{tot} \cdot \left(\frac{L}{D}\right) \cdot \left(\frac{e_{bat}}{g}\right) \cdot \left(\frac{W_{bat}}{W_{OE} + W_{PL} + W_{bat}}\right) \tag{2.10}$$

As aircraft weight remains constant throughout the flight, the logarithmic relation is removed in Equation (2.10). The efficiency of the conversion from stored energy, up and till propulsion is depicted by η_{total}, Equation (2.9) can be adjusted by equating $\eta_{tot} = \eta_{gt} \cdot \eta_p$. Care should be taken to determine the change in structural weight (included in W_{OE}) when the type and weight of the energy source is changed. If the propulsive system is changed (battery electric instead of kerosene) the fuel system changes which can result in a change of the weight of the system. As a different energy source is used for the same range, a change in weight for the energy source is expected due to a different specific energy. As the aircraft structure has to accommodate for this weight change, the structural weight and therefore the operational empty weight changes as well.

A different approach has to be taken if a hybrid propulsion system is assumed, with a constant weight and a depleting weight energy source. De Vries et al. have derived the Breguet equation (shown in Equation (2.11)) for an aircraft with constant power split between the constant and depleting weight energy sources (in their case fuel and battery electric hybrid) [35]. It is able to account for different layouts of the hybrid propulsion system.

$$R = \eta_3 \cdot \left(\frac{e_{bat}}{g}\right) \cdot \left(\frac{L}{D}\right) \cdot \left(\eta_1 + \eta_2 \cdot \frac{\phi}{1-\phi}\right) \cdot ln\left(\frac{W_{OE} + W_{PL} + \frac{g}{e_{bat}} \cdot E_{0,tot} \cdot \left(\phi + \frac{e_{bat}}{e_f} \cdot (1-\phi)\right)}{W_{OE} + W_{PL} + \frac{g}{e_{bat}} \cdot \phi \cdot E_{0,tot}}\right) \tag{2.11}$$

The efficiencies depicted by η_1, η_2 and η_3 depend on, the architecture of the propulsive system. If the system has a mechanical node architecture, which means the electrical power is converted to mechanical power before being summed to the power from the gas turbine, $\eta_1 = \eta_{gt}$, $\eta_2 = \eta_{em}$ and $\eta_3 = \eta_p$. An electrical node architecture involves the gas turbine power to be converted to electrical power, and the electrical power streams from the turbine and batteries meet before being converted to mechanical power. In this architecture $\eta_1 = \eta_{gt} \cdot \eta_{eg}$, $\eta_2 = 1$ and $\eta_3 = \eta_{em} \cdot \eta_p$ [35]. $E_{0,tot}$ is the total energy carried on the aircraft at the initiation of the cruise

phase from all energy sources [35]. Variable ϕ is the proportion of the total energy requirement of the aircraft is provided by the constant weight energy source.

Even tough a constant power split might not lead to the best design, the equation will provide an initial value for the performance of the design [35]. As De Vries et al. state in their paper, full electric and conventional flight are limit cases of Equation (2.11) (for a detailed derivation the reader is referred to [35]). This results in $\phi = 1$ meaning constant weight energy source (e.g. battery powered aircraft) flight and $\phi = 0$ a depleting weight energy source (e.g. conventional aircraft). With Equation (2.9) to Equation (2.10) a set of equations is obtained which allows modelling of the performance of current aircraft as well as expected the performance of conceptual aircraft.

Piano-X

Piano-X is commercial software developed by Lissys to determine aircraft performance data. Piano-X determines the aircraft performance from flight physics, but employs flight data to correct for effects that are not modelled [40]. Piano-X features a set of 250 existing aircraft, for which performance can be determined for various flight conditions [41]. From existing aircraft, parameters can be adjusted to see the effect of changes in for mission or aircraft design. Jensen et al. compared results from Piano-X to Eurocontrols BADA Revision 3.6. for the specific air range (distance travelled through the air per unit of fuel) at near optimal cruise speed and altitude. The discrepancy for regional jets, narrowbody and widebody aircraft was 2.69%, 1.76% and 5.82%, respectively [40].

As Piano-X is used to review current aircraft with detailed flight data, detailed information of an aircraft has to be known to review a design. Furthermore, Piano-X is used to review aircraft with conventional configuration (aircraft layout or propulsion system) which limits the reviewing capability for more radical future designs [42].

2.4.3 Fleet and traffic simulation models

Simulating air traffic consists of determining what missions are flown by aircraft and determination of which aircraft the missions is flown with. As a decision on how to model the one directly influences the other, both are discussed in this section. The ICAO has published a manual in which it has set out different methods of forecasting future air traffic demand and predicting fleet movement [43].

Three methods will be discussed as they are regarded as applicable to this research project, for a more comprehensive account the reader is referred to the ICAO document [43]. As modelling future air traffic demand depends on several external factors, most models allow for different scenarios to determine the range of outputs. For example the SRESS scenarios of the IPCC, which in practice result in low, medium and high air traffic demand outputs.

Trend projection

The method of trend projection requires knowledge of the historic growth and a historic size of the parameter to be estimated (a base year) [43]. The ICAO measures size of demand in Revenue Passenger Kilometre (RPK) for passenger demand and in Revenue Tonne Kilometre (RTK) for freight demand [44]. Availability is measured in Available Seat Kilometre (ASK) and Available Tonne Kilometre (ATK) for seat and cargo availability, respectively. An extrapolation is performed to determine the size of the parameter in the future. Care has to be taken to use the appropriate trend curve to obtain the highest quality fit. Growth in aviation demand is expressed in year-on-year percentage increase which leads to the relation shown in Equation (2.12)[3][6].

$$x = x_0 \cdot (1 + g)^t \tag{2.12}$$

The overall value of the parameter in the base year is represented by x_0. The growth rate is represented by g and t is the time span corresponding to the growth rate. When reporting on the entire sector of aviation, the growth rate is reported as the change in global RPK by IATA [3][6]. Terekhov et al. have used this approach connecting the growth in aviation demand with the growth of the future aircraft fleet [45]. The size of the aviation sector and the growth rates have a regional dependency. Some regions have a long history in aviation and are considered developed, in other regions aviation is still relatively new and expanding faster [46].

The location of emissions is a factor in the atmospheric interactions of the emissions and as such on the environmental impact of aviation [23]. Owen et al. recognise this dependency in the FAST model and subdivide the demand forecast in near term and long term demand [32]. For near term demand, the growth forecast of the ICAO Committee on Aviation Environmental Protection (CAEP) Forecasting an Economic Sub-Group

(FESG) are used which has provided expected growth numbers intra- and between regions up and till 2050 in the CAEP9 report of 2013 [46]. Owen et al. had access to data up and till 2026 in 2010 and used a longer term aviation demand model between 2026 and 2050. This model uses a logistic function or S-curve which will be discussed in the following section.

Logistic function

The method of using a logistic function has been used by the FESG in the 1999 IPCC report [18]. The rationale behind this approach is that in a developing market air traffic demand grows rapidly and in excess of GDP growth, whereas in a mature market air traffic demand growth approaches a rate equal to the GDP growth [18]. As the function is used for long term modelling, it is assumed all regional markets will reach maturity and follow the relation shown in Equation (2.13).

$$\frac{RPK}{GDP} = \frac{K}{1 + a \cdot e^{-b \cdot t}} \tag{2.13}$$

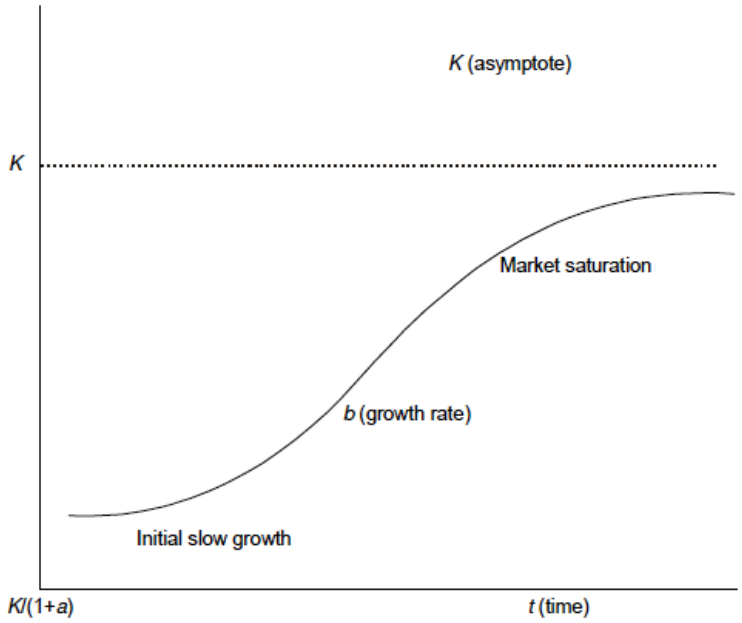

Figure 2.4: Shape of the logistic function. Image from the ICAO manual on traffic forecasting [43]

In Equation (2.13) K equals the asymptotic value of the relation which is illustrated in Figure 2.4. Care should be taken to note this is not an asymptotic value for air traffic demand, but the approached maximum ratio between GDP and RPK. Parameter a is the scaling factor which scales K to the minimum value. b is the growth rate which determines the rate in which the RPK over GDP ratio moves from the minimum to the maximum value. The IPCC report has determined the values for parameters K, a and b in the period from 1960 to 1995 [47]. Their respective values are presented in Equation (2.14).

$$\begin{aligned} \frac{RPK}{GDP} &= \frac{26.24}{1 + 9.04 \cdot e^{-0.73 \cdot t}} \\ K &= 26.24 \\ a &= 9.04 \\ b &= 0.73 \end{aligned} \tag{2.14}$$

Gravimetric model

The gravimetric model is used to determine the traffic between two locations. The scale of the locations is irrelevant, it can model the traffic between airports as well as continents. The model takes into account an array of factors which are expected to increase or decrease air traffic demand between two locations [43]. Examples of these factors are demographics, socio-economic, travel time, other modes of transport and service availability. The factors are determined historically and forecasts are available for the future. The historic data

is used to determine the coefficients of the function. The AIM model makes use of the gravimetric model to determine the demand between city pairs by use of Equation (2.15)[30].

$$ln(N_{OD}) = \beta_0 + \beta_1 \cdot ln(P_o \cdot P_d) + \beta_2 \cdot ln(I_o \cdot I_d) + \beta_3 \cdot ln(f_{od} + vot \cdot t_{od}) + \sum_i \beta_i D^i_{od} \tag{2.15}$$

The variable N_{OD} is the passenger demand between the origin and destination city. P are the populations of the metropolitan areas of the city, whereas I is the per capita household income. f is the route fare. vot and t are the passenger's value of time and travel time between the cities, respectively. β are the coefficients of the parameters and D_i captures other factors of the connection between the two cities [30]. The coefficients β are estimates, and the demand is calibrated by scaling to the known demand in the base year.

As the gravimetric model takes in a diverse range of factors, it is possible to model the effect of regional and local developments expected to influence demand. A high spatial resolution of emissions can be modelled, as travel between cities can be simulated to follow historic flight paths or great circle distances. The model requires the availability of long term forecasts for the factors in order to model demand. The quality of the demand forecast relies heavily on the quality of the forecasted factors.

2.4.4 Fleet composition and flight simulation

When air traffic demand is known, aircraft can be assigned to fill the demand. In order to do so a fleet composition can be either derived from demand or assigned to demand.

Trend projection

Trend projection for the aircraft fleet follows the same rationale as trend projection for air traffic demand. First, the aircraft fleet in the base year is determined in conjunction with the missions flown by which aircraft. This results in figures for the Available Seat Kilometres (ASK) and Available Tonne Kilometre (ATK). The trend in ASK or ATK is extrapolated to determine the expectation in future availability. Air traffic availability and demand are related through the load factor (LF) as shown in Equation (2.16).

$$RPK = LF \cdot ASK \tag{2.16}$$

The load factor allows the forecasted trends in RPK (and load factor) to be translated into ASK, which can in turn be used to determine fleet size and operations. Owen et al. make use of the projected ASK (Owen et al. use the equivalent SKO) from by the FESG up and till 2026 [32]. The ASK data provided is disaggregated into route- and aircraft groups, which allowed for a higher spatial resolution of aircraft emissions. For the period after 2026, the FAST model uses RPK data based on GDP growth. Owen et al. compute efficiency gains over the period after 2026 on an ASK basis, but do not specify how ASK is determined from RPK. The retirement and replacement of older aircraft types is modelled through the fleet rollover method of Greene and Meisenheimer.

Terekhov et al. use a similar method to determine the future fleet and operations, but complement the model with ordered aircraft data [45]. The ICAO FESG traffic growth forecast (in RPK) is compared to the expectation of delivered orders, and if required additional aircraft are added to the fleet to accommodate for deficiency between availability and demand. For years where no order data is known yet, or orders have not yet been placed, the fleet is modelled based on demand. Aircraft are retired and replaced if necessary based on the retirement curves derived by the ICAO CAEP FESG [46].

Profit optimisation

The profit optimisation model tries to incorporate the factors airlines take into account to maximise profit through aircraft selection [44]. Profit is maximised by maximising the margin between revenue and expenses. In the decision process of adding an aircraft to the fleet, an airline will choose an aircraft that is projected to generate the highest profit. Examples of factors that can increase revenue are travel time and comfort, whereas cost minimisation takes in factors such acquisition, crew, maintenance and fuel costs.

The AIM model developed by Dray et al. employs a function to optimise net present value for the decision model of new technology adoption [30]. The model uses aircraft groups, which disaggregate the global fleet into nine size categories based on the amount of seats an aircraft has. When a new aircraft within the group retires or is added to the fleet to satisfy demand, the technology the aircraft is equipped with is determined by maximising the profit generated. The AIM model assumes equal revenue is generated by the different technologies, which leads to an operating expense minimisation. For every route a fleet is composed which reduces the overall expenses on that route.

2.5 Model selection

A range of possible models and submodels for designing a tool which is able to evaluate the impact of innovation in the aviation sector have been presented in Section 2.4. Several conditions have been determined for the tool to be successful, such as user-friendliness and applicability. A discussion for the criteria on which the model selection will be performed is provided in Section 2.5.1. Afterwards the model options and the performance towards the selected criteria is discussed in Section 2.5.2. Finally, the multi criteria analysis and model selection is presented in Section 2.5.3.

2.5.1 Criteria

In this section, the selection criteria are presented to be used to determine the system architecture selection.

- **User-friendliness:**
  A measure of how easy and pleasant the tool is to use. This measure is positively impacted by clear graphics, visual feedback, as small set of required input parameters and a low response time.
- **Accuracy:**
  A measure of how truthful the results are expected to be. Using peer reviewed models and data, as well as industry standards, increases confidence in the accuracy of the results.
- **Versatility:**
  A measure of how well-equipped the tool is to handle a wide variety of cases. Next to a base case scenario, it would be preferred that the tool is able to accommodate for individual, as well as a set of, technological and operational measures to determine the associated impact.
- **Feasibility:**
  A measure of how well the system architecture is suited to allow completion within the project duration and the availability of the required data sources.
- **Robustness:**
  A measure of how well the system architecture is suited to unexpected or extreme input parameters. Preferably, such inputs can be resolved or are not accepted with an accompanying warning to negate illogical results or a tool crash.

2.5.2 Model options

A discussion of the modular composition is provided, along with the performance in the selection criteria, for five model options.

Option 1

The first model consists largely of the Aviation Integrated Modelling project, but is complemented with a Breguet based performance analyser. The model involves an iteration loop in which first the air traffic demand between origins and destinations is determined and secondly the air traffic supply. From the determined supply, the cost for an air fare is set and the new demand based on the fare is determined. This process is repeated until convergence is met. The effect of technological and operational innovation is modelled as a change in fuel use per flight phase and a change in acquisition cost of aircraft. The Breguet performance analyser determines the change in fuel usage and cost is an input to the model (or can be determined by a cost module).

The iterative process decreases the user-friendliness of the model due to the long response time (90 minutes for a solution from base year 2015 till 2050), but increases accuracy due to the inclusion of fare costs. The robustness of the model is negatively affected, as unexpected inputs can cause the model to become stuck in an iteration loop. The versatility profits from this form of innovation modelling. Most of the work in the project will be directed at developing the performance module within the AIM model to allow for a range of innovation scenarios, developing an emission location inventory module and interface development. This impacts the feasibility of the project positively.

Option 2

This model option is analogous to the FAST model investigated in the Section 2.4. The air traffic demand is determined for the base year and is extrapolated by expected (regional) growth rates into the future. The same procedure is followed for the global fleet composition and the routes flown by the fleet. The aircraft performance

module is based on data obtained from Piano-X and is extrapolated for the representative fleet to allow for the determination of the location and quantity of aircraft emissions. Future innovation is modelled as an annual efficiency improvement, neglecting the influence of a specific operational or technical modification.

Due to the non-iterative computational procedure, a solution can be determined at a low computational cost, benefiting the user-friendliness of the model. The accuracy of the model will be negatively impacted as costly innovations are not reflected back into the air fares and subsequently decrease air traffic demand. The argumentation for the versatility of the model could be performed along the lines of high versatility, as the annual fuel efficiency increase can account for the influence of every possible operational or technical alteration. However, in this report the versatility of the model is regarded as low, as specific innovations are neglected, the effect of the year of introduction of an innovation is neglected and the effect on emissions of different innovations is neglected.

Development of a non-iterative model based on extrapolated growth positively influences the feasibility, however high quality representative data acquisition for the base year for air traffic demand, air traffic availability and aircraft movement has a strong negative impact on the feasibility for the project execution for this system architecture. The non-iterative, small set of input parameters are expected to benefit the robustness of the model positively.

Option 3

The third option for the system architecture shares the same air traffic demand module as the previous model, the air traffic demand is determined for a base year and is extrapolated for future demand by expected regional growth rates. Based on the traffic demand, aircraft are scheduled along routes by a profit optimisation function, which leads to a global fleet composition. Aircraft performance data is extracted from the BADA database and efficiency improvements are modelled as a steady annual fuel efficiency increase.

As the model is non-iterative, the computational cost of the system architecture is suppressed, positively impacting the user-friendliness. The accuracy of the model is regarded higher than compared to the second model option as the profit optimisation module approaches actual aircraft operations. The versatility of the model with regard to the modelling of technical and operational innovation is determined to be low due to the same rationale provided for model option 2. Development of the model is more complicated as compared to model option 2, due to the inclusion of a profit optimisation module, and suffers from the same requirement for relevant, representative and high quality data for the base year. The extra required input to run the fleet and movement module reduces robustness, but retains a high score.

Option 4

The fourth model option is a combination of the first model option and the second model option. The air traffic demand module from model one is retained, but expanded with a simplified route for air traffic demand. As the AIM module contains options for the different SSP's (Shared Socioeconomic Pathways), the demand module can be run for these different scenarios and the determined air traffic demand quantities saved. This predetermined air traffic demand data can then be used for a simplified computation to determine coarse results for a scenario at a low computational cost. When a set of scenarios has been explored, the most interesting scenarios can then be run in the air traffic demand module to include feedback of the innovation costs into air traffic demand. Downstream, the system retains a similar architecture as the first model option.

The simplified, computational cost reducing air traffic demand option increases the user-friendliness as indicative results can be obtained faster as compared to the iterative demand module. The accuracy is impacted as the feedback towards air traffic demand of operational costs is halted. Versatility of the model is relatively high due to the supplementation of Breguet based models to determine the impact of fuel use of the relevant flight phases. As the modification to the air traffic demand module is regarded as small, the feasibility of the project is not considered to change considerably as compared to the first model option. The model is more exposed to input values that cause the model to crash, as compared to model options two and three leading to a lower robustness score.

Option 5

The fifth model option can be considered a mix between model option two and three. The air traffic demand projection is performed by extrapolating base year data, and the fleet and aircraft movement is performed by a profit optimisation function. The aircraft performance is analysed by use of extrapolated Piano-X data supplemented by Breguet based model to determine the change in aircraft emissions.

The model option benefits from the low amount of input parameters and low computational cost, which leads to quick resolution of a scenario and therefore a high user-friendliness rating. The accuracy of the model is average, as no feedback exists between the cost of an operational or technical change and the air fare. Versatility is high as the Piano-X data, edited by a fuel change per flight phase, can allow for a large set of operational and technical modifications. Feasibility is negatively impacted due to the required set of data and high development cost. The robustness of this model is quite high due to the small set of input parameters.

	Air traffic demand module	**Fleet and traffic module**	**Aircraft performance module**
Option 1	AIM O-D gravity model	AIM multinomial logit model	Piano-X extrapolated with added Breguet based models
Option 2	Baseyear extrapolation	Baseyear extrapolation	Piano-X extrapolated with annual fuel efficiency increase
Option 3	Baseyear extrapolation	Profit optimisation	BADA data with annual fuel efficiency increase
Option 4	AIM O-D gravity model with simplified option	AIM multinomial logit model	Piano-X extrapolated with added Breguet based models
Option 5	Baseyear extrapolation	Profit optimisation	Piano-X extrapolated with annual fuel efficiency increase

Table 2.4: Overview of the system architecture options

2.5.3 Result

The result of the multi criteria analysis can be found in Table 2.5. The highest overall score has been attributed to option 4. The architecture of the model is based on AIM, contributing to a high accuracy and feasibility. By using AIM as a database for the flight data, using the fleet composition module and replacing the performance model by a Breguet based model, the model is constructed. This increases the user-friendliness, versatility and robustness by a limited set of input parameters, low computational cost and the versatile Breguet range equation. Model option 1 and 4 are competitive, but the user-friendliness of model option 4 drives the selection towards that option. A compromise is made on accuracy in favour of user-friendliness. The method of constructing the model is further elaborated upon in Chapter 3.

	User friendliness	**Accuracy**	**Versatility**	**Feasibility**	**Robustness**	**Result**
Weight factor	0.3	0.2	0.2	0.2	0.1	1.0
Option 1	4	9	8	8	7	6.9
Option 2	9	6	6	6	9	7.2
Option 3	9	7	6	5	8	7.1
Option 4	8	8	8	8	7	7.9
Option 5	9	7	6	5	8	7.1

Table 2.5: Result of the system architecture multi criteria analysis.

3 | Methodology

The following chapter discusses the construction method of how the model assesses the impact of technology or policy on aircraft emissions. First, an introduction to the model composition and the general architecture of the model is presented in Section 3.1. The model can be discerned into three modules: an air traffic model, a performance and a fleet composition and activity module, which are discussed in Section 3.2, Section 3.3 and Section 3.4 respectively.

3.1 Model introduction and architecture

The goal of the model is to assess how choices concerning policy or technology options will influence the impact of aviation on the global climate in the twenty-first century. The model can be used as well to provide insight in the technological progress required to have a certain impact. The impact is expressed in this model in emissions of carbon dioxide, nitrous oxides, soot and carbon monoxide as compared to a base scenario.

Furthermore, the model outputs flight movements and water vapour emissions which can be used in a contrail formation model. The model is composed of three modules (as visualised in Figure 3.1): an air traffic module, an aircraft performance module and a fleet and air traffic module.

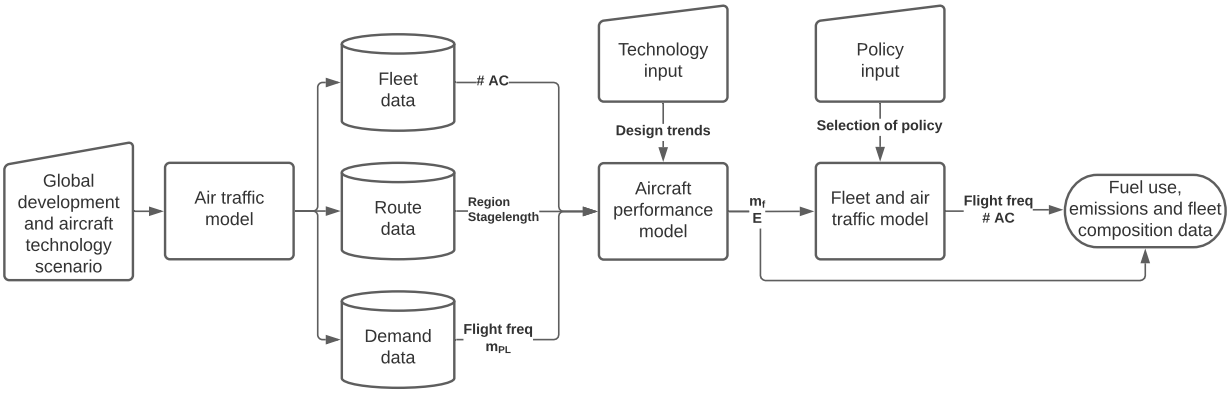

Figure 3.1: Model architecture

As a first step a data set is required which contains flight information representative for the global fleet and its development through time. Required information from this model consists of aircraft size category, payload weight, flight frequency, route distance and route origin and destination. Several data sets are provided with the model and can be chosen through the model input parameters. For a list of the input parameters and an explanation the reader is referred to Appendix A. the control inputs are contained within the technology input and policy input block.

The aircraft type, payload and distance data is supplied to the performance model. For every route and payload combination, the fuel and energy required by the aircraft to fly the route is determined. In this module, the effect of choices in aircraft design trends is assessed. The aircraft designs generated from the input parameters are not guaranteed to be able to fly certain routes. The ability for a design to fly a route is determined by reviewing if a design and route combination violates the maximum take-off or landing weight for a payload range combination. The output of fuel use for an aircraft design for a route is used in the fleet module.

Before the fuel consumption is used as input data for the fleet model, the fuel burn per mission is divided by the Revenue Tonne Kilometre (RTK) per mission to determine the fuel required per RTK per aircraft design. The highest fuel reduction per RTK as compared to the base aircraft (reference aircraft), is then used in the fleet activity and composition module. The highest fuel reduction per RTK is used in the fleet activity module to provide preference in scheduling aircraft, such that the largest overall reduction in fuel consumption is achieved. This process is further elaborated upon in Section 3.4.

In the fleet activity and composition module, a time step is performed from the run start year until the final model run year. First a procedure is run to determine the total amount of active aircraft per size category in a region. Retirement, destruction and freighter curves are imposed to subtract the aircraft unavailable for passenger flights. The rates of retirement, destruction and freighter conversion are used as policy control variables. Second hand market sales are simulated by redistributing the surplus amount of aircraft in a region towards regions with a deficit. The remaining deficit is equal to the amount of newly built aircraft in a region. The summation of these procedures leads to the total amount of aircraft available.

The average RTK capacity an aircraft can fly in a year is then obtained by dividing the amount of flown RTK in a region by the amount of active passenger aircraft. In the flight scheduling routine the average amount of RTK an aircraft can fly in a year, the annual RTK capacity, is used for the number of routes it is able to serve. In the scheduling routine, the amount of available RTK's are distributed according to available aircraft in a region per generation per size category.

The scheduling routine starts with the route in which the highest potential fuel reduction per RTK can be obtained, and assesses if the aircraft with the lowest fuel consumption is available. When available, the aircraft are scheduled to the route. When unavailable, the scheduler determines whether the required amount of RTK can be filled by new aircraft slots in the region. If no new aircraft are available, the procedure is repeated for the aircraft which has the next lowest fuel consumption on the route. The procedure runs until every route has an aircraft scheduled to it.

When the fleet model has run until the final year, every flight is assigned to a specific aircraft generation, size category and design. The fuel and energy consumption are then determined by multiplying the specific route flight frequency to the corresponding aircraft fuel and energy usage. The fuel consumption is multiplied by emission indices to determine the aircraft emissions.

3.2 Air traffic model

In order to assess the scale of the environmental impact of technology or policy choices, a data set is required consisting of current and future flight movements. The data contains the carried payload, the origin and destination of the route, the stage length and flight frequency. Furthermore, the fleet composition by build year and region for the start year are required as an input for the model in this work.

The data set for the air traffic model used in this work is the Aviation Integrated Model (AIM), but it is possible to supply any data set as long as it contains the data specified above. The AIM model has been developed at the University of Cambridge by Reynolds et al. to assess the interaction with aviation and its effects on local and global economy, local and global environmental effects [48].

Within AIM, the possibility exists to assess the impact of specified aircraft technologies on these factors. The AIM model time steps from 2015 until the supplied final year and balances supply and demand, while accounting for the interrelation between the local and global economic and environmental effects. A simulation in AIM of these factors will finish within several hours. Even tough the computational cost is not excessive for a comprehensive model as AIM, it is considered as too expensive to be used directly in the model in this work due to the severe impact on user-friendliness.

The feedback from aircraft performance on operational costs and air traffic demand is not incorporated in the model in this work. Apart from the increase in computational cost, it would require a larger set of input parameters from the user, further decreasing the user-friendliness. Therefore, the output of the AIM model is supplied as a database to the model in this work for the five Shared Socioeconomic Pathway scenarios (SSP). The SSP's are defined by the IPCC and represent five different scenarios with varying mitigation and adaptation challenges in reducing climate change, as shown in Figure 3.2 [31]. The SSP's set the parameters for global socio-economic development and in turn the development of the inter- and intraregional aviation sector. Selection of a different SSP scenario will edit the frequency and location of air traffic.

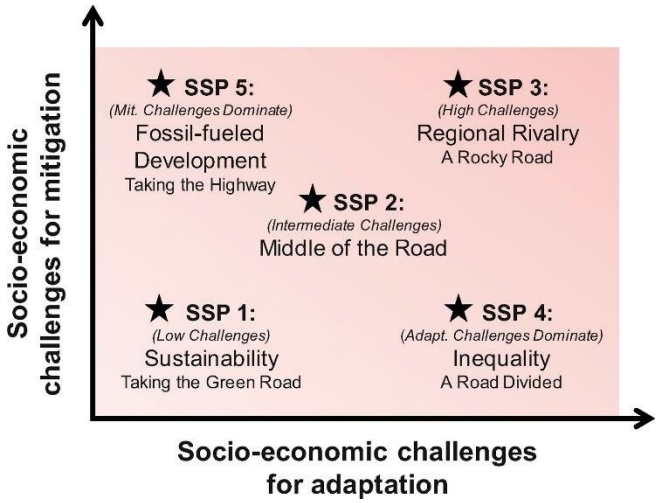

Figure 3.2: Chart visualising the representation of the five Shared Socioeconomic Pathways (image taken from Daigneault et al. [49])

Five databases corresponding to the five different SSP scenarios are obtained from the AIM model and serve as the flight data for this work. AIM allows the user to model specific aircraft technology or use an annual trend in aircraft fuel efficiency. A basic technical scenario of an annual 1.1% fuel economy increase is used for the database to reflect the general trend in aircraft performance as determined by Zheng et al. [12]. If a specific scenario is to be modelled which does not coincide with the five SSP scenarios, the AIM model can be run once with the specific input for that scenario, after which the output data set can be used in the model from this work to assess the influence on global emissions, energy requirements and fleet composition.

A brief summary of how demand and supply is assessed in the AIM model is provided in Section 3.2.1 and Section 3.2.2, as these serve as the base for the air traffic database in this model. For a more specific description of the mechanics of the model the reader is referred to the AIM documentation by Dray [30]. The data from the air traffic module has to be processed before it can be used as an input for the subsequent modules, for which the procedure is explained in Section 3.2.3.

3.2.1 Demand in the Aviation Integrated Model

The AIM model makes use of a gravimetric model to determine the demand between city pairs by use of Equation (3.1)[30].

$$ln(N_{od}) = \beta_0 + \beta_1 \cdot ln(P_o \cdot P_d) + \beta_2 \cdot ln(I_o \cdot I_d) + \beta_3 \cdot ln(f_{od} + vot \cdot t_{od}) + \sum_i \beta_i D^i_{od} \tag{3.1}$$

The variable N_{od} is the passenger demand between the origin and destination city. P are the respective populations of the metropolitan areas of the city, whereas I is the per capita household income. f is the route fare. vot and t are the passenger's value of time and travel time between the cities, respectively. β are the scaling coefficients of the parameters and D_i captures other factors of the connection between the two cities [30]. The gravimetric model is used to describe the "pull" between the points, in this case two cities. The coefficients β are determined through regression and control the relative "push" or "pull" effect of the parameter.

AIM has been validated by simulating the passenger demand between 2005 and 2015 where it was found that demand is within 10% of the actual demand per airport, except for several exceptions of Asian multi airport systems [50]. The subdivision between these airports is less accurately modelled, which leads to a difference in route length for flights arriving and departing from the multi airport cities. As the relative difference in travelled distance is small as compared to overall route distance, the inaccuracy is not considered to have a large impact on results of the model in this work.

3.2.2 Supply in the Aviation Integrated Model

In AIM, several procedures are performed to determine the supply. These consist out of an itinerary choice model, a fare model, an airport delay model and an aircraft size choice model. Each of these models interact directly or indirectly with the demand model. Therefore, in AIM the demand and supply are determined through iteration until supply and demand converge [30]. In this section the aircraft choice model is further

elaborated upon as the output is used directly in the model in this work. The aircraft choice model distributes demand on a route over the aircraft size categories. In AIM nine different aircraft size categories are used to represent the global fleet as listed in Table 3.1. For each aircraft size category a reference aircraft is defined to determine the aircraft performance, which will be further discussed in Section 3.3.

Size Category	Seat Range	Reference Aircraft
Small regional jet	30-69	Canadair CRJ 701
Large regional jet	70-109	Embraer 190 STD
Small narrowbody	110-129	Airbus A319
Medium narrowbody	130-159	Airbus A320
Large narrowbody	160-199	Boeing 737-800
Small twin aisle	200-249	Boeing 787-800
Medium twin aisle	259-299	Airbus A330-300
Large twin aisle	300-399	Boeing 777-300ER
Very large aircraft	400+	Airbus A380-800

Table 3.1: Aircraft size categories and reference aircraft from AIM. Table from Dray et al.[30]

The demand for a segment among the nine aircraft size categories is distributed in AIM through a multinomial logic Equation (3.2).

$$pr_{mns} = \frac{e^{U_{mns}}}{\Sigma_j e^{U_{mnj}}} \tag{3.2}$$

$$U_{mns} = \theta_0 + \theta_1 d_{mn} + \theta_2 h_m + \theta_3 h_n + \theta_4 N_{mn} + \theta_5 LF_{mn} + \theta_6 R_m + \theta_7 R_n + \theta_8 NLCC_{mn} + \theta_9 HHI_{mn}$$

The proportion of the demand filled by aircraft size category s on the route from airport m to airport n is represented by pr. j depicts the summation over all nine aircraft size categories. θ is the scaling parameter for the variables in the equation where d is the segment distance, h is a factor accounting for the hub status of an airport in review. N, LF and R are the number of passengers on the segment, the load factor and the longest runway length for the airports and segment, respectively. To account for specific aircraft preference by airlines, the number of low-cost carriers operating on the segment ($NLCC$) and airline passenger share (HHI) is included in the equation.

As the number of aircraft operating a route is calculated, the segment availability can be determined by the total available seats operating the segment. Dray et al. found the global fleet to be within 10% of the actual fleet for all size categories, except the small regional jet [50]. The fleet is underpredicted by 30% for this size category with the possible provided reasons for the discrepancy being constraints at small airports and airlines with limited capital which are not reflected in AIM [50].

The discrepancy is considered to be of a small effect on the model in this work, as flights are passed to a higher aircraft size category. As the passenger capacity of these aircraft is twice or more, the increase in the fleet numbers for these aircraft is limited. It is expected that the fuel and emissions output of the model is lower than when the small regional jet would be more accurately modelled. The increased capacity of the higher size category aircraft leads to fewer flights (at the same load factor), and as fuel consumption generally scales with a lower factor than capacity, the overall fuel consumption is reduced.

3.2.3 Flight data processing

The AIM model provides a database of flight data, but processing is required to use the data in the subsequent modules. The processing operations are discussed in this section and consist of formulating how the load factor is defined, adjustment of the segment distance for a non-optimal flight trajectory, determination of the payload mass, coupling the "to" and "from" route between a city pair and imposing the operational limitations set by the payload range diagram of the reference aircraft.

Non-optimal flight trajectory

The segment distance between two city pairs is defined as the great circle distance between the airports. AIM uses a ground track extension model to account for (lateral) routing inefficiencies as depicted in Figure 3.3. The method has been developed by Reynolds in 2009 by researching the relation between actual and flown flight

trajectories, who found a routing inefficiency of 13% on average for European A320 aircraft [51]. The relation between the actual distance flown and the great circle distance is provided by Equation (3.3).

$$d_{act,nm} = \mu_{1,r_n r_m} + \mu_{2,r_n r_m} d_{GC,nm} \tag{3.3}$$

d is the distance flown between airport n and m, μ are parameters which account for typical routing inefficiency within a region which is expressed by r [30]. Two lower limits are imposed on the actual distance flown: for routes less than 100 nautical miles, the flown distance is set to be 30% higher than the great circle distance. For routes with a great circle distance larger than 100 nautical miles, a lower limit is imposed of an 8% increase over the great circle distance if the regional inefficiencies resulted in an actual flight distance lower tan this distance.

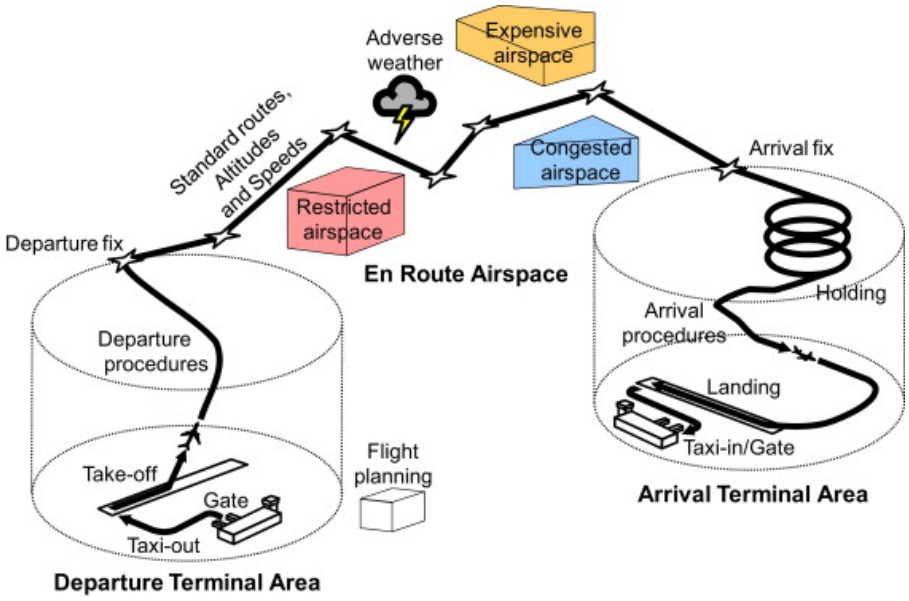

Figure 3.3: Image depicting causes for routing inefficiencies (image taken from Reynolds et al. [51])

Payload mass

The payload mass per flight is determined through two steps. First, the load factor from AIM is, as discussed in the preceding section, expressed as the amount of passengers on a flight as compared to the average seating capacity. By multiplying the average passenger payload mass ($m_{pax,ave} = 100kg$), the average seating capacity (S_{avg}) and the load factor (LF), the passenger payload mass on a flight ($m_{pl,pax}$) is determined as stated in Equation (3.4).

$$m_{pl,pax} = m_{pax,ave} \cdot S_{avg} \cdot LF \tag{3.4}$$

The belly freight mass is estimated from typical passenger-to-freight ratios $\%_{fr}$ for a region pair based on ICAO data by AIM [30]. The freight mass is added to the passenger mass to obtain the total payload mass as expressed in Equation (3.5). If the total payload mass is in excess of the maximum payload capacity of the reference aircraft, the freight payload mass is reduced to carry as much freight payload to fill the maximum payload capacity.

$$\begin{aligned} m_{pl,fr} &= m_{pl,pax} \cdot \%_{fr} \\ m_{pl,tot} &= m_{pl,pax} + m_{pl,fr} \end{aligned} \tag{3.5}$$

Segment pairs

The fleet activity module of the model in this work uses a procedure to ensure that aircraft that fly a segment from airport A to B, can not afterwards fly from airport C to D. The procedure ensures that aircraft fly the return flight as well to prevent the flight scheduler procedure to output an unfeasible flight schedule. The segment pairing procedure first provides each flight segment with a unique identifier. The second step is coupling each flight with the corresponding return flight in that year. For example, the route from airport A to B in year 2028 is coupled to the route from B to A in year 2028.

Payload range limitations

In AIM, two restrictions are imposed on aircraft: both the maximum payload capacity and maximum range for the reference aircraft can not be exceeded. The developers of AIM acknowledge that the payload range diagram for the reference aircraft has more limitations, such as the maximum take off weight (MTOW) and the maximum fuel weight (MFW). The maximum fuel weight is defined as the maximum fuel capacity the aircraft can carry, converted to weight by multiplying the volume by density. However, the argumentation by the developers of AIM is that the reference aircraft is representative of several aircraft with different MTOW and MFW, and that flights in excess of the payload range diagram of the reference aircraft are filled by aircraft which can operate with the specific weights [30].

When the model in this work would follow the same procedure, the performance model will restrict the flights outside the boundaries of the payload range diagram and the base case for the model can not be resolved. If the performance model would pass the flights, the results would impact the physical basis of the model, as the performance model has been developed and calibrated with payload and range combinations within the capabilities of the reference aircraft.

The adaptation of the flights that fall outside the boundaries of the payload range diagram is performed by conserving the total RTK of the segment. The payload range diagram for the Boeing 777-300ER can be found in Figure 3.4. The diagram shows that on average half the payload capacity is utilised on the aircraft, resulting in an average load factor of 0.5. For flights that exceed the payload range diagram, but lie before the point of MFW (marked by yellow in Figure 3.4), the flight frequency is increased. The total amount of payload carried on the segment by the aircraft size category is determined by multiplying the flight frequency (q) with the payload weight per flight by Equation (3.6). The total payload weight is divided by the maximum possible payload weight for the segment range as provided by the payload range diagram, and rounded up to determine the new flight frequency. Then, the total payload weight is divided by the new flight frequency to result with the new payload weight per flight.

$$\begin{aligned} m_{pl,tot} &= q \cdot m_{pl} \\ q_{new} &= \left\lceil \frac{m_{pl,tot}}{m_{pl,pos}} \right\rceil \\ m_{pl,new} &= \frac{m_{pl,tot}}{q_{new}} \end{aligned} \tag{3.6}$$

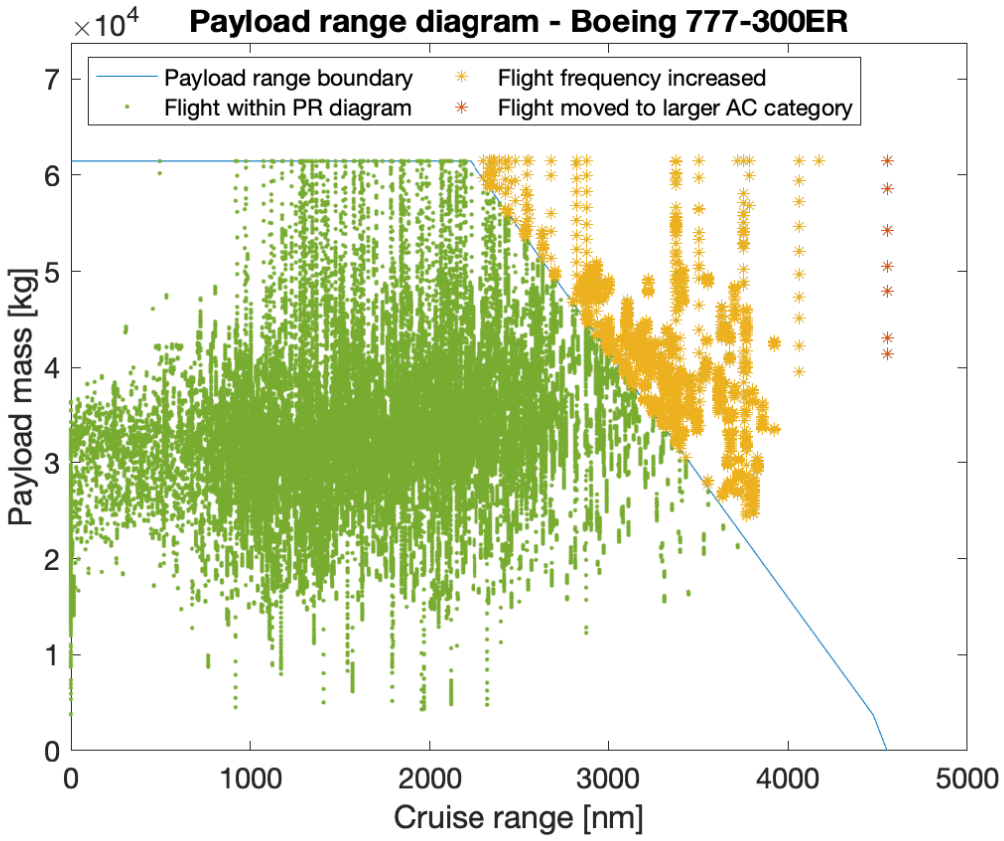

Figure 3.4: Payload range diagram including flight

Flights that are in excess of the MFW are scheduled to the next larger aircraft size category. An overview of the amount of routes that have an increased flight frequency or are rescheduled is provided in Table 3.2. Imposing the payload range boundaries on the flight data is most significant for the size categories four to eight.

Size category	**Increased flight frequency** [%]	**Mission to higher size category** [%]	**Total** [%]
1	0.07	0.00	0.07
2	0.00	0.01	0.01
3	0.01	0.06	0.07
4	1.15	0.38	1.52
5	1.67	3.25	4.90
6	0.92	0.00	0.92
7	3.60	0.00	3.60
8	3.45	0.01	3.45
9	0.37	0.00	0.37

Table 3.2: Relative amount of flights that are adapted to fall within the payload range diagram.

3.3 Performance model

In the performance model, the trends in aircraft technology are assessed on their impact in fuel and energy use. In this section the mechanics of the performance model are discussed. First, the performance model of AIM is discussed and the choice of how the performance model is constructed in this work is explained in Section 3.3.1. The manner in which the technology trends in the input parameters influence the performance model is elaborated upon in Section 3.3.2. The method of construction of the performance model and determination of fuel and energy usage per segment is presented in Section 3.3.4.

3.3.1 AIM performance model

The performance model in AIM uses an interpolation of Lissys Piano-X fuel usage data to obtain the fuel use of an aircraft segment combination [42]. Piano-X is constructed with performance parameters from aircraft manufacturers and is considered an accurate tool to estimate fuel consumption of aircraft. The interpolation is performed over the segment distance and payload load factor. As mentioned in Section 3.2.3 this process does not account for the payload range capability of the reference aircraft. The interpolation leads to Equation (3.7).

$$m_{f,sp} = \eta_{sp,0} + \eta_{sp,1} \cdot d + \eta_{sp,2} \cdot d \cdot LF_{pl} + \eta_{sp,3} \cdot d^2 + \eta_{sp,4} \cdot LF_{pl} + \eta_{sp,5} \cdot d^2 \cdot LF_{pl} \tag{3.7}$$

The variables in the equation are m_f for fuel mass per flight, where s refers to the aircraft category and p to the routes. η are the interpolated scaling variables used to factor the trajectory corrected segment distance d and the payload weight factor LF_{pl}.
The interpolation of the Piano-X data leads to quick and accurate results for aircraft that are similar to the reference aircraft. In order to model future technology in aircraft design AIM is equipped with two options.

One is an assumed annual fuel efficiency increase which is imposed on the fuel use equation. Imposing an annual fuel efficiency increase allows to resolve the impact of more efficient aircraft on the emissions of the aviation sector, but does not account for the required advances in technology to obtain the fuel use reduction.

The second option is by adding specific technology options and reviewing their effect on the individual missions segments. This is performed by discounting the fuel use for the mission segment. For example, aircraft with electric taxiing ability would be modelled by reducing the fuel use in the taxi segments by a specified amount. The downside of this way of modelling technological advances is that it requires high detail information of the effect on every mission segment.

The main reason for construction of the model in this work is the difference between the models in the way the performance is assessed. The model in this work is designed to determine the effect of advances in aircraft technology without specification of the exact technology and its influence on every stage in the aircraft mission. Instead, the model assesses the effect of future aircraft technology by using technology trends. In this way, the model allows for assessment of specific technology (by its effect on the trend) as well as the required advancement in a technology field for a change in the climate impact of the aviation sector.

3.3.2 Technology trends

The model in this work strives to assess the impact of technology trends in fuel usage and aircraft emissions. These technology trends are provided through the input parameters. The manner in which these input parameters are used to model the technology trends are discussed in this section.

Consumable fuel specific energy

The specific energy ($\frac{MJ}{kg}$) of the consumable fuel is provided by this parameter. This is set at $43.1 \frac{MJ}{kg}$ for jet A-1 fuel, but can be adapted to assess the effect of a change in jet fuel blend or fuel type. It should be noted that care has to be taken to assess the impact of a more drastic change to the propulsion system on the other performance parameters, such as structural and aerodynamic performance. The specific energy is used in the performance model, where it scales the required energy to travel a distance to a mass reduction. A higher specific energy of the fuel leads to lower mass required to fly the same distance and reduces overall fuel consumption.

Non-consumable fuel specific energy

The performance model allows for modelling of non-consumable or constant weight fuels, of which an example is electric batteries. Two input parameters are involved in modelling the specific energy of the constant weight fuel. The first input parameter is the specific energy in $\frac{Wh}{kg}$ in the base year. The second input parameter is the annual exponential growth in specific energy computed by Equation (3.8).

$$e_{f,c} = e_{f,c0} \cdot (1 + e_{f,c,inc})^t \tag{3.8}$$

The parameter $e_{f,c}$ is the specific energy in year t. $e_{f,c0}$ is the specific energy in the base year and $e_{f,c,inc}$ is the annual exponential growth. The trend is sampled in the design years where new aircraft enter the market. The trend is visualised in Figure 3.5 for a base year specific energy of $300\frac{Wh}{kg}$ and 3% yearly increase in constant fuel specific energy.

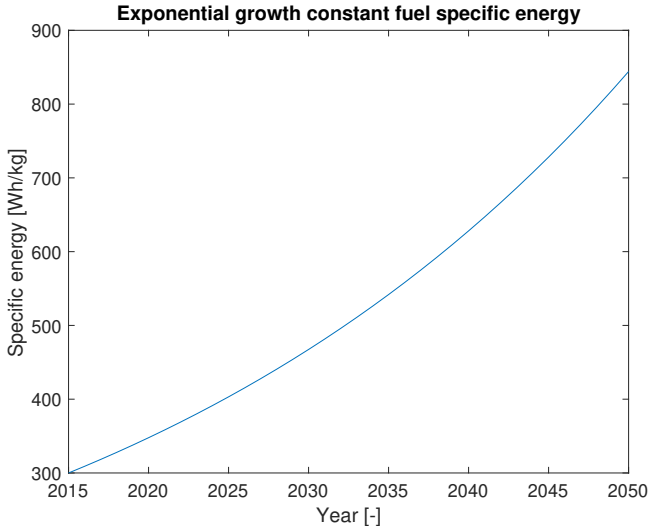

Figure 3.5: Specific energy trend for a base year specific energy of $300\frac{Wh}{kg}$ and 3% yearly increase in constant fuel specific energy.

Power share

The power delivered to the aircraft can be selected to be split in a range from zero to one, specifying the ratio of the total power to be delivered by the constant weight fuel. Setting the parameter to zero specifies all power to be delivered by consumable fuel, resulting in an aircraft with a conventional propulsion system. When a fully constant weight fuel aircraft is to be simulated, the power split variable Φ is set to one.

The power split ratio can be chosen to be modelled in two ways: constant power split through all aircraft generations or a step wise increase per generation. In either option, Φ_0 sets the power share ratio for the first new aircraft generation. If Φ_{step} is set at one, subsequent aircraft generation design will have Φ increased with Φ_{inc} per generation. Setting Φ_0 at 0.25 with a step wise increase of $\Phi_{step} = 0.25$ and designing four new aircraft generations with constant weight power splits of 0.25, 0.5, 0.75 and 1.0 for aircraft generation one, two, three and four, respectively.

Propulsive efficiency

The propulsive efficiency is modelled by Equation (3.9), which is asymptotic in 1. The initial propulsive efficiency is specified by the input parameter $\eta_{p,0}$. The difference between the initial propulsive efficiency is provided by subtracting the ideal efficiency (1) with the initial propulsive efficiency. The scaling parameter k controls the pace in which the exponent approaches zero, and in turn the pace in which propulsive efficiency approaches the ideal efficiency level of one. The trend (visualised in Figure 3.6) is added to allow the user to model propulsive technology such as counter rotating open rotor engines, but should be set at low values for a realistic trend.

$$\eta_p = \eta_{p,0} + (1 - \eta_{p,0}) \cdot (1 - e^{-t \cdot k}) \tag{3.9}$$

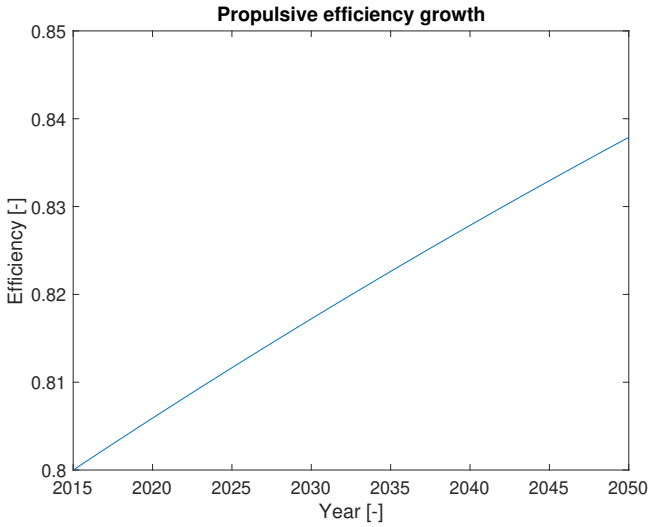

Figure 3.6: Propulsive efficiency trend for a base year propulsive efficiency of 80% and $k = 0.006$ yearly increase in constant fuel specific energy.

Aerodynamic efficiency

The initial aerodynamic efficiency of the reference aircraft has been determined from Piano-X data, and are contained within the model in this work. The annual increase of aerodynamic efficiency ($LD_inc = 0.8\%$) is modelled by an exponential growth equation in the same manner as the constant fuel specific energy. The formula used is listed in Equation (3.10).

$$LD = LD_0 \cdot (1 + LD_{inc})^t \tag{3.10}$$

Structural efficiency

The structural efficiency is modelled by an annual decrease in operative empty weight (OEW). A decrease in operative empty weight, when all other weights are unchanged, leads to lower mass for the same mission and therefore to lower fuel usage. This process is performed by Equation (3.11). The parameter OEW_{inc} in the denominator depicts the increase in efficiency such that positive trend in efficiency results in a decrease of operation empty weight.

$$OEW = \frac{OEW_0}{(1 + OEW_{inc})^t} \tag{3.11}$$

3.3.3 Performance model parameters

The performance parameters for the nine reference aircraft are required for the base aircraft and to model the design trends for future generations of aircraft. The data is obtained from Piano-X data containing the fuel use for payload and range combinations. The aircraft used from the Piano-X model are listed in Table 3.3.

Size Category	Seat Range	Reference Aircraft	Piano-X Aircraft
Small regional jet	30-69	Canadair CRJ 701	Canadair CRJ 701
Large regional jet	70-109	Embraer 190 STD	Embraer 190 STD
Small narrowbody	110-129	Airbus A319	A319-131 75t
Medium narrowbody	130-159	Airbus A320	A320-214 77t
Large narrowbody	160-199	Boeing 737-800	B737-800 NG (172)
Small twin aisle	200-249	Boeing 787-800	B787-8 (baseline v 10)a
Medium twin aisle	259-299	Airbus A330-300	A330-300 242t p
Large twin aisle	300-399	Boeing 777-300ER	B777-300 ER (700)
Very large aircraft	400+	Airbus A380-800	A380-861 (uae1)

Table 3.3: Aircraft groups and reference aircraft data from Piano-X. Aircraft groups and size classes taken from Dray et al.[30]

The model used in this work for the performance model is based on the Breguet range equation. To ensure that the models simulate the same mission, input parameters were taken or derived from Piano-X data to be used in the performance data estimation. An overview of these parameters is shown in Table 3.4.

Variable	Source	Variable	Source
W_{pl}	Input	$\frac{L}{D}_{Cr}$	Piano-X
R_{Bl}	Input	$\frac{L}{D}_{De}$	Piano-X
$W_{f,FL}$	Piano-X	R_{Cl}	Piano-X
W_{TO}	Piano-X	R_{Cr}	Piano-X
$W_{f,TaxiOut}$	Piano-X	R_{De}	Piano-X
$W_{f,Climb}$	Piano-X	M_{Cr}	Piano-X
$W_{f,Cruise}$	Piano-X	h_{Cr}	Piano-X
$W_{f,Descent}$	Piano-X	R_{Div}	Piano-X
$W_{f,Block}$	Piano-X	E_{Loi}	Piano-X
$W_{f,Reserve}$	Piano-X	$\%_{Con}$	Piano-X
$\frac{L}{D}_{Cl}$	Piano-X		

Table 3.4: Input parameters for the fuel weight determination

The Breguet range equation is shown in Equation (3.12) [35]. The equation describes the relation between the range an aircraft is able to fly in steady horizontal flight, depending on propulsive, aerodynamic and structural performance parameters in combination with the payload. R depicts the range in meters. η_{gt} and η_p are the non-dimensional gas turbine and propulsive efficiency, respectively. The non-dimensional aerodynamic efficiency is depicted by $\frac{L}{D}$. e_f represents the energy density of the fuel (Jet-A1 equals $43.1 MJkg^{-1}$), whereas g equals the gravitational acceleration ($g = 9.81 ms^{-2}$). The initial and final weight of the aircraft in Newton is represented by W_i and W_f, respectively.

$$R = \eta_{gt} \cdot \eta_p \cdot \left(\frac{L}{D}\right) \cdot \left(\frac{e_f}{g}\right) \cdot ln\left(\frac{W_i}{W_f}\right) \tag{3.12}$$

The initial and final weight can be further specified by use of Equation (3.13). As the operative empty weight (W_{OE}) and payload weight (W_{PL}) remain constant during commercial flight, the difference between the initial and final weight is the amount of fuel (W_f) burned during the mission segment.

$$\begin{aligned} W_i &= W_{OE} + W_{PL} + W_{f,i} \\ W_f &= W_{OE} + W_{PL} + W_{f,f} \\ W_i - W_f &= W_{OE} + W_{PL} + W_{f,i} - W_{OE} - W_{PL} - W_{f,f} = W_{f,i} - W_{f,f} = \Delta W_f \end{aligned} \tag{3.13}$$

The fuel burned can be further subdivided per mission segment as shown in Equation (3.14). After each mission segment the weight is reduced by the fuel burned during that segment, except for the reserve fuel.

$$W_{f,total} = W_{f,ESW} + W_{f,Ta} + W_{f,TO} + W_{f,Cl} + W_{f,Cr} + W_{f,De} + W_{f,Ldg} + W_{f,Taxi} + W_{f,Res} \tag{3.14}$$

The reserve fuel is composed of three components as shown in Equation (3.15). The divergence fuel is carried to be able to cruise to an alternate destination. The loiter fuel is carried to have adequate fuel when an aircraft is put into a holding pattern awaiting to continue the mission. The contingency fuel is carried to overcome for other than planned cruise conditions.

$$W_{f,Res} = W_{f,Div} + W_{f,Loi} + W_{f,Con} \tag{3.15}$$

The Breguet range equation is valid for steady, horizontal flight which occurs during the phases in which the cruise, reserve and loiter fuel is burned. A common way to resolve the required fuel for the other flight phases is by use of weight or fuel fractions. An empirically determined ratio of the initial and final weight over a flight phase is used to specify the fuel used in the relevant flight phase ($\frac{W_i}{W_f}$). Table 3.5 contains values for the fuel fractions as determined by Roskam in 1989 [36].

In the performance model in this work, the fuel fractions were updated to correspond to the aircraft performance found in the Piano-X data. This resulted in new fuel fractions for the climb and descent phases as listed in Table 3.5. It was found that the fuel usage for the engine warm up, taxi, take off and landing, taxi and shutdown phase are modelled by setting the engine to a standard engine setting. This made the fuel usage independent of the payload weight. As the engine size depends on the thrust to weight ratio of the aircraft, the fuel usage during these flight phases was defined as a fraction as compared to the maximum take off weight (MTOW) as illustrated by Equation (3.16).

Segment	**Roskam**	**Size category**								
	1-9	1	2	3	4	5	6	7	8	9
Engine start, warm-up (ESW)	0.990	6.5e-4	6.2e-4	6.1e-4	7.1e-4	4.8e-4	4.8e-4	4.2e-4	3.1e-4	4.4e-4
Taxi (Ta)	0.990	6.5e-4	6.2e-4	6.1e-4	7.1e-4	4.8e-4	4.8e-4	4.2e-4	3.1e-4	4.4e-4
Take-off (TO)	0.995	6.0e-4	6.2e-4	5.7e-4	6.0e-4	6.0e-4	4.7e-4	5.5e-4	5.5e-4	3.2e-4
Climb (Cl)	0.980	0.973	0.973	0.979	0.978	0.977	0.983	0.980	0.984	0.980
Descent (D)	0.990	0.997	0.997	0.996	0.996	0.996	0.998	0.998	0.997	0.997
Landing, taxi, shutdown (LTS)	0.922	8.8e-4	8.2e-4	8.1e-4	9.5e-4	9.6e-4	4.7e-4	4.7e-4	6.1e-4	8.8e-4

Table 3.5: Overview of the fuel fractions as specified by Roskam [36] and updated fuel fractions including MTOW fraction fuel weights for mission segments.

$$W_{f,FP} = \frac{MTOW}{f_{FP}} \tag{3.16}$$

At the start of the mission an aircraft carries all fuel weights in Equation (3.14), but during a regular mission the fuel burned ($W_{f,block}$) consists of the fuel weights shown in Equation (3.17).

$$W_{f,total} = W_{f,Taxi} + W_{f,To} + W_{f,Clb} + W_{f,Cr} + W_{f,Des} + W_{f,Ldg} + W_{f,Taxi} = W_{f,Block} \tag{3.17}$$

As fuel is consumed during the flight, the weight of the aircraft decreases during the flight. By use of equation Equation (3.14) the weight at the start of each flight phase can be defined. These weights are shown in Equation (3.18) to Equation (3.25).
At the gate before the engine is started and the aircraft is taxied to the runway, the aircraft weight is equal to Equation (3.18).

$$W_{Start} = W_{OE} + W_{PL} + W_{f,Taxi} + W_{f,To} + W_{f,Clb} + W_{f,Cr} + W_{f,Des} + W_{f,Ldg} + W_{f,Taxi} + W_{f,Res} \tag{3.18}$$

Before take-off, the startup and taxi fuel is consumed, and the weight is reduced to Equation (3.19).

$$W_{To} = W_{OE} + W_{PL} + W_{f,To} + W_{f,Clb} + W_{f,Cr} + W_{f,Des} + W_{f,Ldg} + W_{f,Taxi} + W_{f,Res} \tag{3.19}$$

After the take-off is performed the weight and the aircraft starts the climb segment the weight is expressed by Equation (3.20).

$$W_{Clb} = W_{OE} + W_{PL} + W_{f,Clb} + W_{f,Cr} + W_{f,Des} + W_{f,Ldg} + W_{f,Taxi} + W_{f,Res} \tag{3.20}$$

At the start of the cruise segment the weight of the aircraft can be determined by Equation (3.21).

$$W_{Cr} = W_{OE} + W_{PL} + W_{f,Cr} + W_{f,Des} + W_{f,Ldg} + W_{f,Taxi} + W_{f,Res} \tag{3.21}$$

After the cruise segment and before descent is initiated the aircraft weight equals Equation (3.22).

$$W_{De} = W_{OE} + W_{PL} + W_{f,Des} + W_{f,Ldg} + W_{f,Taxi} + W_{f,Res} \tag{3.22}$$

As the landing is initiated the aircraft weight is expressed by Equation (3.23).

$$W_{Ldg} = W_{OE} + W_{PL} + W_{f,Ldg} + W_{f,Taxi} + W_{f,Res} \tag{3.23}$$

After touchdown the aircraft starts taxiing toward the gate with a weight equal to Equation (3.24).

$$W_{Taxiin} = W_{OE} + W_{PL} + W_{f,Taxi} + W_{f,Res} \tag{3.24}$$

On arrival at the gate and the engines are shutdown the final aircraft weight is composed of Equation (3.25).

$$W_{Final} = W_{OE} + W_{PL} + W_{f,Res} \tag{3.25}$$

The Breguet Equation (3.12) can be rewritten to isolate the equation for the consumed fuel during the flight phase as shown in Equation (3.26).

$$\begin{aligned} W_f &= (e^B - 1) \cdot (W_{FP}) \\ B &= \frac{R \cdot g}{\eta_{gt} \cdot \eta_p \cdot e_f \cdot \frac{L}{D}_{FP}} \end{aligned} \tag{3.26}$$

Implementation of Breguet model

To be able to define the aircraft weight at every mission segment the aircraft operational empty weight has to be derived from the Piano-X data. The empty weights are determined subtracting the payload and fuel weight from the aircraft take off weight by Equation (3.27) and are listed in Table 3.6.

$$W_{OE} = W_{TO} - W_{PL} - W_{FL} \tag{3.27}$$

Aircraft	**OEW (kg)**
Canadair CRJ 701	19.731
Embraer 190 STD	27.720
Airbus A319	41.771
Airbus A320	42.666
Boeing 737-800	41.413
Boeing 787-800	122.198
Airbus A330-300	130.400
Boeing 777-300ER	168.781
Airbus A380-800	301.100

Table 3.6: Overview of aircraft OEW

From the aircraft operative empty weight, the consumed fuel during every mission segment can be determined. This requires definition of two aircraft missions: the regular aircraft mission and the aircraft mission including reserve segments. The regular mission consist of the aircraft flying from airport A to airport B, as illustrated by Figure 3.7.

Reserve fuel is carried by the aircraft, as it should be able to account for unperceived alterations to the planned mission. To determine the amount of reserve fuel required, a mission including the aircraft's additional segments is defined. The amount of fuel loaded unto the aircraft is the fuel required to fly this mission as illustrated by Figure 3.8. The extra fuel weight loaded to fly segment five up and till segment nine compose the aircraft reserve fuel.

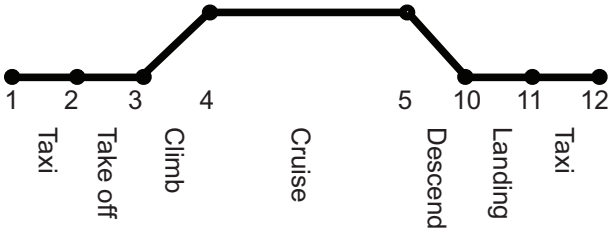

Figure 3.7: Regular aircraft mission from airport A to airport B

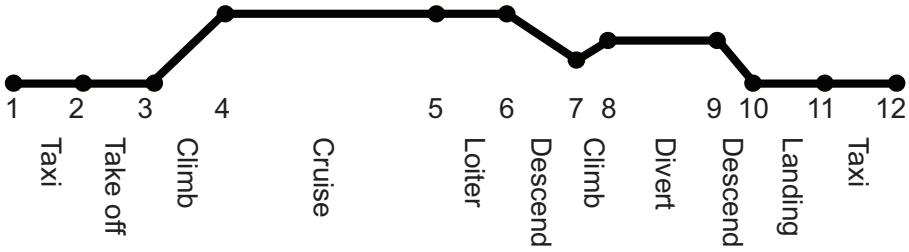

Figure 3.8: Aircraft mission with reserve fuel segments

By use of fuel fractions, the aircraft weight at station nine can be determined. First the aircraft mass zero fuel weight (W_{ZF}) is determined by adding the payload weight (W_{PL}) to the operative empty weight (W_{OE}) as shown by Equation (3.28).

$$W_{ZF} = W_{OE} + W_{PL} \tag{3.28}$$

The fuel fractions from Roskam can be used to determine the weights between station nine and twelve by use of Equation (3.29) and Equation (3.31) [36]. For the landing and descent phase the contingency fuel is added to the aircraft. The contingency fuel is expressed as a percentage of the segment fuel as shown in Equation (3.30).

$$W_{10} = \frac{W_{12}}{ff_{LTS}} \tag{3.29}$$

$$W_{10c} = W_{10} + (W_{10} - W_{11}) \cdot \%_{con} \tag{3.30}$$

$$W_9 = \frac{W_{10c}}{ff_{Descend}} \tag{3.31}$$

$$W_{9c} = W_9 + (W_9 - W_{10c}) \cdot \%_{con} \tag{3.32}$$

In the diversion segment, the aircraft cruises towards a different destination airport for which the distance has been predefined. The diversion distance, loiter time and contingency fuel percentage for the reference aircraft are listed in Table 3.7. The Breguet range equation is then used to determine the fuel fraction for the diversion segment by Equation (3.33).

The diversion distance is set at 200 nautical miles or 370.2 km as reported by typical for international missions by Airbus and Zheng et al. [52][12]. The values for loiter time and contingency fuel are stipulated by the ICAO in Annex 6 and are equal to 30 minutes and five percent, respectively [53].

Size category	**Diversion distance (km)**	**Loiter time (minutes)**	**Contingency fuel (%)**
1-9	370.2	30	5

Table 3.7: Overview of aircraft reserve parameters based on typical diversion distance as reported by Airbus and loiter and contingency fuel specified by the ICAO [52][53],

$$\begin{aligned} B &= \frac{R_{Divert} \cdot g}{\eta_{Cruise} \cdot e_f \cdot \frac{L}{D}_{Cruise}} \\ ff_{Divert} &= e^B \\ W_8 &= \frac{W_{9c}}{ff_{Divert}} \end{aligned} \tag{3.33}$$

The aircraft weight at station six is determined by the use of a series of fuel fractions as shown by Equation (3.34) and Equation (3.35).

$$W_7 = \frac{W_8}{ff_{Climb}} \tag{3.34}$$

$$W_6 = \frac{W_7}{ff_{Descend}} \tag{3.35}$$

The loiter phase is part of the reserve fuel segments and occurs if an aircraft has to wait for e.g. a landing slot. As aircraft are flown to maximise endurance instead of range in the loiter phase, the aircraft is operated at different settings which leads to different values for the propulsive and aerodynamic efficiency. The loiter equation is shown in Equation (3.36).

$$E = \frac{R}{V} = \eta_{gt} \cdot \eta_p \cdot \left(\frac{L}{D}\right) \cdot \left(\frac{e_f}{g \cdot V}\right) \cdot ln\left(\frac{W_i}{W_f}\right) \tag{3.36}$$

The loiter distance is determined by multiplying the loiter duration by the loiter speed as shown in Equation (3.37).

$$\begin{aligned} R_{Loiter} &= E \cdot V_{Loiter} \\ B &= \frac{R_{Loiter} \cdot g}{\eta_{Cruise} \cdot e_f \cdot \frac{L}{D}_{Cruise}} \\ ff_{Loiter} &= e^B \\ W_5 &= \frac{W_6}{ff_{Loiter}} \end{aligned} \tag{3.37}$$

The aircraft weight at station four is determined by the Breguet range equation for the cruise phase as shown in Equation (3.38), where the cruise distance is taken from the Piano-X data.

$$\begin{aligned} B &= \frac{R_{Cruise} \cdot g}{\eta_{Cruise} \cdot e_f \cdot \frac{L}{D}_{Cruise}} \\ ff_{Cruise} &= e^B \\ W_4 &= \frac{W_5}{ff_{Cruise}} \end{aligned} \tag{3.38}$$

$$W_{4c} = W_4 + (W_4 - W_5) \cdot \%_{con} \tag{3.39}$$

Through a series of fuel fractions the aircraft weight at station zero can be determined as shown in Equation (3.40) to Equation (3.44).

$$W_3 = \frac{W_{4c}}{ff_{Climb}} \tag{3.40}$$

$$W_{3c} = W_3 + (W_3 - W_{4c}) \cdot \%_{con} \tag{3.41}$$

$$W_2 = \frac{W_{3c}}{ff_{TakeOff}} \tag{3.42}$$

$$W_{2c} = W_2 + (W_2 - W_{3c}) \cdot \%_{con} \tag{3.43}$$

$$W_1 = \frac{W_{2c}}{ff_{Taxi}} \tag{3.44}$$

$$W_0 = \frac{W_1}{ff_{StartUp}} \tag{3.45}$$

By resolving Equation (3.29) to Equation (3.44) the aircraft weight at the start of the mission can be determined. The unknown parameter η is the equivalent cruise efficiency.

Error minimisation

Using the Breguet range equation to resolve the consumed fuel weight per flight phase requires knowledge of the propulsive, aerodynamic and structural efficiency. These are supplemented by the mission parameters consisting of payload weight and block range. The aerodynamic, structural and mission parameters are obtained from the Piano-X data to ensure that every model is run with the same input parameters.

Piano-X does not provide the propulsive efficiency parameters. In order to run the model initial parameters are assumed of 0.38 and 0.8 for the gas turbine and propulsive efficiency, respectively. The model assumes an equivalent overall efficiency for the propulsion efficiencies resulting in $\eta_{eq} = 0.3040$. With the initial value for the equivalent efficiency, the model can be run, and the overall efficiency can be optimised to minimise the Normalised Root Mean Square Error (NRMSE) between fuel consumption data per flight phase. First the Root Mean Square Error (RMSE) is determined using Equation (3.46). The NRMSE is then determined by normalising the RMSE with the average fuel weight value in the flight phase Equation (3.47).

$$RMSE = \sqrt{\frac{\sum_i^n (\hat{y} - y)^2}{n}} \tag{3.46}$$

$$NRMSE = \frac{RMSE}{\bar{y}} \tag{3.47}$$

The optimisation is performed by constraining the efficiency value per flight phase to lie between zero and one. The gas turbine and propulsive efficiency are unknown and are represented by an overall efficiency, η which is determined by minimising the root-mean-square error between the data sets. The overall efficiency depends on a range of parameters such as engine type, air density and airspeed. As Piano-X is developed with manufacturers and fuel usage data from airlines, the minimisation of the root-mean-square error as compared to the Piano-X data set will result in an overall efficiency which resembles the way aircraft are operated.

Determination of η

The root-mean-square error and the performance parameters from the optimisation are presented in Table 3.8 to Table 3.9, respectively. The normalised-root-mean-square and R^2 accuracy parameters are listed in Appendix B. The best fit of the model is found in the determination of the cruise fuel, block fuel and take off weight which can be found in Figure 3.9 and Figure 3.10. As the Breguet model is valid in steady, horizontal flight, it would be expected that the performance of the model in determining these weights is accurate. This is confirmed by the R^2 values close to one and the low NRMSE for the flight phases. The higher take off mass for the B737-800 NG is listed in Figure 3.9 and is equal to 960 kilograms.

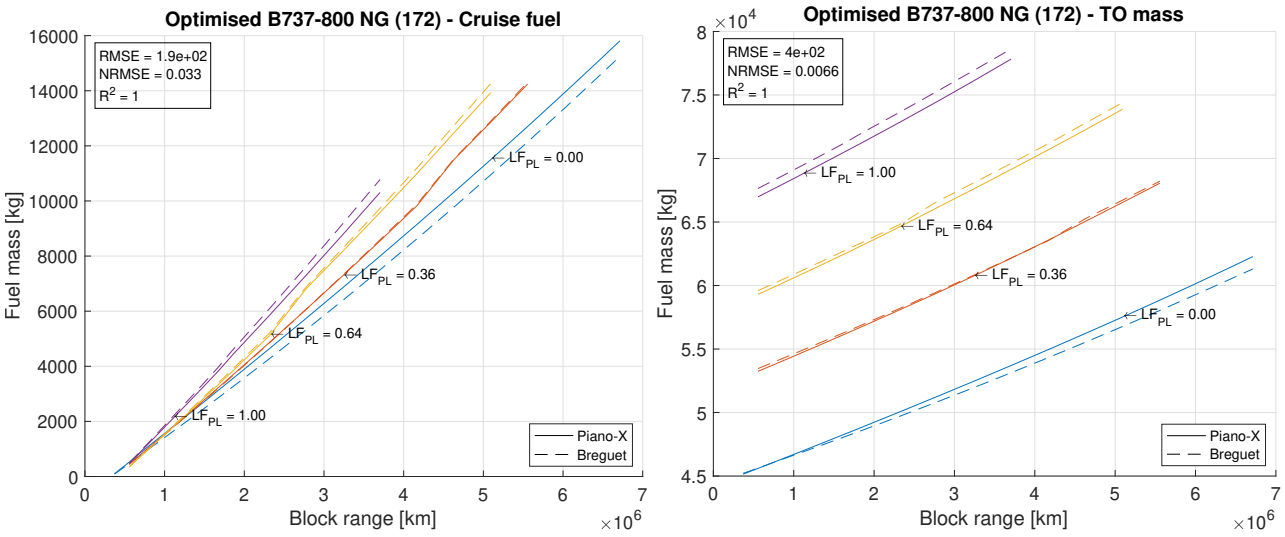

Figure 3.9: Cruise fuel mass and take off mass for the Boeing 737-800 NG from Piano-X and the model in this work for four payload load factors ranging from zero to 1.

The higher take off mass (neglecting required fuel is equivalent to ten extra passengers) has an impact on the determined overall propulsive efficiency. The higher take off weight will cause the overall propulsive efficiency to be higher. The fuel masses used in the optimisation are constant, so with an increased mass at take off, the overall propulsive efficiency increases to result in the same fuel burn. Usage of the Breguet model is expected to result in a difference in fuel mass estimation due to the simpler manner of modelling an aircraft mission. The optimisation used in the model in this work incurs a decreased modelling error due to the Breguet model as reported in literature on Breguet range estimation by Bovet et al. [37]. As the Breguet model allows for modelling of a larger set of technology options, the modelling error is accepted.

	Climb	Cruise	Descent	Block	Reserve	TO weight
Canadair CRJ 701	46	140	6	188	418	430
Embraer 190	60	250	8	315	544	550
A319-131	78	234	19	302	281	417
A320-214	95	213	17	312	182	363
B737-800 NG	85	192	17	371	448	438
B787-8	78	553	22	688	952	1075
A330-300	134	382	22	586	1474	1385
B777-300 ER	168	367	45	859	1361	1224
A380-861	458	728	53	1340	2972	2788

Table 3.8: Root mean square error for model optimisation.

The climb, descent and reserve fuel determination encounter lower modelling accuracy. The R^2 modelling accuracy parameter is negative for the reserve and descent fuel estimation. A negative value for R^2 is encountered when the residual is larger than the difference between the mean of the target variables to the target variables. This indicates a poor relation between the modelling variables and output variable.

For the climb and descent phases, the modelling error is caused by the difference between the model used in Piano-X and the model in this work. Piano-X models the entire flight trajectory of the aircraft, which results in discontinuous steps in these phases as illustrated in Figure 3.11. The method of fuel fractions models the

fuel usage in these phases as continuous, which leads to reduced modelling performance. The performance is increased by the fuel fraction update with Piano-X fuel data and the absolute difference is small as compared to the block fuel as shown in the root-mean-square table in Table 3.8.

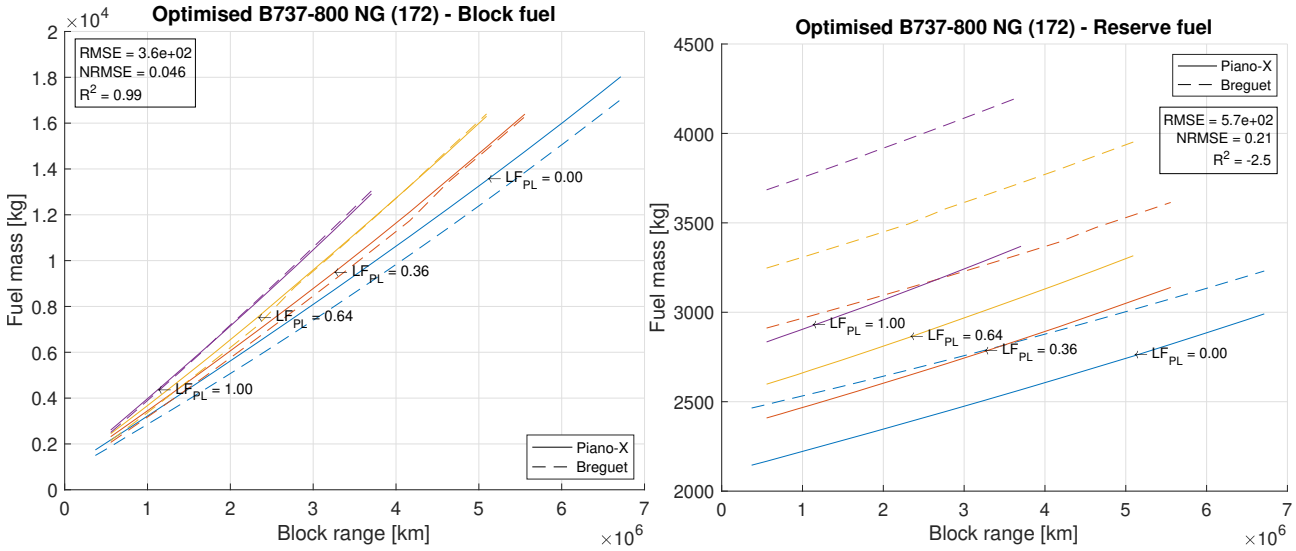

Figure 3.10: Block and reserve fuel mass for the Boeing 737-800 NG from Piano-X and the model in this work for four payload load factors ranging from zero to 1.

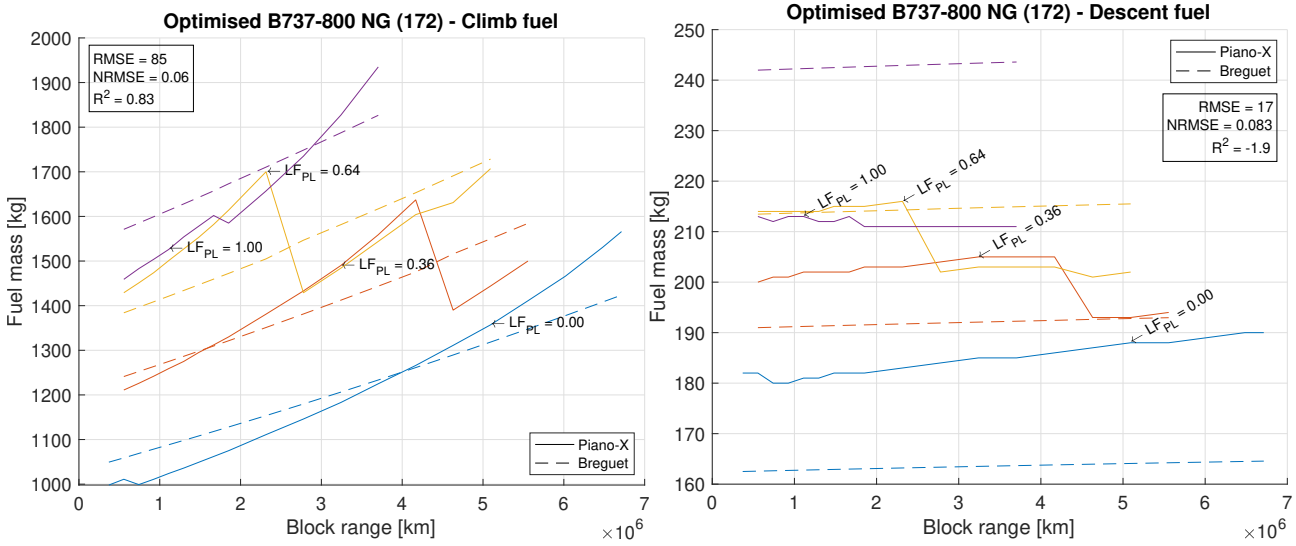

Figure 3.11: Climb and descent fuel mass for the Boeing 737-800 NG from Piano-X and the model in this work for four payload load factors ranging from zero to 1.

The result of the optimisation for the fuel fractions for the climb and descent phase and the overall propulsive efficiency are listed in Table 3.9. The fuel fractions for the climb and descent phases are situated around the values provided by Roskam (0.980 for climb and 0.990 for descent) [36]. For the descent phase, the fuel fraction by Roskam indicates higher fuel consumption (the fuel fractions are higher).
With increasing aircraft size category, the overall propulsive efficiency increases. The widebody aircraft operate with engines with an increased bypass ratio over the narrowbody aircraft, explaining the increase in overall propulsive efficiency.

	ff_{cl} [−]	η_{cr} [−]	ff_{de} [−]
Canadair CRJ 701	0.9729	0.2439	0.9968
Embraer 190	0.9732	0.2498	0.9967
A319-131	0.9794	0.3081	0.9961
A320-214	0.9775	0.2988	0.9964
B737-800 NG	0.9768	0.2857	0.9963
B787-8	0.9827	0.3831	0.9977
A330-300	0.9798	0.3425	0.9977
B777-300 ER	0.9840	0.3566	0.9974
A380-861	0.9797	0.3586	0.9971

Table 3.9: Performance parameters for model optimisation.

The reserve fuel weight is inaccurately modelled through the Breguet equation as illustrated in Figure 3.10. The performance model used in this work is developed to be as accurate as possible at acceptable computational cost and user-friendliness of the model. Therefore, single performance parameters are used for the aerodynamic and overall propulsive efficiency, these inaccurately reflect the loiter phase which is performed at a lower flight level. The parameters are altered by operation on a lower flight level and lead to increased fuel usage.

A sensitivity analysis has been performed to determine the influence on the overall fuel consumption in the other flight phases and determined the effect is limited. The sensitivity analysis is presented in Table 3.10 where it is shown that, except for the reserve fuel weight, the difference in fuel and take off mass with the exact reserve fuel mass is less than one percent. The remainder of the difference between the results from Piano-X can be explained by the higher detail in which a flight mission is modelled in Piano-X. Piano-X models step wise climbing in the cruise altitude as the aircraft decreases weight. As the weight of the aircraft decreases, the altitude at which the highest fuel efficiency is obtained increases. The model in this work assumes constant parameters throughout the flight mission.

	$\Delta Climb$	$\Delta Cruise$	$\Delta Descent$	$\Delta Block$	$\Delta Reserve$	$\Delta TOweight$
Canadair CRJ 701	0.0002	0.0018	0.0015	-0.0007	0.3539	0.0097
Embraer 190	-0.0002	0.0017	0.0014	-0.0003	0.3746	0.0076
A319-131	-0.0008	0.0032	0.0025	0.0012	0.1008	0.0033
A320-214	-0.0007	0.0037	0.0029	0.0046	0.0618	0.0025
B737-800 NG	0.0006	0.0029	0.0020	0.0027	0.1627	0.0030
B787-8	-0.0008	0.0017	-0.0003	0.0013	0.1685	0.0030
A330-300	-0.0008	0.0035	0.0010	0.0020	0.2304	0.0055
B777-300 ER	-0.0014	0.0039	0.0013	0.0011	0.1655	0.0029
A380-861	0.0025	0.0011	-0.0002	0.0024	0.2610	0.0051

Table 3.10: NRMSE sensitivity to reserve fuel of the Boeing 737-800 NG.

Verification and validation of Piano-X data

Piano-X performance results have been verified for the AERO2k project by Eyers et al. in [54]. For the AERO2k project, Piano trip fuel results were compared to fuel determined by flight planning tools of British Airways and Virgin. As compared to the trip fuel determined by British Airways, on average, Piano underestimated the trip fuel by 2.3%. The data from the Virgin flight planner differed on average by 3%. For several aircraft larger deviations exist, which were considered to be caused by a different configuration of aircraft model in Piano such as different engines.

Eyers et al. validated the results from Piano to the fuel requirements determined from airline operational data. The airline operational data was for an aircraft which was operated on a multitude of routes for short haul as well as long haul (aircraft type and operator are unknown due to commercial sensitivity). The performance data from Piano was found to underestimate fuel consumption by 2.23%. The R^2 value for the Piano data as compared to operational flight data was determined to be 0.997 [54].

The main reasons for deviation between the data from the flight planners and airline operational data was thought to be difference between aircraft configuration between the airlines and Piano. The deviation caused by the modelling difference is considered to be of minor effect on the performance in this work. As the reference aircraft represents a range of aircraft the goal of the model is not reflecting a specific aircraft configuration, but the average of the fleet in the size category, the error due to modelling difference in configuration is of less effect.

3.3.4 Performance model mechanics

The design parameters discussed in the preceding section are used to determine the fuel and energy use on every aircraft and relevant route combination. The performance model is run for per aircraft generation per aircraft type. The design parameters are imported from the aircraft design module and the segment parameters from the flight data module. Afterwards, the procedure to determine the fuel mass is explained step by step in the following paragraphs.

Cruise distance

As a first step the cruise distance has to be determined from the block distance and payload weight factor. This is performed by an interpolation for the cruise distance over the block range and block distance, resulting in Equation (3.48).

$$d_{cr} = \zeta_0 + \zeta_{1,s} \cdot d_{bl} + \zeta_{2,s} \cdot LF_{PL} + \zeta_{3,s} \cdot d_{bl} \cdot LF_{PL} \tag{3.48}$$

The fit of the linear interpolation results in a high accuracy fit as shown in Table 3.11. The values for R^2 are close to one, the normalised-root-mean-square error is on average less than one percent for all aircraft and the root-mean-square error is less than fifteen nautical miles at its maximum. Considering the discontinuous distances found in the climb and descent phases, the performance of the cruise distance interpolation is considered accurate enough to be used in the performance model. This is caused due to the cruise distance making up a large share of the block distance as compared to the climb and descent phases.

Size category	R^2 [-]	NRMSE [-]	RMSE [nm]
1	0.999	0.013	13.4
2	0.999	0.012	13.92
3	0.999	0.001	9.67
4	0.999	0.011	13.87
5	0.999	0.013	14.66
6	0.999	0.003	8.00
7	0.999	0.005	10.96
8	0.999	0.003	5.90
9	0.999	0.003	7.96

Table 3.11: Model fit parameters for the cruise distance interpolation.

Iteration non-consumable fuel

In order to model aircraft that operate with a power split over a consumable and non-consumable fuel, the Breguet equation has to be modified. De Vries et al. have derived the Breguet equation (shown in Equation (3.49)) for an aircraft with constant power split between the constant and depleting weight energy sources (in their case fuel and battery electric hybrid) [35]. It is able to account for different layouts of the hybrid propulsion system.

$$R = \eta_p \cdot \left(\frac{e_f}{g}\right) \cdot \left(\frac{L}{D}\right) \cdot \left(\eta_{gt} + \eta_{em} \cdot \frac{\phi}{1-\phi}\right) \cdot ln\left(\frac{W_{OE} + W_{PL} + \frac{g}{e_{bat}} \cdot E_{0,tot} \cdot \left(\phi + \frac{e_{bat}}{e_f} \cdot (1-\phi)\right)}{W_{OE} + W_{PL} + \frac{g}{e_{bat}} \cdot \phi \cdot E_{0,tot}}\right) \tag{3.49}$$

The equation can be rewritten to determine the consumed fuel as expressed by Equation (3.50).

$$\begin{aligned} A &= \eta_p \cdot \left(\frac{e_f}{g}\right) \cdot \left(\frac{L}{D}\right) \cdot \left(\eta_{gt} + \eta_{em} \cdot \frac{\phi}{1-\phi}\right) \\ B &= W_{OE} + W_{PL} \\ C &= \frac{g}{e_{bat}} \cdot \left(\phi + \frac{e_{bat}}{e_f} \cdot (1-\phi)\right) \\ D &= \frac{g}{e_{bat}} \cdot \phi \\ E_{0,tot} &= B \cdot \frac{e^{\frac{R}{A}} - 1}{C - e^{\frac{R}{A}} \cdot D} \end{aligned} \tag{3.50}$$

The weight of the consumed fuel and the weight of the consumable fuel can then be determined by Equation (3.51).

$$\begin{aligned} W_f &= (1-\phi) \cdot \frac{g}{e_f} E_{0,tot} \\ W_{bat} &= \phi \cdot \frac{g}{e_{bat}} E_{0,tot} \end{aligned} \tag{3.51}$$

As the constant fuel (battery) weight does not deplete throughout the mission, an iteration is required to determine the mass at the start of the mission from the zero fuel weight. This is due to the fact that the consumable fuel mass is known at the end of the procedure, but is used as input parameter at the start. At the first iteration, the battery mass is set at zero. The weight of the consumable and non-consumable fuel is added over each flight phase until the weight of the aircraft at the gate before the start of the mission is determined. The required non-consumable fuel mass is used in the next iteration to determine the energy requirement of the aircraft for the flight. This process is repeated until the absolute difference in battery mass as compared to the previous iteration is less than one percent of the battery mass determined in the current iteration, as shown in Equation (3.52).

$$\Delta = \frac{m_{bat,i} - m_{bat,i-1}}{m_{bat,i}} \tag{3.52}$$

For specific range, power split ratio and constant fuel specific energy combinations, the denominator becomes negative. This occurs in the condition specified in Equation (3.53). In this situation the weight of the non-consumable fuel converges to a negative, unfeasible, solution. This occurs at the combination of low specific energy for the non-consumable fuel, a high power split ratio (large share of non-consumable fuel power) and long ranges. The low specific energy prevents the aircraft design to fulfil the mission and pushes the solution to a non-real (negative) answer. In these situations, the performance model registers the aircraft as unable to fly the mission.

$$\begin{aligned} \frac{g}{e_{bat}} \cdot \left(\phi + \frac{e_{bat}}{e_f} \cdot (1-\phi)\right) &< \frac{g}{e_{bat}} \cdot \phi \cdot e^{\frac{R}{A}} \\ 1 + \frac{e_{bat}}{\phi \cdot e_f} &< e^{\frac{R}{A}} \end{aligned} \tag{3.53}$$

A feasibility check is performed on the MTOW and maximum landing weight (MLW) as well. If a specific aircraft-mission combination is in excess of one of these weights in the relevant flight phase, the performance model specifies the combination as impossible to be used in the fleet activity model.

Low specific energy of the non-consumable fuel can result in a significant increase in the computational cost of the performance model. The mass of the constant fuel converges towards infinity as a unit of constant fuel mass leads to a small increase in available energy. As the non-consumable fuel mass converges to an unfeasible solution, the increase in computational cost does not lead to increased accuracy of the performance model. To counter this effect, the performance model registers the sign of change in battery mass of the last 50 iterations. If the sign in the past 50 iterations has not been negative (battery mass has increased the past 50 iterations) and the battery mass exceeds an unfeasible high mass (mass of the earth as 6^{24} is used) the aircraft design is registered to be unable to perform the mission.

When the weight of the aircraft at the start of the mission has been determined and the unfeasible solutions have been registered, the actual fuel and energy use can be determined. As the constant fuel weight has been determined through the iteration, it does not change. Therefore, the energy usage can be determined for the cruise phase by the simplified Equation (3.54). The fuel during the taxi, take-off, climb, descent and landing, taxi in and shutdown phases is determined by fuel fractions as explained in Section 3.3.3.

$$E_{cr} = (W_{OE} + W_{PL} + W_{bat}) \cdot e_f \cdot \left(\frac{e^{\frac{R}{A}} - 1}{g \cdot (1 - \phi)} \right) \tag{3.54}$$

3.4 Fleet activity and composition model

The fleet activity and composition model simulates the composition of the active global fleet and the scheduling of flights. The composition of the active fleet is required to assign specific aircraft to specific flights. This is done by time stepping from the first year of the model run to the final year. The model in this work uses the fleet data by build year for the start year of the run and fleet totals by aircraft type and region for the subsequent years from AIM. As AIM models factors that influence the amount of RTK's an aircraft can fly in a year, such as airport congestion and route delays, this allows the model in this work to model these changes.

If user provided flight and fleet data are used, the RTK capacity in the base year is determined and used in subsequent years to model the fleets total amount of aircraft. This procedure is explained in Section 3.4. The flight scheduling routine is presented in Section 3.4.1 and the determination of fuel, energy and emission totals is described in Section 3.4.2.

Active fleet

As a first step the amount of active aircraft are determined. The stock of active aircraft by build year is loaded from the previous year. The aircraft that are retired or destroyed are subtracted from the fleet by use aircraft type specific retirement curves. A retirement (and destruction) curve provides the proportion of aircraft that are active at a given age [55]. The retirement curves used in this model are the same as used in AIM and were determined by Dray in 2013. Dray developed the retirement curves for narrowbody, widebody, turboprop, executive and regional aircraft. This was done by analysing a database which contained active aircraft by type, year and manufacture age. Dray fitted the results to a logistic function as shown in Equation (3.55).

$$\frac{N_{active}}{N_{active} + N_{retired}} = \frac{1}{1 + e^{-a_1 - a_2 \cdot t}} \tag{3.55}$$

N represent the number of aircraft, where a are the fitting parameters. t is the time in years measured from the manufacturing year. The retirement curve and the data used to develop the retirement curve is visualised in Figure 3.12.

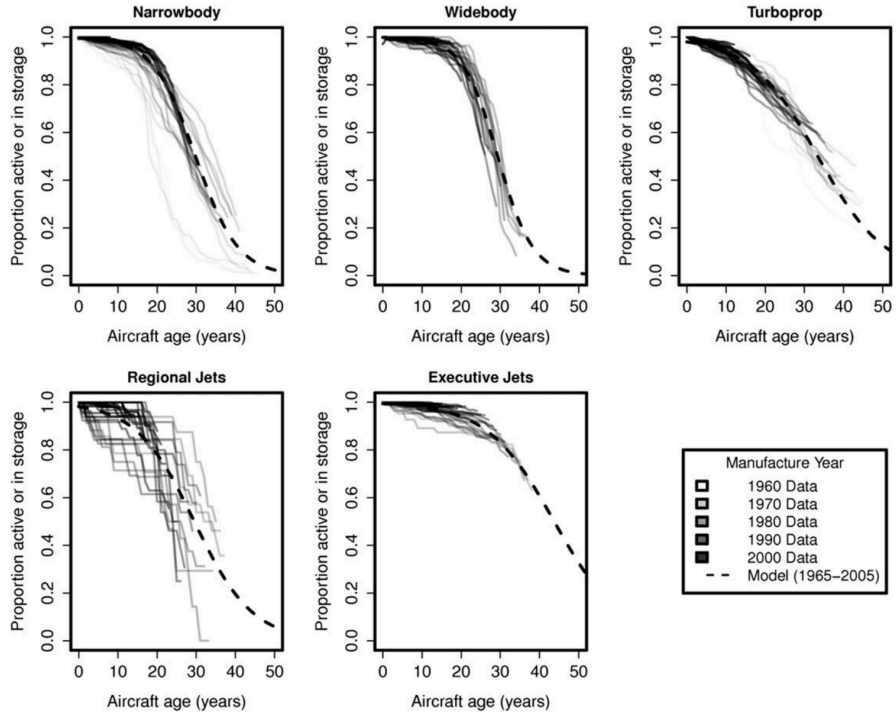

Figure 3.12: Retirement curves as developed by Dray (illustration taken from Dray [55])

The amount of retired aircraft in a year is equal is determined by dividing the retirement curve for the current build year by the retirement curve for the previous build year. As the sum of the active and retired aircraft is equal over the years, these terms cancel. For each aircraft category the aircraft per build year are multiplied by Equation (3.56) to obtain the active aircraft, where the difference is the amount of retired (or destroyed) aircraft.

$$\frac{\frac{N_{active,i}}{N_{active,i}+N_{retired,i}}}{\frac{N_{active,i-1}}{N_{active,i-1}+N_{retired,i-1}}} = \frac{N_{active,i}}{N_{active,i-1}} \tag{3.56}$$

For narrowbody aircraft, the retirement curve of aircraft built in the 1960s shows retirements that occurred significantly earlier than the average. Dray found that this was caused mainly by the economic situation in the 1980s [55]. High oil prices pushed the aircraft market in favour of new aircraft with significant fuel reductions as compared to the second hand market. The combination with economic downturn in the US lead to lower demand for aircraft, further reducing the second hand market. The surplus of 1960 built aircraft lead to the aircraft being retired earlier than aircraft built in subsequent decades [55]. Currently, the same surplus of aircraft is observed due to the impact of the Covid pandemic on the aviation sector, but aircraft retirements are not yet seen to increase as reported by Cirium [56]. If retirement would increase this would lower the average aircraft age and reduce fuel consumption and in turn emissions on the short term. The longer term impact depends mainly on the new average retirement age.

The fleet of active aircraft contains passenger aircraft and dedicated freighter aircraft. In the same manner as the retirement curves Dray determined freighter curves for narrowbody, widebody and turboprop aircraft [55]. By Equation (3.57) the proportion of freighter aircraft can be determined and subtracted from the active fleet and the remainder is the active fleet of passenger aircraft.

$$\frac{N_{active,freighter}}{N_{active}} = \frac{1}{1+e^{-f_1-f_2 \cdot t}} \tag{3.57}$$

Freighter conversions were found to occur mainly for economic reasons by Dray [55]. The increased age of an aircraft causes its value to decrease and pushes the business case in favour of utilisation as a freighter aircraft. Therefore, the increase with aircraft age leads to a higher proportion of aircraft utilised as a freighter. Freighter aircraft have a higher average age than passenger aircraft and extend the operational lifetime of an aircraft.

Freighter aircraft make up a relatively larger share of the widebody aircraft fleet. Motivation for a freighter conversions were found to consist of carrying capacity, range and noise level (for nighttime operations) by

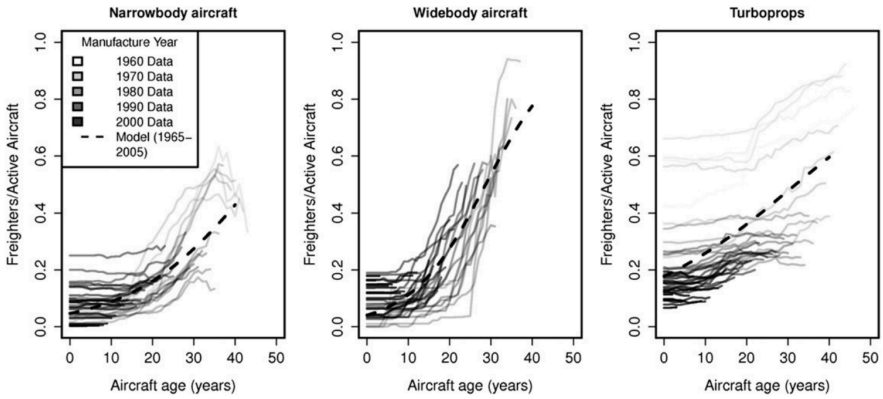

Figure 3.13: Freighter curves as developed by Dray (illustration taken from Dray [55])

Dray [55]. Based on Figure 3.13 and Table 3.12 widebody aircraft have favourable characteristics towards these properties, were narrowbody freighter conversions are rarer.

Apart from aircraft age, the development of the airfreight market is an important factor as well (bulk or parcel freight) which leads to a higher spread around the average and the modelled freighter curve in Figure 3.13 [55]. The parameters for the retirement and freighter curves are taken from AIM and listed in Table 3.12.

SC	$\mathbf{a_1}$	$\mathbf{a_1}$	$\mathbf{t_{r,50}}$	$\mathbf{f_1}$	$\mathbf{f_1}$	$\mathbf{t_{f,50}}$
1	5.9307	-0.1997	29.7	-3.3371	0.0371	90.0
2	5.9307	-0.1997	29.7	-3.3371	0.0371	90.0
3	5.9307	-0.1997	29.7	-3.3371	0.0371	90.0
4	5.9307	-0.1997	29.7	-3.3371	0.0371	90.0
5	5.9307	-0.1997	29.7	-3.3371	0.0371	90.0
6	5.8707	-0.1946	30.2	-4.7963	0.1654	29.0
7	5.8707	-0.1946	30.2	-4.7963	0.1654	29.0
8	6.5492	-0.2225	29.4	-2.2657	0.0789	28.7
9	6.5492	-0.2225	29.4	-2.2657	0.0789	28.7

Table 3.12: Retirement and freighter curve parameters, $\mathbf{t_{r,50}}$ is the age at which 50% of aircraft are retired, $\mathbf{t_{f,50}}$ is the age at which 50% of active aircraft are converted to freighters (parameters from AIM [30])

The determination of the active aircraft can be compared to the amount of required aircraft per aircraft type per region to obtain the regional deficit or surplus. To simulate the second hand market, the amount of surplus aircraft are distributed to regions with shortages. This procedure deviates from the manner in which the second hand market is simulated in AIM. AIM determines the second hand market using a range of (economic) variables which are out of scope for the model in this work. A simplified model is therefore used to distribute the surplus of aircraft. A share of the total aircraft is stored (temporarily or before retirement) at storage locations. Regions with a deficit and with high amount of stored aircraft are modelled to attract a larger proportion of the second hand market by Equation (3.58). The fraction of stored aircraft in the region per aircraft type (N_{st}) is divided by the total global, stored amount of the aircraft type ($N_{st,tot}$). This fraction is multiplied by the global surplus of aircraft ($N_{sh,tot}$).

$$N_{in,sh} = \frac{N_{st}}{N_{st,tot}} \cdot N_{sh,tot} \tag{3.58}$$

If the amount of second hand aircraft distributed to the region is larger than the deficit, the amount of second hand aircraft coming into the region is reduced to equal the deficit. The remainder of second hand aircraft are distributed according to the size of the deficit as shown by Equation (3.59). The amount of second hand aircraft flowing into a region, in addition to the amount determined in Equation (3.58), is $N_{de,ad}$. $N_{de,rem}$ and $N_{de,tot,rem}$ are the remaining deficit in the region and the total global deficit after the redistribution of aircraft based on storage proportion, respectively. The remaining global surplus of aircraft is represented by $N_{de,tot,rem}$.

$$N_{ad,sh} = \frac{N_{de,rem}}{N_{de,tot,rem}} \cdot N_{de,tot,rem} \tag{3.59}$$

After the second hand distribution has been performed, the required amount of new aircraft in a region per aircraft category can be resolved. The new aircraft in the region is then determined by the remaining deficit. The total procedure from the fleet of the previous year to the amount of aircraft required in the current year is illustrated in Equation (3.60).

$$N_{i,new} = N_{i,tot,req} - (N_{i-1,tot} - N_{i,ret} - N_{i,fr} + N_{i,sh,in} - N_{i,sh,out}) \tag{3.60}$$

3.4.1 Flight scheduling

From the active total fleet of aircraft, the flight schedule can be determined. First the pool of available RTK is determined by multiplying the amount of active aircraft by the average RTK capacity per aircraft by Equation (3.61). This results in a pool of available RTK to be flown per aircraft generation and fuel type for a given size category.

$$RTK_{ava,g,t} = RTK_{ave} \cdot N_{g,t} \tag{3.61}$$

The amount of available new aircraft is multiplied by the average RTK as well, resulting in an amount of RTK to be divided over the aircraft generations for the size category. This procedure is performed in the flight scheduler. The flight scheduler module requires a list of flights performed in the current year for the aircraft size category. The flight scheduler selects which generation and fuel type the new aircraft added to the fleet will consist of. The selection procedure is modelled by selecting new aircraft on the highest reduction of fuel usage per RTK, as the highest reduction of operational costs is obtained by the specific aircraft on that route. The fuel usage per RTK ($O_{g,t,seg}$) is determined by dividing the mass of fuel ($m_{f,g,t}$) for the flight amount of RTK (RTK_{seg}) through Equation (3.62).

$$O_{g,t,seg} = \frac{m_{f,g,t}}{RTK_{seg}} \tag{3.62}$$

The fuel usage per RTK from Equation (3.62) is subtracted from the base aircraft (generation one) fuel usage per RTK. This is done to evaluate which aircraft has the largest reduction in operational costs. The list is then sorted on the largest potential reduction in fuel usage per RTK.
The list of routes to be flown in the current year and the pool of available RTK are inputs for the aircraft distribution module, for which the procedure is visualised in Figure 3.14. Per route the required amount of RTK to fill all flights on the segment are passed to the distribution module. The required RTK are determined by equation (3.63).

$$RTK_{od} = q_{od} \cdot m_{pl,od} \cdot D_{act,od} \tag{3.63}$$

The distribution module checks which aircraft has the lowest fuel consumption (per RTK) for the route and evaluates if enough RTK are available from that aircraft. If the stock of RTK for the aircraft is larger than required, the aircraft are scheduled to the route. When flights are scheduled, the stock of available RTK is reduced by the required RTK's for the flight.

When the stock of available RTK is larger than zero but smaller than required, the amount of flights that can filled with the stock is scheduled. For the remainder of flights on the route the available amount of RTK is reviewed if it can fulfil the flights.

If the stock of available flights is enough to fill more than one flight, the flights are scheduled and the stock of available RTK's is reduced by the required RTK's for the flight. The amount of new aircraft are that are deployed are registered.

If flights remain unscheduled, the procedure is repeated for the aircraft with next lowest fuel consumption per RTK until all flights are scheduled in the current year. The amount of new aircraft per generation and fuel type are added to the fleet with the current year as build year. The register containing which aircraft operates which flight is stored.

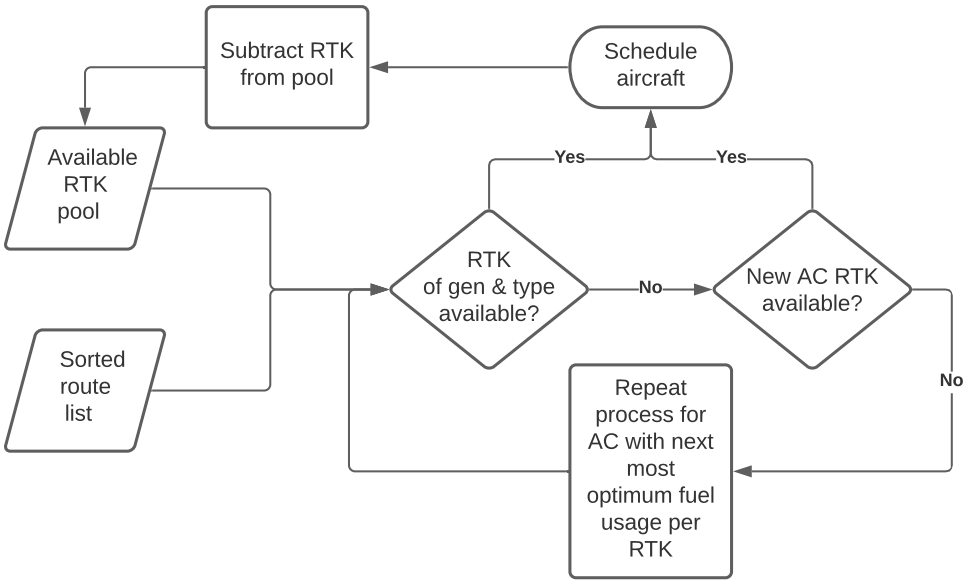

Figure 3.14: Aircraft distribution procedure

3.4.2 Fuel and emission totals

The performance module outputs the fuel and energy use for every aircraft generation, fuel type and mission combination. This data is combined with the flight frequency of every aircraft per mission to obtain the fuel and energy use per route. This is done through Equation (3.64). m_f is the mass of the consumable fuel and E_f is the energy amount for the non-consumable fuel. q represents the flight frequency for the aircraft generation and fuel type between the origin and destination. The fuel mass and energy requirement can then be summed to determine the totals per route, region, generation, aircraft or year.

$$\begin{aligned} m_{f,tot,od} &= m_{f,gt,od} \cdot q_{gt,od} \\ E_{f,tot,od} &= E_{f,gt,od} \cdot q_{gt,od} \end{aligned} \tag{3.64}$$

Through multiplying the fuel mass with the emission indices, the emissions due to aviation are determined. An emission index specifies the amount formed of a chemical substance as a reference substance is consumed. In this model, the reference substance is Jet-A1. Equation (3.65) shows how this is computed for carbon dioxide and water. During the chemical reacting of Jet-A1, 3.155 kilograms of carbon dioxide is formed, such that the emission index (EI_{CO2}) is equal to 3.160. The emission index for water is $EI_{H2O} = 1.231$. Both emission indices are from Lee et al. [1][2].

$$m_{CO2} = m_{f,tot} \cdot EI_{CO2} m_{H2O} = m_{f,tot} \cdot EI_{H2O} \tag{3.65}$$

For the nitrogen oxides (NO_x), unburned hydrocarbons (HC) and carbon monoxide (CO) emission species, the formation process is modelled differently. Formation of these species depend on engine type, engine setting and operating conditions, which makes the emission indices dependent on aircraft type and mission segment. The emission indices are determined from the mean values found in Piano-X data for the climb, cruise, descent and ground segments for each reference aircraft. Fuel consumption during the mission segments is multiplied by the corresponding emission index and are summed to find the total emissions per mission as depicted in Equation (3.66). The index e represents the emission species and the index p is the mission segment.

$$m_e = \Sigma_{e=1}^{e=4} m_{f,p,e} \cdot EI_{p,e} \tag{3.66}$$

4 | Results

The following chapter presents a review of the results obtained from the model. First, in Section 4.1 the results of a simulation, with equal input parameters as used in AIM, is compared to the results of AIM to discuss model performance and discrepancies. Afterwards a case study is presented in Section 4.2 in which the requirements for battery electric flight and the expected scale of impact are investigated to demonstrate the capabilities of the model.

4.1 Model validation with AIM

To compare the results from the model in this work with the simulation ran in AIM, the model in this work is run with equal input parameters. As the AIM simulation was run with an improvement in aircraft technology resulting in an annual fuel efficiency increase of 1.1% per year, the model in this work was run with the introduction of a new generation of aircraft every year. An equal improvement in propulsive, aerodynamic and structural efficiency was determined, resulting in an average 1.1% fuel reduction over all missions for the aircraft size category. First the output of the air traffic model is discussed in Section 4.1.1. The result of the global fleet are presented in Section 4.1.2. The fuel consumption and aircraft emissions of carbon dioxide and nitrous oxides are analysed in Section 4.1.3.

4.1.1 Air traffic model results

The results for the development of global air traffic are measured in revenue passenger kilometre (RPK) and revenue tonne kilometre (RTK). The results are visualised in Figure 4.1 and Figure 4.2 for the five SSP scenarios. Both graphs illustrate that RPK and RTK are conserved throughout the model. This is further confirmed by the modelling accuracy parameters in in Table 4.1 and Table 4.2, where the difference is attributed to rounding error. In the model in this work a procedure is performed to ensure aircraft operate within the payload range diagram for the reference aircraft (procedure elaborated upon in Section 3.2.3). During this procedure, conservation of RTK is applied to ensure that the amount of air traffic modelled is equal to the air traffic scenario input. Both the graphs and tables indicate this process is executed successfully.

Another source for a discrepancy in RPK or RTK can occur when routes are assigned to aircraft. As the RPK and RTK input in the model are equal to the output, the fleet activity model performs flight assignment accurately and ensures an aircraft is assigned to every route.

In the graphs Figure 4.1 and Figure 4.2, a discontinuity between 2018 and 2019 is observed, which originates in AIM. As AIM switches from reported data to projections, the model experiences a small discontinuity. As the AIM data is used in the model in this work, the same step increase in RPK and RTK is experienced.

	RMSE $[km \cdot 10^9]$	**NRMSE** [%]	**R2** [-]
SSP1	5.508	0.32	1.000
SSP2	1.247	0.08	1.000
SSP3	1.266	0.10	1.000
SSP4	1.261	0.09	1.000
SSP5	1.248	0.06	1.000

Table 4.1: Modelling accuracy for revenue passenger kilometer

	RMSE $[kg{\cdot}km{\cdot}10^{10}]$	**NRMSE** [%]	**R2** [-]
SSP1	7.088	0.33	1.000
SSP2	1.205	0.06	1.000
SSP3	1.235	0.08	1.000
SSP4	1.226	0.07	1.000
SSP5	1.193	0.05	1.000

Table 4.2: Modelling accuracy for revenue tonnes kilometer

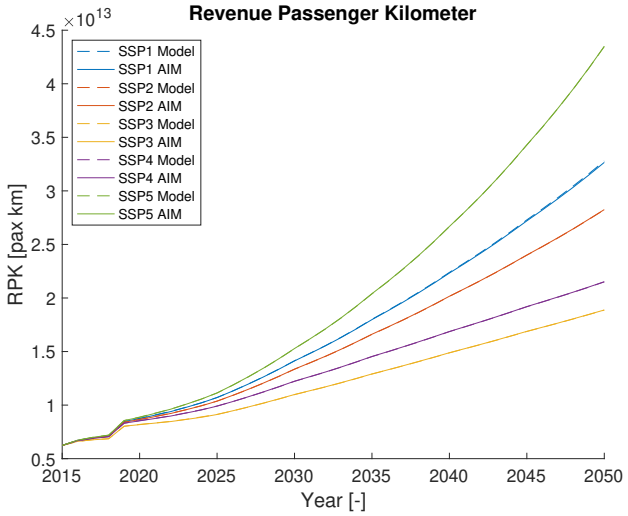

Figure 4.1: Model and AIM global revenue passenger kilometre results for the five SSP's

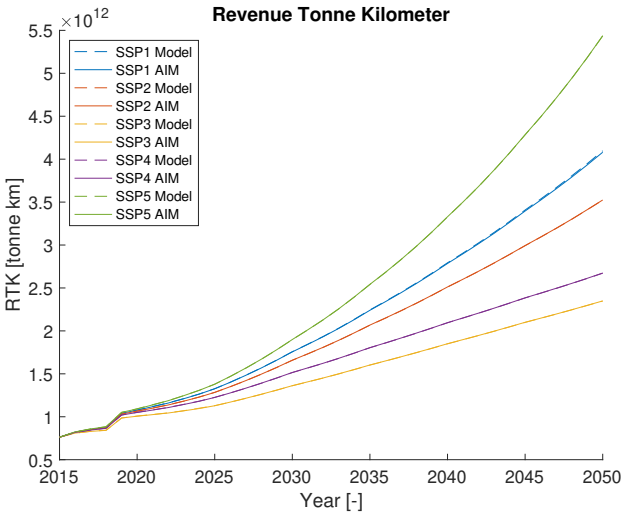

Figure 4.2: Model and AIM global revenue tonne kilometre results for the five SSP's

4.1.2 Fleet model results

In the fleet model, the fleet composition is determined from the air traffic data and AIM input data. In Figure 4.3 the global fleet size is graphed from AIM and the model in this work. A small difference is observed between the two data sets. In the model in this work a procedure is performed to ensure aircraft operate within the payload range diagram for the reference aircraft (procedure elaborated upon in Section 3.2.3). During this procedure, conservation of RTK is applied, to ensure the modelled amount of air traffic is equal. This procedure results in decreased payload on a flight or moving the flight to a larger aircraft size category. As payload on a flight is decreased, the flight frequency is required to go up, in order to conserve RTK on a route. In turn, the required amount of aircraft are increased.

If the flight is moved to an aircraft of a higher size category, the fleet size of the aircraft size category unable to fly the mission is decreased, as fewer flights are required. In turn, the payload is increased for the aircraft of the higher size category and a review is performed if the aircraft is able to operate the mission with increased payload. If not able, the payload is decreased and the flight frequency and the fleet size are increased. The effect of increasing the global fleet is larger, resulting in a larger global fleet as compared to AIM. This is confirmed by Table 4.3 where the average modelling discrepancy is one percent or less.

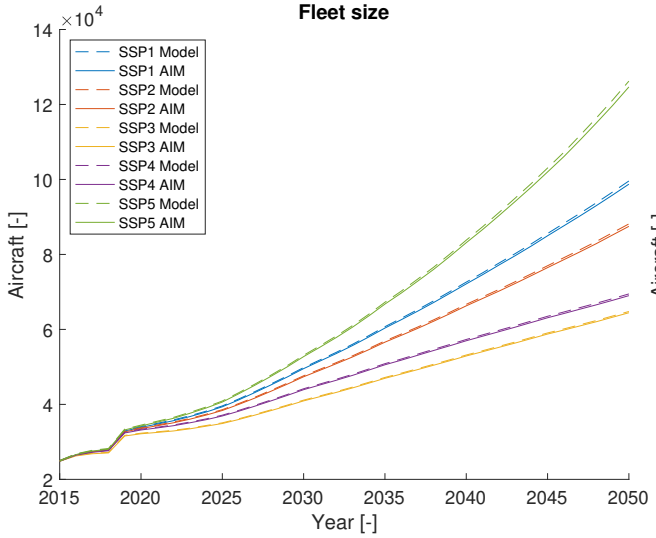

Figure 4.3: Model and AIM global fleet size for the five SSP's

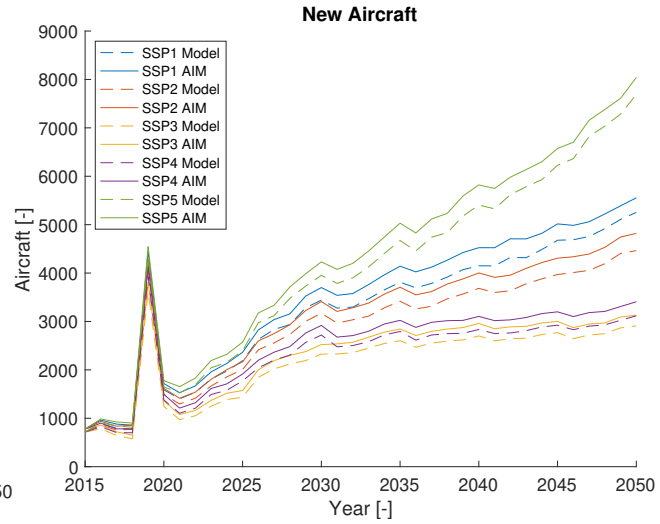

Figure 4.4: Model and AIM global amount of yearly new aircraft for the five SSP's

A larger discrepancy is observed for the amount of new aircraft entering the fleet each year. The discrepancy is caused by the difference in modelling of the second hand market between AIM and the model in this work. In AIM, the second hand market is modelled by taking into account a range of economic factors which are out of the scope for the model in this work. The second hand market in this work is modelled by redistributing excess aircraft in a region to regions with a deficit. This effect leads to a high level of employment for the existing current fleet, reducing the amount of aircraft that are stored. Both effects decrease the amount of new aircraft required in a year, which is observed in Table 4.4. The average modelling discrepancy for new aircraft entering the fleet in the five SSP's is equal to 8%.

	RMSE [-]	**NRMSE** [%]	**R2** [-]
SSP1	428	0.75	1.000
SSP2	357	0.67	1.000
SSP3	229	0.52	1.000
SSP4	296	0.63	0.999
SSP5	685	1.06	0.999

Table 4.3: Modelling accuracy for the global fleet size

	RMSE [-]	**NRMSE** [%]	**R2** [-]
SSP1	269	7.70	0.964
SSP2	255	8.15	0.955
SSP3	198	8.53	0.942
SSP4	215	8.58	0.938
SSP5	292	6.75	0.980

Table 4.4: Modelling accuracy for new aircraft entering the fleet

Another modelling difference is encountered in the distribution of second hand aircraft. AIM determines the amount of acquired and sold second hand aircraft as a fraction of the total amount of aircraft per size category in the region. If a net decrease occurs, the fraction is subtracted from each aircraft by build year. When a net increase of aircraft occurs, the fraction is added. This procedure can lead to a shift in average, global aircraft age. When in region A, with an average aircraft age of twelve years, a net decrease of aircraft occurs e.g. ten aircraft and in region B, with an average aircraft age of fifteen years, an increase occurs of ten aircraft, the average age of the ten aircraft will have increased by three years to fifteen years.

In the model in this work, the aircraft that leave a region due to a net decrease are redistributed, conserving the age of the aircraft. This effect can be seen in Figure 4.5 where the global, average aircraft age of AIM exceeds the average age from the model in this work from 2022 up and till 2038. This in turn increases the amount of new aircraft entering the fleet. As the average aircraft age increases (due to a reduction in the aviation sectors growth), a larger share of aircraft are retired and employed as freighters. As fewer aircraft are available within a region, a larger amount of new aircraft are required. This can be seen over the entire range of years in Figure 4.4. The larger amount of new aircraft entering the fleet in AIM results in a lower average aircraft age from 2038 on in Figure 4.5. The relatively large difference in modelling observed for new aircraft entering the fleet is dampened by the different second hand market model, resulting in an average modelling error of less than one percent as shown in Table 4.5.

	RMSE [**year**]	**NRMSE** [%]	**R2** [-]
SSP1	0.085	0.65	0.981
SSP2	0.082	0.61	0.978
SSP3	0.111	0.79	0.966
SSP4	0.075	0.54	0.971
SSP5	0.079	0.62	0.991

Table 4.5: Modelling accuracy for average aircraft age

The graph in Figure 4.6 depicts the share supplied by the newest available generation of the new aircraft. The graph is an output of the model, showing the adoption of a new aircraft generation. If a new generation of aircraft has increased performance over the previous generations in fuel consumption, the line is expected to be equal to one over the entire time span. As a new generation is introduced every year with a 1.1% increase in fuel efficiency as compared to the previous generation, the model is expected to select the latest generation. If more specific aircraft designs are modelled which feature an increase in the performance of one parameter, but causes a penalty to another performance parameter, Figure 4.6 will indicate the scale of adoption of the aircraft design based on fuel efficiency. As for example an aircraft design will feature an increase in aerodynamic performance with an increase in structural weight, depending on the relative in- and decreases, the situation can occur where the aircraft design is more efficient on long-range routes, but features a higher fuel consumption on short range

routes. New aircraft selection would lead to an adoption factor lower than one, as short range routes will be operated by the more economical, older generation aircraft.

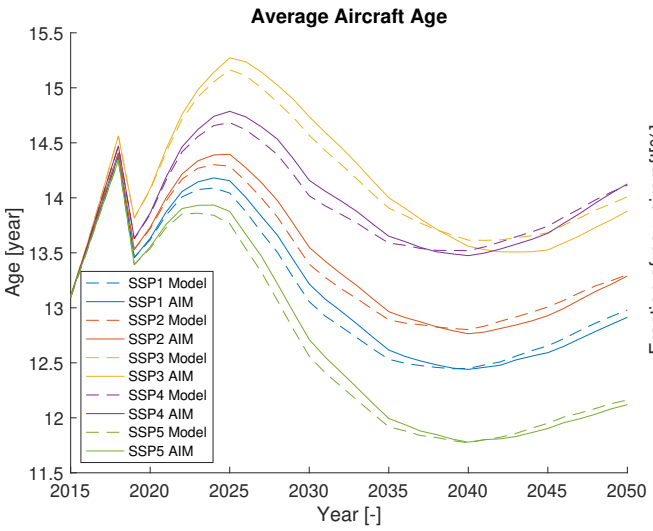

Figure 4.5: Model and AIM global average aircraft age for the five SSP's

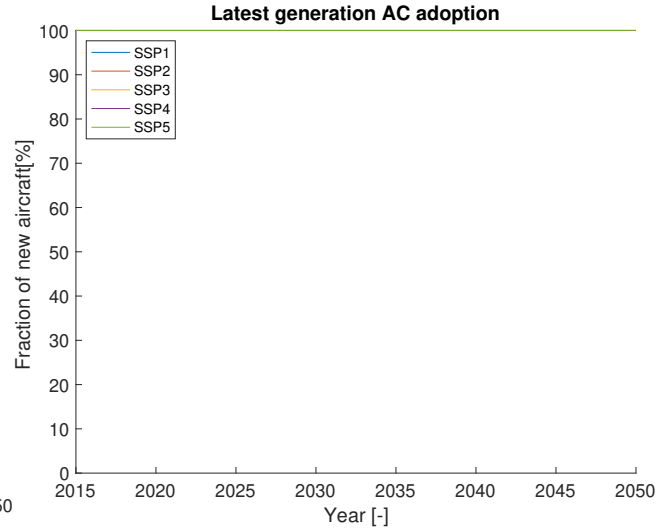

Figure 4.6: Model share of new aircraft supplied from the latest available generation amount for the five SSP's

4.1.3 Performance model results

The fuel usage and emissions are determined by the fuel usage per aircraft and are multiplied with the flight frequency determined in the fleet activity model. The fuel consumed by the global fleet per year is visualised in Figure 4.7. The model in this work underestimates fuel consumption as compared to AIM up and till the year 2030. The fuel consumption is higher for all SSP's in the following years leading to an average modelling discrepancy of 3% as listed in Table 4.6.

	RMSE $[kg \cdot 10^{11}]$	**NRMSE** [%]	**R2** [-]
SSP1	1.639	3.34	0.992
SSP2	1.233	2.74	0.993
SSP3	0.879	2.49	0.988
SSP4	0.973	2.49	0.991
SSP5	2.206	3.86	0.993

Table 4.6: Modelling accuracy for fuel consumption

The underestimation is caused by the flights that are rescheduled to a higher aircraft size category by the payload range limitations and are performed more efficiently on a fuel per passenger basis. Afterwards, as the average aircraft age in this work increases and exceeds the average aircraft age in AIM, the global fuel consumption increases and exceeds the fuel results from AIM.

Furthermore, the 1.1% increase in fuel efficiency is modelled as an average for all missions flown by the aircraft size category. Missions will exist with a fuel consumption decrease which are lower or higher than the specified increase. As differences occur between mission flight frequency, the fuel consumption is increased as compared to AIM, where the fuel efficiency increase is modelled equally for every range and payload combination.

Finally, the Breguet equation used in the model in this work introduces a modelling discrepancy. Where AIM uses a regression over load factor and range for each aircraft size category, the Breguet model in this work makes use of fuel fractions to determine the fuel consumption in the taxi, take-off, climb, descent and landing phases. Furthermore, the cruise phase is modelled as a straight line, where the step climb modelled in Piano-X (performance data source for AIM and the model in this work) is not incorporated. The simpler model has been developed to allow for a more diverse range of aircraft technology options, but does influence the modelling accuracy. Overall the modelling accuracy is higher than reported in literature (due to an update of the fuel fractions and overall propulsive efficiency) by Bovet et al [37].

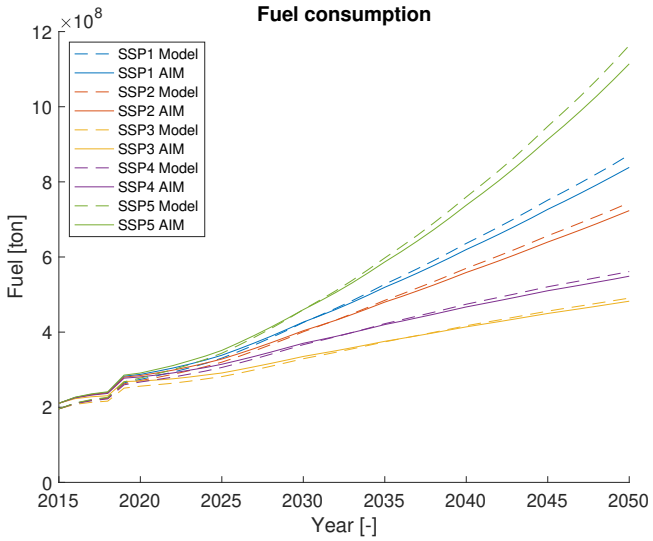

Figure 4.7: Model and AIM global fuel consumption for the five SSP's

The global emissions of carbon dioxide and nitrous oxides are visualised in Figure 4.8 and Figure 4.9, respectively. The carbon dioxide emissions show the same pattern as the fuel consumption, which is expected due to the manner in which the emission is modelled. The formation of carbon dioxide is determined by a multiplication of the fuel consumption with the emissions index. This leads to a similar modelling discrepancy as for fuel consumption as listed in Table 4.7.

	RMSE $[kg \cdot 10^{11}]$	**NRMSE** [%]	**R2** [-]
SSP1	5.341	3.45	0.992
SSP2	3.998	2.82	0.993
SSP3	2.744	2.46	0.988
SSP4	3.106	2.52	0.990
SSP5	7.203	4.00	0.993

Table 4.7: Modelling accuracy for CO2 emissions

	RMSE $[kg \cdot 10^{9}]$	**NRMSE** [%]	**R2** [-]
SSP1	1.355	1.69	0.998
SSP2	0.693	0.95	0.999
SSP3	0.348	0.62	0.999
SSP4	0.343	0.55	1.000
SSP5	2.136	2.27	0.998

Table 4.8: Modelling accuracy for NOx emissions

The difference in emission results for the nitrous oxides emissions is lower than observed for fuel consumption and carbon dioxide emissions. The nitrous oxides emissions are computed per mission segment through multiplying the respective fuel consumption in the mission segment with the respective emission index. The emission index is computed from the average nitrous oxide emissions from the Piano-X emission data. The average modelling discrepancy is equal to 1.5% as presented in Table 4.8. The reduction in modelling error as compared to fuel usage is caused by a combination of two effects. The largest modelling difference for fuel consumption due to the Breguet model is observed for the smaller aircraft size categories and for all aircraft in the descent phases. For both the smaller aircraft size categories and the descent phases, the emission index for NO_x is smallest. This results in the largest share of NO_x emissions being computed in the more accurately modelled flight phases, and in turn in emission quantities closer to the results observed in AIM.

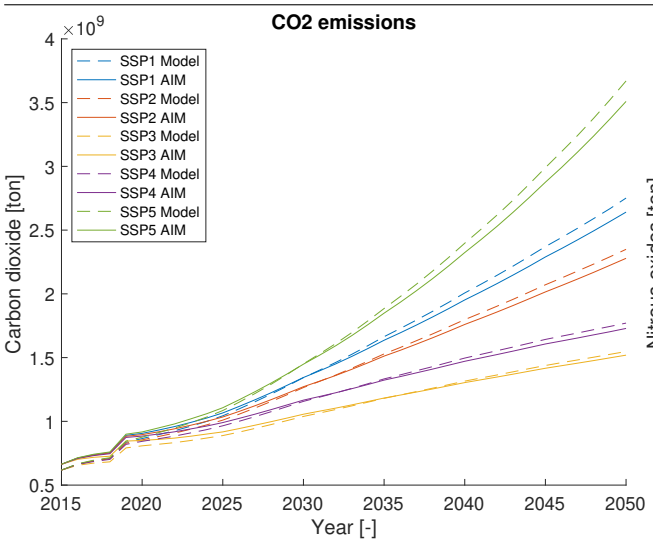

Figure 4.8: Model and AIM global carbon dioxide emissions for the five SSP's

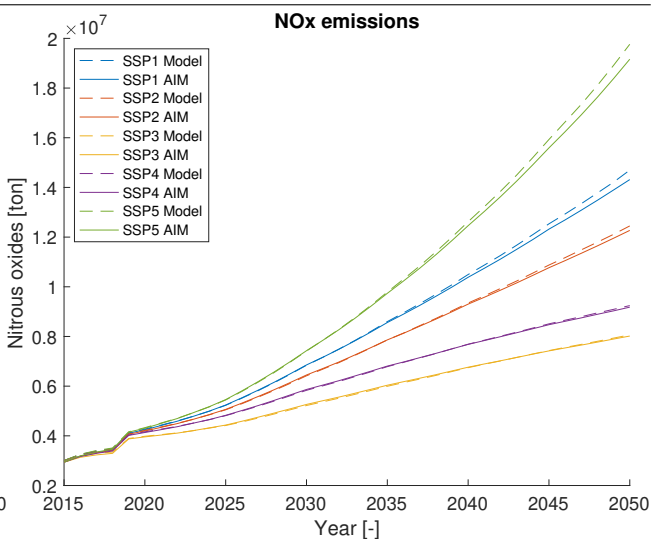

Figure 4.9: Model and AIM global nitrous oxide emissions for the five SSP's

4.2 Case studies battery electric aircraft

The model in this work was designed as a tool to investigate the effect of future aircraft technology on the climate impact of aviation. To illustrate the potential of the model, two cases are presented for the SSP 2 scenario. Both cases involve hybrid electric power split ratio's (ϕ) ranging from 0 to 1 in steps of 0.25. Both cases are run with two different values for the annual increase of battery specific energy (g_{bat}). The lower value of 3.78% is equal to the advancement in electric battery specific energy found for lithium energy cells from values reported by Ding et al. and Lobberding et al. between 1990 and 2019 [57][58].

The model is run simultaneously with a 50% increase compared to the base value for the annual battery specific energy increase (5.67%). This is done to investigate the effect of a higher technology trend in this field. The case studies differ in the technology trends modelled. Case 1 involves an annual increase of the performance parameters leading to a reduction in fuel consumption of 1.1% for conventionally powered aircraft. Case 2 involves a higher trend in annual efficiency increase to 1.5%.

First the market share which are served by the hybrid electric aircraft is presented for both test cases in Section 4.2.1. The rate in which hybrid electric aircraft are introduced to the global fleet is discussed in Section 4.2.2. The case studies are reviewed on the impact on aircraft emissions in Section 4.2.3.

4.2.1 Battery electric aircraft traffic share

The market share of battery electric hybrid aircraft is presented for both the case studies is presented on an RPK basis in Figure 4.10 and Figure 4.11. The largest market share on an RPK basis for both test cases is found for the aircraft with a quarter of the power supplied by electric batteries with a trend in specific energy for batteries of 5.67%. The first generation for which hybrid electric flight starts to operate a share of the market is the fourth generation, introduced in the year 2040.

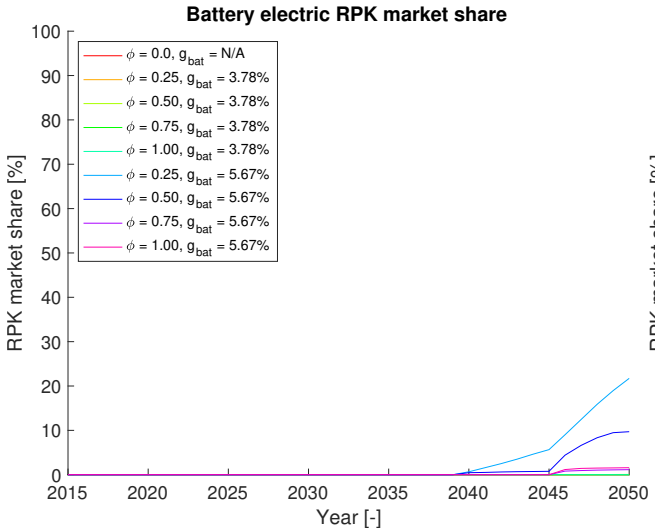

Figure 4.10: Case study 1: RPK market share of battery electric hybrid aircraft with an annual fuel efficiency increase of 1.1% for SSP2.

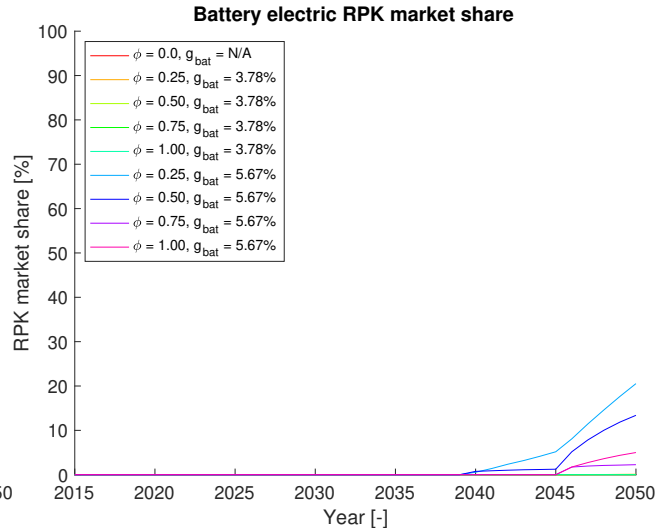

Figure 4.11: Case study 2: RPK market share of battery electric hybrid aircraft with an annual fuel efficiency increase of 1.5% for SSP2.

The period from 2035 to 2050 for the RPK market share is displayed in Figure 4.12 and Figure 4.13. The market share for aircraft with a specific energy increase of 3.78% compose a negligible share of the air traffic market (less than 1%). The cases where the annual increase in specific energy for electric batteries is equal to 5.67% are able to serve a significant share of the total air traffic market. For both cases, the hybrid electric aircraft with a quarter of the power supplied by the electric system leads to a market share of 21%.

Larger differences are observed for hybrid electric battery aircraft with a higher power ratio. The market share of hybrid electric aircraft with equal power split is increased from 10% to 14% for the second case study. For power splits of 0.75 the market share is doubled and for fully electric aircraft the market share triples. Between a power split of 0.5 to 1 in the second case study, the point is located where an increased power split results in a higher market share. This is illustrated by the larger market share for a power split of 1 as compared to 0.75 in Figure 4.13. At that point, exchanging fuel weight for battery weight leads to more flights with a lower fuel consumption as compared to a conventionally powered aircraft. The energy supplied by the batteries is larger than the increase in energy consumption the aircraft experiences due to the increased aircraft weight.

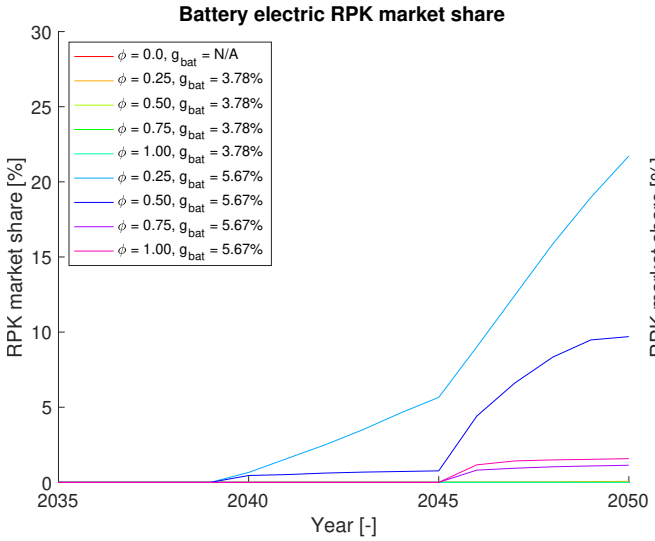

Figure 4.12: Case study 1: RPK market share of battery electric hybrid aircraft with an annual fuel efficiency increase of 1.1% for SSP2 between 2035 and 2050.

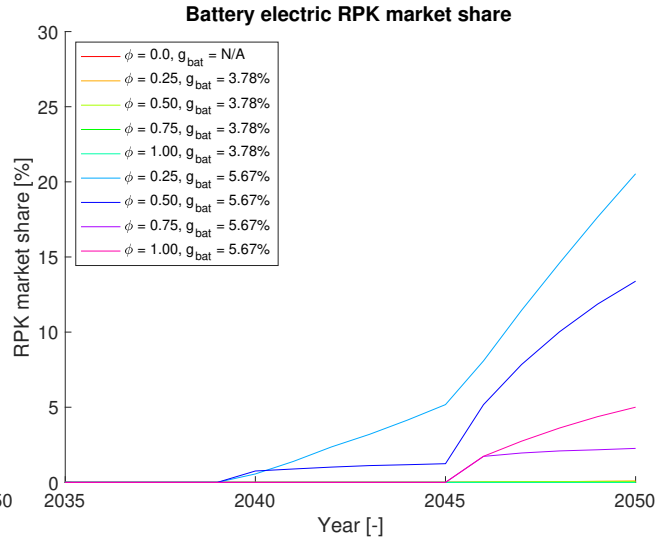

Figure 4.13: Case study 2: RPK market share of battery electric hybrid aircraft with an annual fuel efficiency increase of 1.5% for SSP2 between 2035 and 2050.

The same market shares are found for the market share on RTK basis, as illustrated in Figure 4.14 and Figure 4.15. The market share for all degrees of hybridisation is decreased slightly. This decrease from RPK to RTK is an expected result. Two flights, with the same RPK, can have a different RTK due to different freight masses carried. As weight constraints limit the possibility of hybrid electric aircraft flying certain missions, it is possible for hybrid electric aircraft to serve a higher share of the RPK market as compared to RTK market.

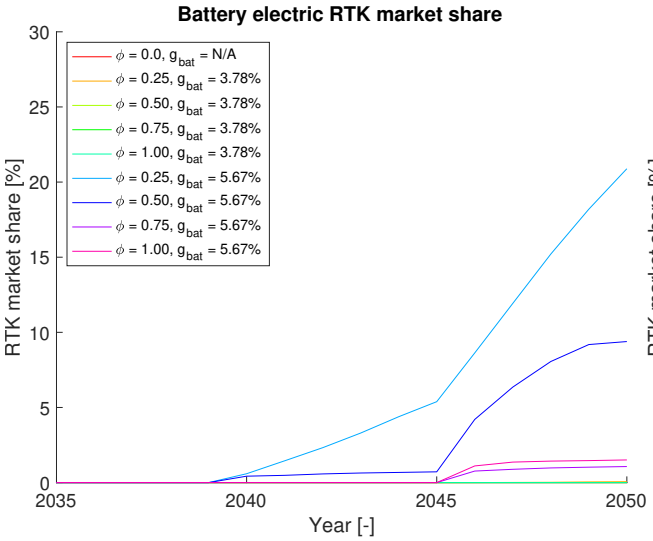

Figure 4.14: Case study 1: RTK market share of battery electric hybrid aircraft with an annual fuel efficiency increase of 1.1% for SSP2 between 2035 and 2050.

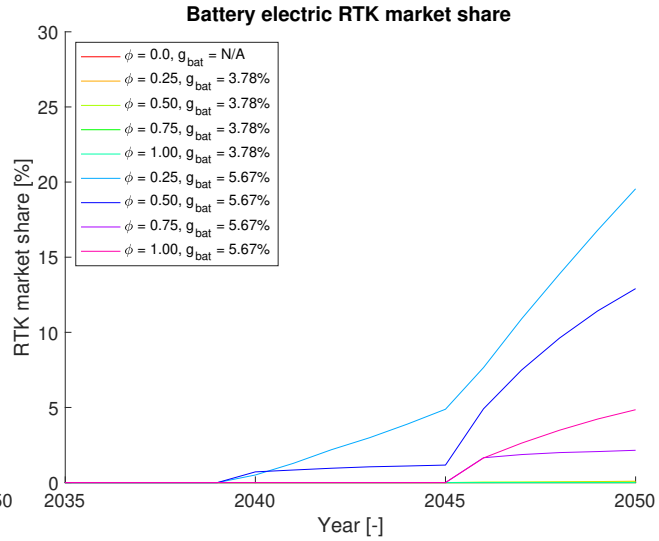

Figure 4.15: Case study 2: RTK market share of battery electric hybrid aircraft with an annual fuel efficiency increase of 1.5% for SSP2 between 2035 and 2050.

4.2.2 Battery electric aircraft fleet share

The share of new aircraft per year filled by hybrid aircraft is shown in Figure 4.16 and Figure 4.17. The graphs illustrate that the market share covered by hybrid electric aircraft is limited by the performance of the aircraft and not the amount of aircraft introduced to the fleet. The amount of hybrid electric aircraft required for the routes where operation by a hybrid electric aircraft leads to the highest fleet reduction is less than the total aircraft introduced by the fleet, as shown by the adoption fraction lower than one in both figures.

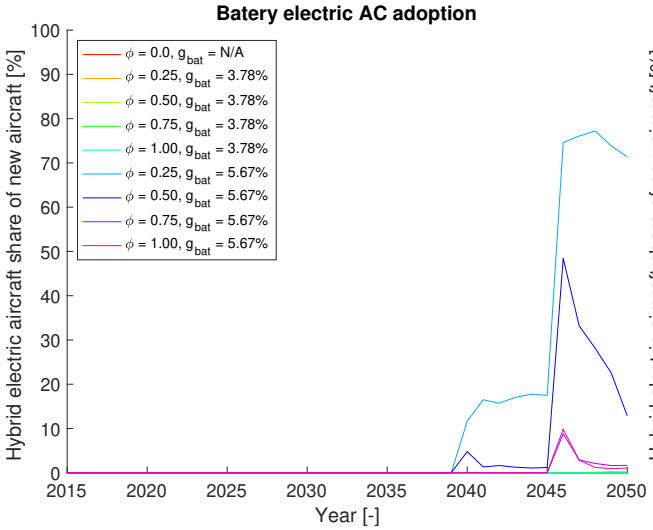

Figure 4.16: Case study 1: Battery electric hybrid aircraft adoption with an annual fuel efficiency increase of 1.1% for SSP2.

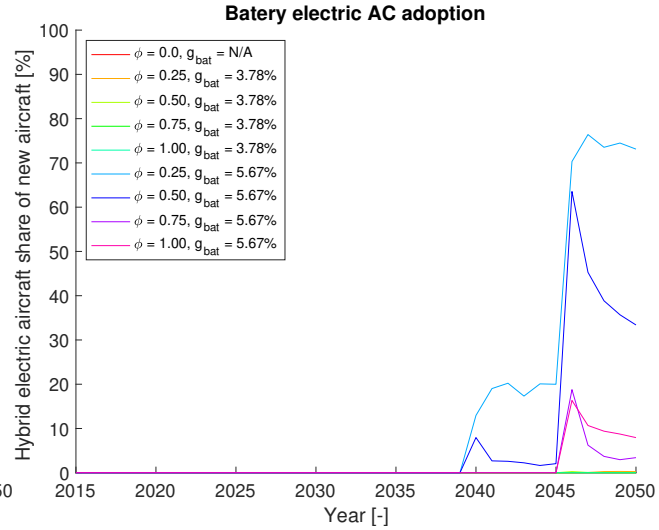

Figure 4.17: Case study 2: Battery electric hybrid aircraft adoption with an annual fuel efficiency increase of 1.5% for SSP2.

The share of hybrid electric aircraft per size category is displayed in Figure 4.18 and Figure 4.19 for aircraft with a quarter of the power supplied by the battery electric system. For the case with an annual aircraft efficiency increase of 1.1% the larger share of hybrid electric aircraft are found in the lower size categories, but is equal for size categories of four and higher. For an annual efficiency increase of 1.5% the share of hybrid electric aircraft is most pronounced at the lower size categories.

Even tough both cases make up equal amounts of the air traffic market share, the division over the aircraft size categories is different. As the annual fuel efficiency of aircraft increases, the operative empty weight and in turn the weight of the aircraft at the start of the mission decreases. The weight penalty of an added unit of mass is larger than compared to an aircraft with a higher operative empty weight. As aircraft of higher size categories spend relatively more time in cruise conditions, at higher efficiency values the difference between the required fuel weight and battery weight is increased as compared to lower efficiency values. This causes the weight penalty of constant fuel to increase and skews the share of hybrid electric aircraft in favour of smaller size categories which operate for a smaller share of the mission length in cruise conditions.

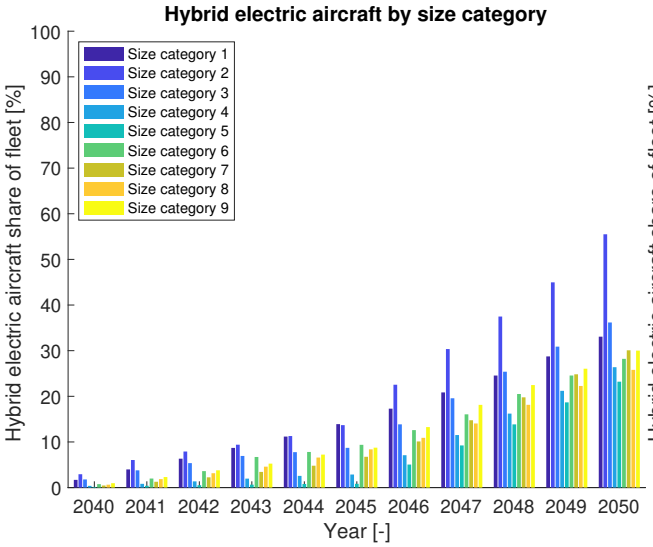

Figure 4.18: Case study 1: Hybrid electric aircraft fleet share per size category for SSP2 for a 0.25 power split ratio and 5.67% annual battery specific energy increase and an annual fuel efficiency increase of 1.1% for SSP2.

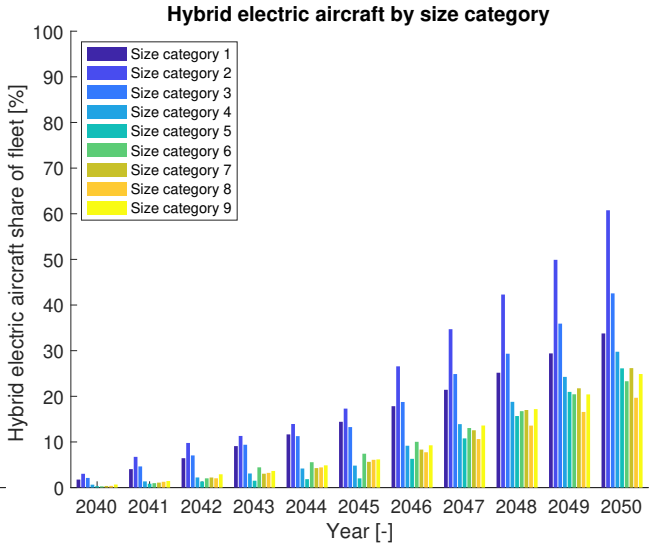

Figure 4.19: Case study 2: Hybrid electric aircraft fleet share per size category for SSP2 for a 0.25 power split ratio and 5.67% annual battery specific energy increase and an annual fuel efficiency increase of 1.5% for SSP2.

The missions flown by the first size category in both case studies for aircraft with a quarter of the power supplied by the battery electric system are shown in Figure 4.20 and Figure 4.21. In both figures, the share of the routes flown by the hybrid electric aircraft is largest for short ranges with low payloads. The largest difference between the cases is found for medium payload and medium to long range missions. For the first case, the majority of routes operated by hybrid electric aircraft are found up to 1.500 kilometres range and 6.000 kilograms of payload. For the second case, the majority of flights for the hybrid electric aircraft are found for a larger spread of ranges up to 2.750 kilometres. It should be noted that the graphs do not indicate which routes the aircraft are capable of flying, but is determined on the basis of the regional fuel reduction per RTK and regional new aircraft requirements.

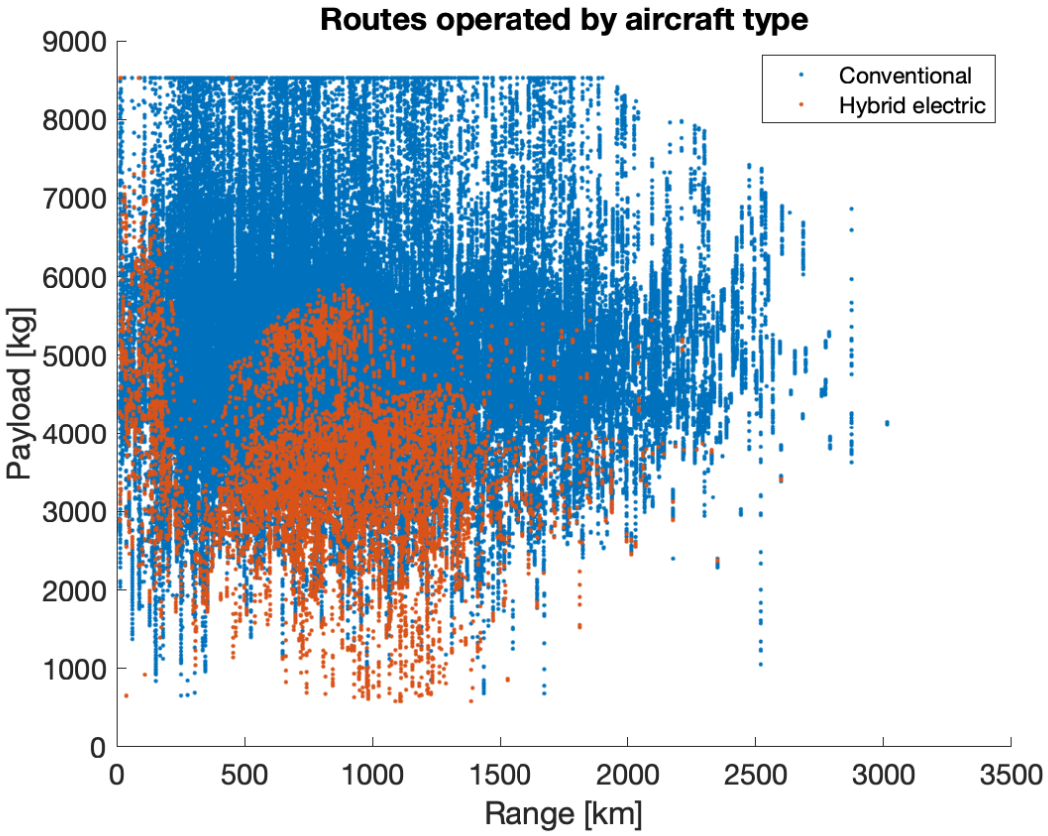

Figure 4.20: Case study 1: Routes operated for the first size category of hybrid electric aircraft with a 0.25 power split ratio, a 5.67% annual battery specific energy increase and an annual fuel efficiency increase of 1.1% for SSP2.

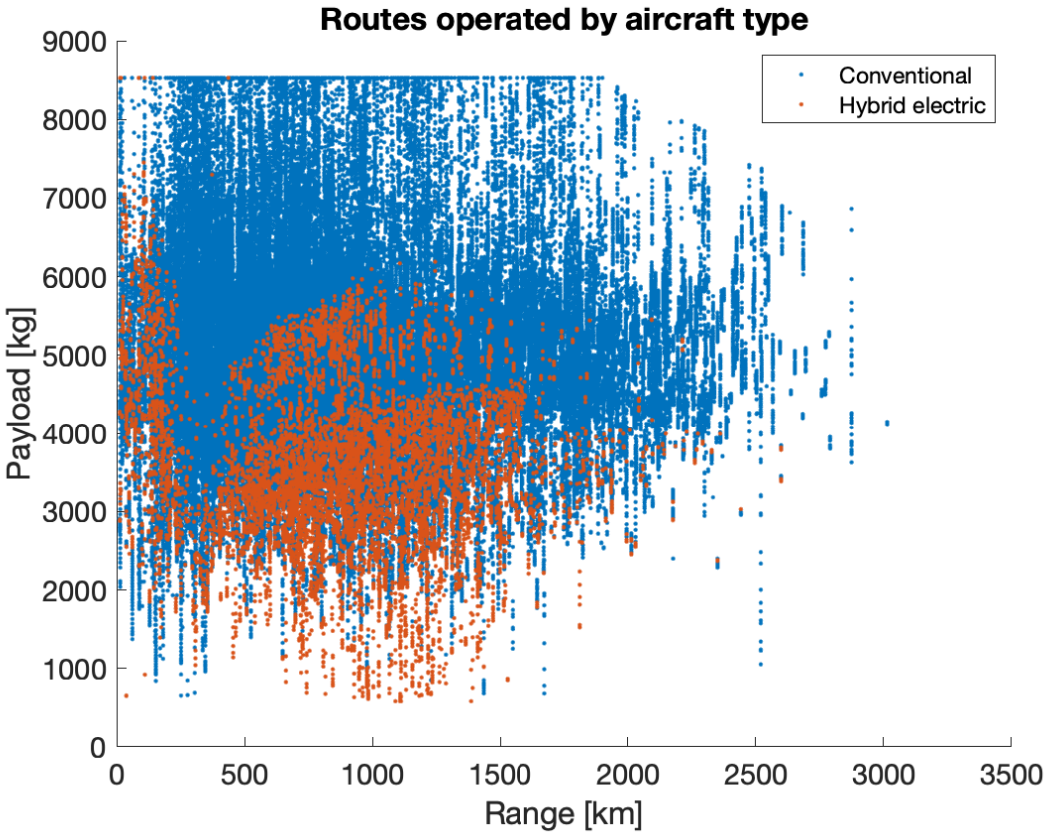

Figure 4.21: Case study 2: Routes operated for the first size category of hybrid electric aircraft with a 0.25 power split ratio, a 5.67% annual battery specific energy increase and an annual fuel efficiency increase of 1.5% for SSP2.

4.2.3 Battery electric aircraft fuel and emission reduction potential

The fuel consumption for both cases is plotted in Figure 4.22 and Figure 4.23. The overall fuel consumption for the second case is lower, as is expected due to the increased annual efficiency increase, as compared to the first case study. For both cases, hybrid electric aircraft operate from 2040 and on wards, but the first visible difference in fuel consumption can be discerned from the year 2044.

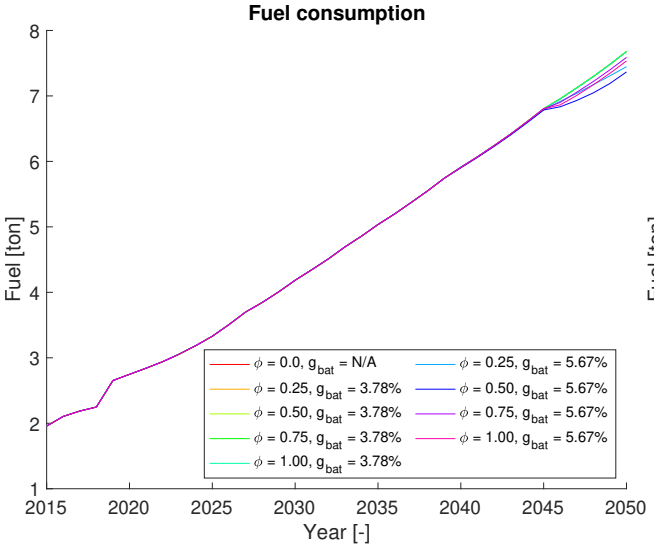

Figure 4.22: Case study 1: Fuel consumption of battery electric hybrid aircraft with an annual fuel efficiency increase of 1.1% for SSP2 between 2015 and 2050.

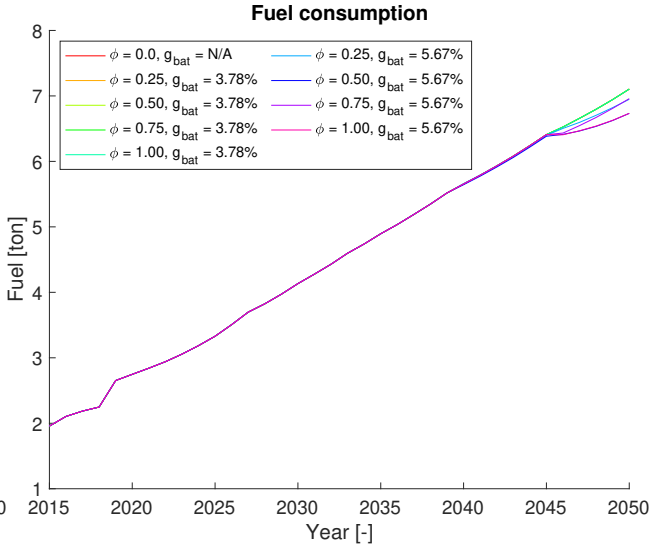

Figure 4.23: Case study 2: Fuel consumption of battery electric hybrid aircraft with an annual fuel efficiency increase of 1.5% for SSP2 between 2015 and 2050.

The same fuel consumption graph is plotted in Figure 4.24 and Figure 4.25 for the period 2035 to 2050. For both cases, the market share of hybrid electric aircraft was largest for aircraft with a power split of 0.25, but the fuel reduction potential is largest for aircraft with a higher power split. A power split of 0.5 has the largest fuel reduction potential for the first case, where in the second case a power split of 0.5 and 1 lead to a similar reduction in fuel consumption.

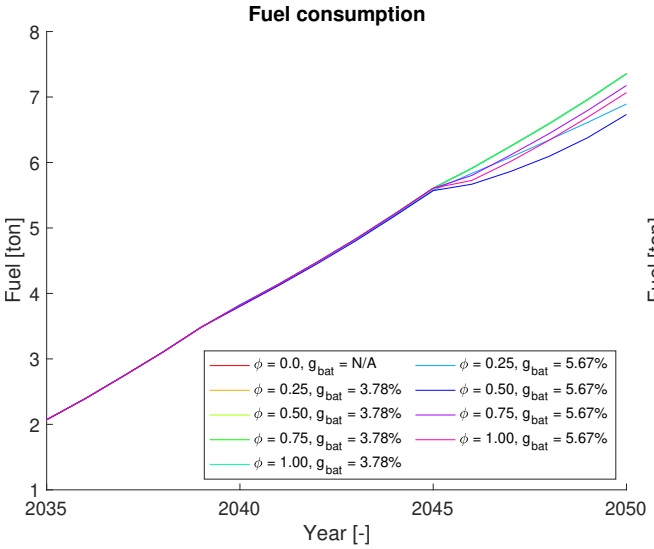

Figure 4.24: Case study 1: Fuel consumption of battery electric hybrid aircraft with an annual fuel efficiency increase of 1.1% for SSP2 between 2035 and 2050.

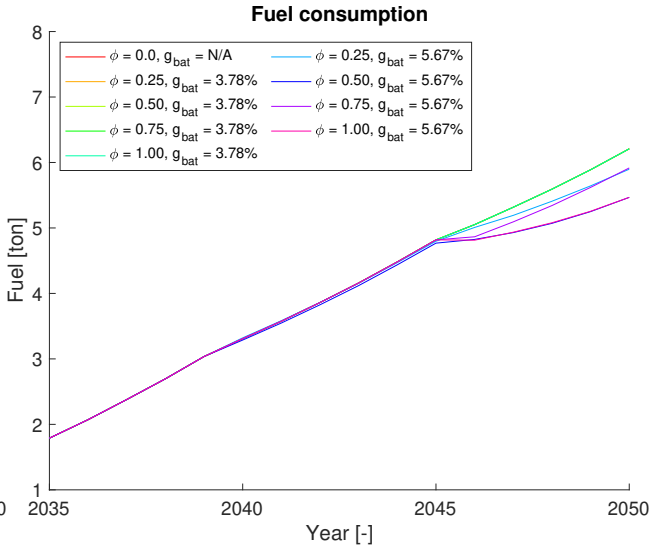

Figure 4.25: Case study 2: Fuel consumption of battery electric hybrid aircraft with an annual fuel efficiency increase of 1.5% for SSP2 between 2035 and 2050.

Hybrid electric aircraft profit less in terms of efficiency from the reduction of aircraft weight, as a fraction of the fuel weight is constant. If all efficiency parameters and the specific energy are equal between the consumable and non-consumable fuel, a hybrid electric aircraft requires a larger amount of energy to fly the same mission. The snowball effect in aviation is then encountered as the increase in required energy in turn leads to a higher aircraft weight which leads a higher energy requirement and so on.

If the energy penalty for a hybrid electric aircraft is smaller than the power split fraction provided by the electric system, the aircraft will have a smaller fuel consumption than the conventionally powered variant. The larger the difference between the penalty in energy requirement and power split ratio, the larger the reduction in fuel consumption will be. This difference is larger for the 0.5 hybrid electric aircraft in case one, and larger for the 0.5 and 1 power split aircraft as compared to aircraft with a power split ratio of 0.25 in both case studies.

The energy requirement in both cases is largest for the 0.5 power split hybrid electric aircraft as shown in Figure 4.26 and Figure 4.27. The energy required for aircraft with a 0.5 power split ratio is substantial, equalling the electric energy generation of China in 2019 [59]. The electric energy requirement for aircraft with a 0.25 power split ratio is reduced for the second case as compared to the first case (due to increased efficiency), but remains substantial. As the overall fuel reduction for the 0.25 power split is marginal and accompanied by a substantial energy requirement, the design option is not regarded as viable on an economic basis. The fully electric aircraft in the second case features a similar energy consumption as the 0.25 power split option, with a larger reduction in fuel consumption, resulting in a more viable economic model for the design.

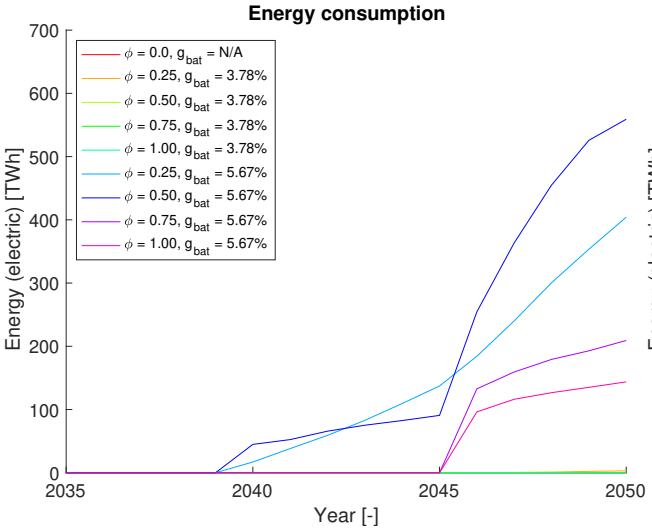

Figure 4.26: Case study 1: Electric energy consumption of battery electric hybrid aircraft with an annual fuel efficiency increase of 1.1% for SSP2 between 2015 and 2050.

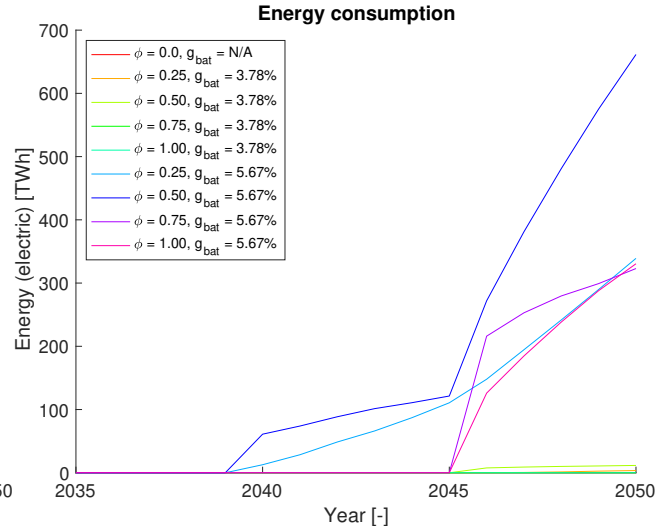

Figure 4.27: Case study 2: Electric energy consumption of battery electric hybrid aircraft with an annual fuel efficiency increase of 1.5% for SSP2 between 2015 and 2050.

As the emissions of carbon dioxide are directly related to the fuel consumption the graphs found in Figure 4.28 and Figure 4.29 shown the same trend as encountered for the fuel consumption.

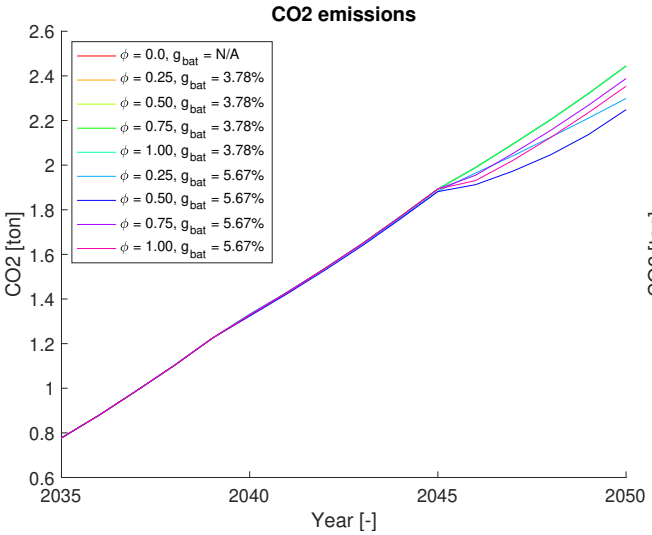

Figure 4.28: Case study 1: Carbon dioxide emission of battery electric hybrid aircraft with an annual fuel efficiency increase of 1.1% for SSP2 between 2035 and 2050.

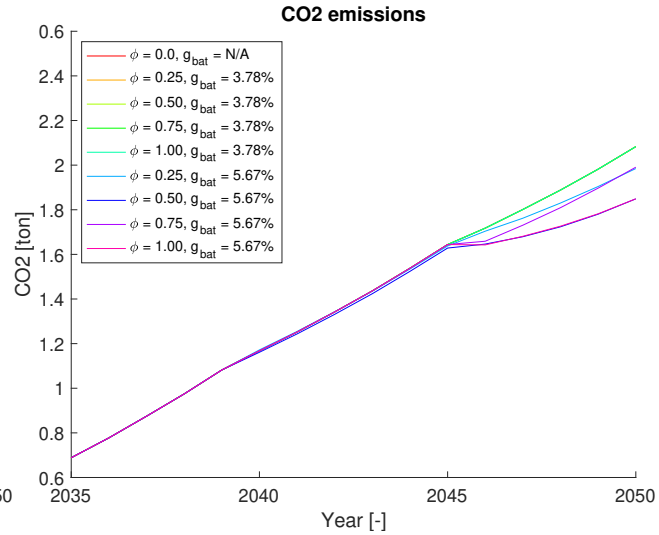

Figure 4.29: Case study 2: Carbon dioxide emission of battery electric hybrid aircraft with an annual fuel efficiency increase of 1.5% for SSP2 between 2035 and 2050.

Nitrous oxide emissions show a large difference between the different power split options for the hybrid electric aircraft as pictured in Figure 4.30 and Figure 4.31. The larger difference is caused by a combination of the manner of modelling and the higher emission indices for specific flight phases. The larger reduction in nitrous oxides is caused by large fuel consumption reductions in flight phases with larger emission indices.

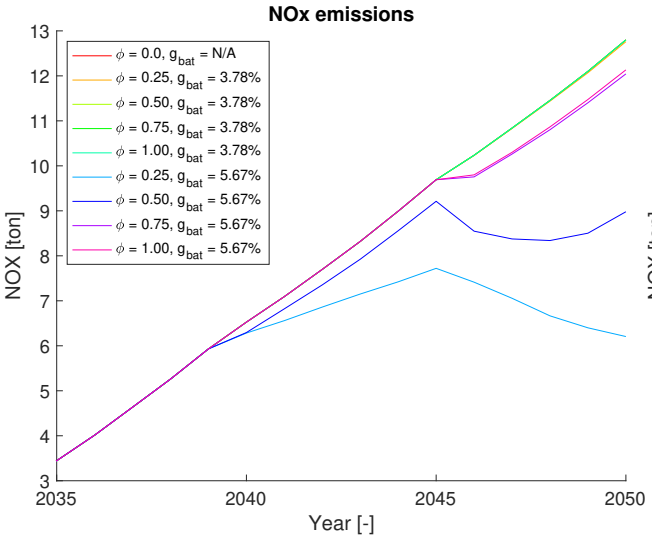

Figure 4.30: Case study 1: Nitrous oxides emissions of battery electric hybrid aircraft with an annual fuel efficiency increase of 1.1% for SSP2 between 2035 and 2050.

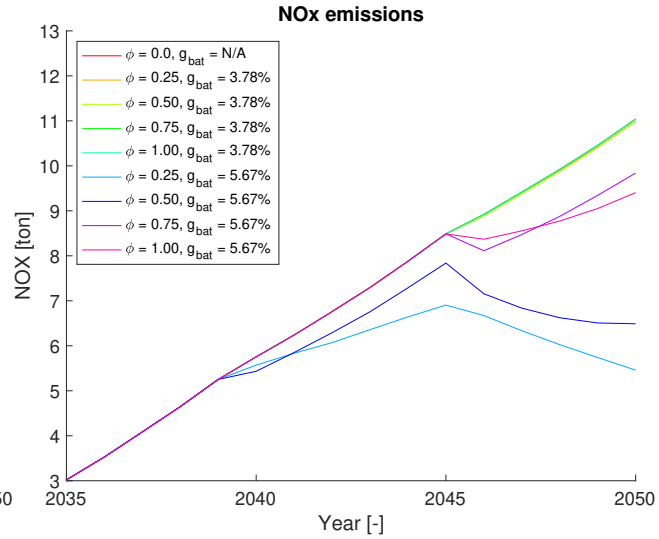

Figure 4.31: Case study 2: Nitrous oxides emissions of battery electric hybrid aircraft with an annual fuel efficiency increase of 1.5% for SSP2 between 2035 and 2050.

5 | Conclusion and recommendation

In this study, a model has been developed which assesses the effect of policy or technology choices on the climate impact of aviation. A subdivision of the global fleet has been made where aircraft are categorised in nine different size categories represented by a reference aircraft of that size category. Air traffic data for the nine different size categories is obtained from the AIM model. The performance model was developed based on the Breguet range equation to allow simulation of a wide range of technology options represented by the propulsive, aerodynamic and structural efficiency parameters. The fleet activity model resolves the amount of active passenger aircraft, the amount of new aircraft in the fleet, and schedules the most fuel efficient available aircraft to a route.

In the model presented in this work, the research question of: *How can a user-friendly model be constructed which can determine the impact of technological and operational development on aviation emissions in the 21st century?* is answered. The performance model is set up by using air traffic input data for different scenarios of global development to simulate air traffic. A model developed on the basis of the Breguet range equation for aircraft, which source a share of the power from a constant fuel source, is used for the performance model. The model is able to assess propulsive, aerodynamic and structural technology options at a low penalty to result accuracy. A small set of input parameters is required to run the model. Depending on the input parameters, a simulation takes between two and twenty minutes.

The model in this work is constructed without implementation of costs. This resulted in a model with low computational cost which requires low knowledge of the costs of the technology under review, but limits the manner in which it is able to resolve how decisions in adopting certain aircraft technology or policy options are made. The model in this work can be improved by implementing a cost model, either by supplementing AIM with the performance model in this work or incorporating a cost model in the model in this work. This would allow airlines in the simulation to strive for profit optimization and result in a decision model which more closely resembles reality. The model in this work minimizes fuel consumption, but neglects the implications of achieving this. In this sense, the model favours aircraft with high aircraft hybridization ratios, neglecting costs of the technology involved in construction of these aircraft and the cost of generating the energy required.
Cost implementation would allow for resolution of the acquisition cost of a technology as well as the cyclical costs of new technology such as battery replacement. The second hand aircraft market which is simulated as the optimum redistribution of excess aircraft towards regions with a deficit could be resolved by a value driven model.
In addition, implementation of costs will allow the policy model to be expanded with the inclusion of fuel taxation or carbon emission rights. This results in a more comprehensive model and increase insight in the tools policymakers have to influence the sectors' climate impact.

The climate impact of the aviation sector is limited to the emissions occurring during flight movements. Implementation of the climate impact in the construction and decommissioning of aircraft would result in a better lifetime assessment of aircraft. This would require extensive knowledge of the materials required to construct these aircraft and their energy source, but would increase the accuracy of aircraft lifecycle emissions. The model in this work is skewed towards aircraft with high hybridization ratios, but incorporating the emissions associated with battery construction and electricity generation would increase insight in the potential of hybrid electric aviation.

It can be concluded that the impact of technological trends and policy options on the share of the aviation sector on climate change can be resolved by the model. The measures are able to limit emissions, but are inadequate to result in the targets set for the aviation sector. The emissions are dictated by the sectors' growth, which outpaces the simulated fuel efficiency increases in this model. This is confirmed by the 300% increase in carbon emissions between 2020 and 2050 for the SSP2 with the current trend of fuel efficiency increase. An increase of 0.4% in annual fuel efficiency of the current trend results in a 250% increase in carbon emissions for the same scenario. To achieve the net-zero emission goals as stated for 2050, aviation fuels will have to become carbon-neutral or the growth of the sector will have to be restricted.

Bibliography

[1] D S Lee, D W Fahey, A Skowron, M R Allen, U Burkhardt, Q Chen, S J Doherty, S. Freeman, P. M. Forster, J. Fuglestvedt, A. Gettelman, R. R. De León, L. L. Lim, M. T. Lund, R. J. Millar, B. Owen, J. E. Penner, G. Pitari, M. J. Prather, R. Sausen, and L. J. Wilcox. The contribution of global aviation to anthropogenic climate forcing for 2000 to 2018. *Atmospheric Environment*, 244(January), 2020.

[2] David S. Lee, David W. Fahey, Piers M. Forster, Peter J. Newton, Ron C.N. Wit, Ling L. Lim, Bethan Owen, and Robert Sausen. Aviation and global climate change in the 21st century. *Atmospheric Environment*, 43(22-23):3520–3537, 2009.

[3] IATA. Industry Forecast - December 2015. Technical report, International Aviation Transport Association, 2020.

[4] IATA. Industry Statistics - Fact Sheet. Technical report, International Aviation Transport Association, 2019.

[5] United Nations Framework Convention on Climate Change. National greenhouse gas inventory data for the period 19902012. *Representation*, 21(82):4–5, 1980.

[6] IATA. IATA - Climate Change, 2019.

[7] ICAO. International Aviation and Climate Change. In *Environmental protection*, number 37 in Assembly of the executive committee, pages 24–26. ICAO, 2010.

[8] ICAO. Effects of Novel Coronavirus (COVID-19) on Civil Aviation: Economic Impact Analysis, 2020.

[9] IATA. Net-Zero Carbon Emissions by 2050, 2021.

[10] European Commission. The European Green Deal, 2019.

[11] Snastasia Kharina and Daniel Rutherford. Fuel efficiency trends for new commercial jet aircraft: 1960 to 2014. Technical Report August, The International Council on Clean Transportation, 2015.

[12] Xinyi Sola Zheng and Dan Rutherford. Fuel Burn of New Commercial Jet Aircraft: 1960 to 2019. Technical Report September, The International Council on Clean Transportation, 2020.

[13] Federal Aviation Administration Office of Environment and Energy. Aviation & Emissions A Primer. Technical Report January, Federal Aviation Administration Office of Environment and Energy, 2005.

[14] D. S. Lee, G. Pitari, V. Grewe, K. Gierens, J. E. Penner, A. Petzold, M. J. Prather, U. Schumann, A. Bais, T. Berntsen, D. Iachetti, L. L. Lim, and R. Sausen. Transport impacts on atmosphere and climate: Aviation. *Atmospheric Environment*, 44(37):4678–4734, 2010.

[15] Don Wuebbles, Mohan Gupta, and Malcolm Ko. Evaluating the impacts of aviation on climate change. *Eos*, 88(14):1–3, 2007.

[16] David R. Williams. Earth Fact Sheet, 2020.

[17] R Friedl. Atmospheric Effects of Subsonic Aircraft : Interim Assessment Report Advanced Subsonic Technology Program of the Edited. Technical report, NASA, 1997.

[18] J.E. Penner, D.H. Lister, D.J. Griggs, D.J. Dokken, and M. McFarland. Aviation and the Global Atmosphere. Technical report, International Panel on Climate Change, 1999.

[19] Thomas F. Stocker, Dahe Qin, Gian Kasper Plattner, Melinda M.B. Tignor, Simon K. Allen, Judith Boschung, Alexander Nauels, Yu Xia, Vincent Bex, and Pauline M. Midgley. *Climate change 2013 the physical science basis: Working Group I contribution to the fifth assessment report of the intergovernmental panel on climate change*, volume 9781107057. Cambridge University Press, 2013.

[20] David Archer, Michael Eby, Victor Brovkin, Andy Ridgwell, Long Cao, Uwe Mikolajewicz, Ken Caldeira, Katsumi Matsumoto, Guy Munhoven, Alvaro Montenegro, and Kathy Tokos. Atmospheric lifetime of fossil fuel carbon dioxide. *Annual Review of Earth and Planetary Sciences*, 37:117–134, 2009.

[21] Gaby Rädel and Keith P. Shine. Radiative forcing by persistent contrails and its dependence on cruise altitudes. *Journal of Geophysical Research Atmospheres*, 113(7):1–9, 2008.

[22] H Mannstein, K Gierens, and P Spichtinger. How to Avoid Contrail Cirrus. *1st CEAS European Air and Space Conference*, pages 2217–2220, 2007.

[23] Christine Fichter, Susanne Marquart, Robert Sausen, and David S. Lee. The impact of cruise altitude on contrails and related radiative forcing. *Meteorologische Zeitschrift*, 14(4):563–572, 2005.

[24] K. Dahlmann, V. Grewe, C. Frömming, and U. Burkhardt. Can we reliably assess climate mitigation options for air traffic scenarios despite large uncertainties in atmospheric processes? *Transportation Research Part D: Transport and Environment*, 46(2):40–55, 2016.

[25] Christine Fichter. Climate impact of air traffic emissions in dependency of the emission location and altitude. Technical report, DLR, 2009. Thesis submitted for the degree of Doctor of Philosophy, Manchester Metropolitan University, Manchester, UK.

[26] Volker Grewe, Sigrun Matthes, and Katrin Dahlmann. The contribution of aviation NO x emissions to climate change: are we ignoring methodological flaws? *Environmental Research Letters*, 14(12), 2019.

[27] U. Schröder, F.P., Kärcher, B., Petzold, A., Baumann, R., Busen, R., Hoell, C., Schumann. Utrafine aerosol particles in aircraft plumes: in situ observations. *Geophysical research letters*, 25(15):2789–2792, 1998.

[28] European Aviation Safety Agency. Study on Aviation and Economic Modelling (SAVE). Technical report, European Aviation Safety Agency, 2010.

[29] O. Oguntona. Longer-term aircraft fleet modelling: narrative review of tools and measures for mitigating carbon emissions from aircraft fleet. *CEAS Aeronautical Journal*, 11(1):13–31, 2020.

[30] Lynnette M Dray. AIM2015: Documentation. Technical report, UCL Energy Institute, London, 2015.

[31] Brian C. O'Neill, Elmar Kriegler, Keywan Riahi, Kristie L. Ebi, Stephane Hallegatte, Timothy R. Carter, Ritu Mathur, and Detlef P. van Vuuren. A new scenario framework for climate change research: The concept of shared socioeconomic pathways. *Climatic Change*, 122(3):387–400, 2014.

[32] Bethan Owen, David S. Lee, and Ling Lim. Flying into the future: Aviation emissions scenarios to 2050. *Environmental Science and Technology*, 44(7):2255–2260, 2010.

[33] Bethan Owen, David S Lee, and Ling Lim. Supporting material for : Flying into the future aviation emissions scenarios to 2050. *Flying*, pages 1–13, 2010.

[34] National Aerospace Laboratory. Executive summary Aviation and Emissions Scenario and Policy Analysis Capabilities of AERO-MS. Technical report, Koninklijk Nederlands Lucht- en Ruimtevaartcentrum, 2012.

[35] Reynard De Vries, Maurice F.M. Hoogreef, and Roelof Vos. Range equation for hybrid-electric aircraft with constant power split. *Journal of Aircraft*, 57(3):552–557, 2020.

[36] J Roskam. *Airplane Design*. DARcorporation, 1985.

[37] Laurent Bovet. How to Correct the Bréguet Range Equation Taking into Account the Fuel Flow Rate of the Aircraft ? In *8th European Conference for Aeronautis and Aerospace Sciences (EUCASS)*, 2019.

[38] J. Lee, S. Lukachko, Ian Waitz, and A. Schafer. Historical and Future Trends in Aircraft Performance, Cost and Emissions. *Annual Review of Energy and the Environment*, 26:167–200, 2001.

[39] Martin Hepperle. Electric Flight - Potential and Limitations. Technical report, Deutsches Zentrum für Luft- und Raumfahrt, 2012.

[40] Luke L. Jensen, Henry Tran, and R. John Hansman. Cruise fuel reduction potential from altitude and speed optimization in global airline operations. *Proceedings of the 11th USA/Europe Air Traffic Management Research and Development Seminar, ATM 2015*, pages 1–10, 2015.

[41] Lissys ltd. Piano-X Aircraft Emissions and Performance - User Guide, 2008.

[42] Lissys ltd. The things that Piano is used for:.

[43] ICAO. International Civil Aviation Organization Manual on Air Traffic Forecasting. Technical report, ICAO, 2006.

[44] ICAO. Introduction to Air Transport Statistics, 2014.

[45] Ivan Terekhov, Thomas Schilling, Malte Niklaß, and Robin Ghosh. Assessing the impact of new technologies in aviation using a global aircraft fleet forecasting model. In *Aegats 2018*, 2018.

[46] ICAO. *Report of the Ninth Meeting of the Committee on Aviation Environmental Protection (CAEP)*. INTERNATIONAL CIVIL AVIATION ORGANIZATION, MONTRÉAL, 2013.

[47] U K Wickrama, S C Henderson, and A Vedantham. Aircraft Emissions: Current Inventories and Future Scenarios. Technical Report January, IPCC, 1999.

[48] Tom G. Reynolds, Steven Barrett, Lynnette M. Dray, Antony D. Evans, Marcus O. Köhler, María Vera Morales, Andreas Schäfer, Zia Wadud, Rex Britter, Henry Hallam, and Richard Hunsley. Modelling environmental & economic impacts of aviation: Introducing the aviation integrated modelling project. *Collection of Technical Papers - 7th AIAA Aviation Technology, Integration, and Operations Conference*, 1(September):569–580, 2007.

[49] Adam Daigneault, Craig Johnston, Anu Korosuo, Justin S. Baker, Nicklas Forsell, Jeffrey P. Prestemon, and Robert C. Abt. Developing Detailed Shared Socioeconomic Pathway (SSP) Narratives for the Global Forest Sector. *Journal of Forest Economics*, 34(1-2):7–15, 2019.

[50] Lynnette M. Dray, Philip Krammer, Khan Doyme, Bojun Wang, Kinan Al Zayat, Aidan O'Sullivan, and Andreas W. Schäfer. AIM2015: Validation and initial results from an open-source aviation systems model. *Transport Policy*, 79(April 2018):93–102, 2019.

[51] Tom G. Reynolds. Air traffic management performance assessment using flight inefficiency metrics. *Transport Policy*, 34:63–74, 2014.

[52] Airbus S.A.S. Aircraft Characteristics Airport And Maintenance Planning. Technical Report Nov 01/20, Airbus, Blagnac, 2005.

[53] ICAO. Annex 6 to the Convention on International Civil Aviation Part I - International Commercial Air Transport - Aeroplanes, AMDT 30.pdf. Technical Report November, ICAO, 2016.

[54] C.J. Eyers, P. Norman, J. Middel, M. Plohr, S. Michot, K. Atkinson, and R.A. Christou. Aero2k global aviation emissions inventories for 2002 and 2025. Technical report, QinetiQ, 2004. LIDO-Berichtsjahr=2005,.

[55] Lynnette Dray. An analysis of the impact of aircraft lifecycles on aviation emissions mitigation policies. *Journal of Air Transport Management*, 28:62–69, 2013.

[56] Cirium. Global aviation recovery is happening, but at a snail's pace, 2021.

[57] Dr. Y. L. Ding, Z. P. Cano, Prof. A. P. Yu, and Prof. Z. W. Chen. Automotive Li-Ion Batteries: Current Status and Future Perspectives. *Electrochemical Energy Reviews*, 1-28:1–82, 2019.

[58] Hendrik Löbberding, Saskia Wessel, Christian Offermanns, Mario Kehrer, Johannes Rother, Heiner Heimes, and Achim Kampker. From cell to battery system in BEVs: Analysis of system packing efficiency and cell types. *World Electric Vehicle Journal*, 11(4):1–15, 2020.

[59] U.S Energy Information Administration. Internation electricity generation, 2021.

A | Model input parameters

- **Run start year:** This parameters specifies the start year of the time frame for which the model is run.
- **Run end year:** This parameters specifies the end year of the time frame for which the model is run.
- **Use AIM database for a SSP:** Selection if an available database from the output of the AIM is used or if a user provided database is used.
- **Database name:** If using a user provided database specify the database name for the model to load the data.
- **SSP:** Name of the SSP scenario to be used in the model.
- **Passenger mass:** The mass per passenger to be used in payload determination.
- **Proces data:** If new flight data is added with the same name it has to be processed first, afterwards data processing can be skipped to reduction computational cost.
- **Specific energy consumable fuel:** Specific energy of the consumable fuel such as Jet-A1, specified in $\frac{MJ}{kg}$.
- **Initial specific energy non consumable fuel:** Specific energy of the non consumable fuel such as electric batteries, specified in $\frac{kWh}{kg}$.
- **Initial propulsive efficiency:** Initial level of the dimensionless propulsive efficiency measured in a scale of zero to one.
- **Initial power split ratio:** Initial level of the power split ratio set in a scale of zero to one.
- **First year new generation of aircraft:** The introduction year of the first new generation of aircraft.
- **Interval between new generations of aircraft:** Interval in years between the first new aircraft generation and the subsequent ones.
- **Annual aerodynamic efficiency increase:** Annual increase in aerodynamic efficiency expressed in percentages to be used as exponential growth.
- **Annual structural efficiency increase:** Annual increase in structural efficiency expressed in percentages to be used as exponential growth.
- **Logarithmic propulsive efficiency increase:** Scaling parameter to be used in the increase in propulsive efficiency.
- **Annual non consumable fuel specific energy increase:** Annual increase in specific energy of the non consumable fuel expressed in percentages to be used as exponential growth.
- **Stepped power split ratio:** Can be set to one to have a step wise increase in power split ratio.
- **Step wise increase in power split ratio:** Step wise increase in power split ratio.
- **Design file:** If using a user provided aircraft design file set to 1.
- **Save design:** To output the aircraft design in this run set to 1.
- **Design filename:** Set the name of the file to save the aircraft design or specify the name of the user provided aircraft design.
- **Early retirement scenario:** Set to one to simulate early retirement.
- **Early retirement age:** Set to the cut off age in which all aircraft are retired if using an early retirement scenario.

- **Start year of early retirement scenario:** Set the year in which the early retirement scenario comes into effect.
- **Region to be simulated:** Set to zero to simulate the global aviation sector, otherwise set to the region identifier provided in the flight data file to simulate that region.

B | Performance model modelling accuracy

	Climb	Cruise	Descent	Block	Reserve	TO weight
Canadair CRJ 701	0.78	0.99	-1.90	0.99	-25.58	0.98
Embraer 190	0.91	0.99	0.56	0.99	-10.64	0.99
A319-131	0.86	1.00	-3.43	1.00	-3.30	1.00
A320-214	0.82	1.00	-4.11	1.00	-0.05	1.00
B737-800 NG	0.83	1.00	-1.93	0.99	-1.22	1.00
B787-8	0.97	1.00	-0.81	1.00	0.40	1.00
A330-300	0.94	1.00	-1.66	1.00	-0.37	1.00
B777-300 ER	0.86	1.00	-6.81	1.00	0.31	1.00
A380-861	0.93	1.00	-2.22	1.00	-1.18	1.00

Table B.1: R square measure of fit for model optimisation.

	Climb	Cruise	Descent	Block	Reserve	TO weight
Canadair CRJ 701	46	140	6	188	418	430
Embraer 190	60	250	8	315	544	550
A319-131	78	234	19	302	281	417
A320-214	95	213	17	312	182	363
B737-800 NG	85	192	17	371	448	438
B787-8	78	553	22	688	952	1075
A330-300	134	382	22	586	1474	1385
B777-300 ER	168	367	45	859	1361	1224
A380-861	458	728	53	1340	2972	2788

Table B.2: Root mean square error for model optimisation.

	Climb	Cruise	Descent	Block	Reserve	TO weight
Canadair CRJ 701	0.059	0.048	0.078	0.047	0.354	0.015
Embraer 190	0.060	0.055	0.080	0.053	0.375	0.015
A319-131	0.063	0.036	0.092	0.036	0.101	0.007
A320-214	0.068	0.035	0.085	0.039	0.062	0.006
B737-800 NG	0.060	0.034	0.083	0.047	0.163	0.007
B787-8	0.026	0.022	0.063	0.023	0.169	0.006
A330-300	0.035	0.015	0.060	0.020	0.230	0.007
B777-300 ER	0.042	0.011	0.082	0.023	0.166	0.005
A380-861	0.053	0.010	0.053	0.016	0.261	0.007

Table B.3: Normalised root mean square error for model optimisation.

	ff_{cl} [−]	η_{cr} [−]	ff_{de} [−]
Canadair CRJ 701	0.9729	0.2439	0.9968
Embraer 190	0.9732	0.2498	0.9967
A319-131	0.9794	0.3081	0.9961
A320-214	0.9775	0.2988	0.9964
B737-800 NG	0.9768	0.2857	0.9963
B787-8	0.9827	0.3831	0.9977
A330-300	0.9798	0.3425	0.9977
B777-300 ER	0.9840	0.3566	0.9974
A380-861	0.9797	0.3586	0.9971

Table B.4: Performance parameters for model optimisation.